Fundamental investigation on the development of tough ion gel-based thin membranes for CO2 separation

張, 勁輝

(Degree)
博士（学術）

(Date of Degree)
2022-09-25

(Date of Publication)
2023-09-01

(Resource Type)
doctoral thesis

(Report Number)
甲第8462号

(URL)
https://hdl.handle.net/20.500.14094/0100477888

Doctoral Dissertation

Fundamental investigation on the development of tough ion gel-based thin membranes for CO_2 separation

高強度イオンゲル型 CO_2 分離薄膜の開発に関する基礎的検討

July 2022

Graduate School of Engineering
Kobe University

ZHANG JINHUI

Contents

Chapter I
General Introduction

I-1 Carbon dioxide (CO_2) emission

Due to the rapid development of industry and the massive use of fossil fuels, the emission of greenhouse gases (GHGs), especially CO_2, is rapidly increasing. The large amount of CO_2 emissions would cause a series of problems to the ecological environment such as global warming, glaciers melting, sea levels rising, etc., and even threatens the survival and development of human beings [1-5]. Power plants using fossil fuels such as coal and natural gas are the largest source of carbon dioxide emissions. In 1850, global CO_2 emissions from fossil fuels is 0.197 billion tons, and the number in 2020 is sharply raised to 34.81 billion tons [6]. The results from the recent Intergovernmental Panel on Climate Change (IPCC) reports suggested that the CO_2 emissions should be reduced by 55% before 2030 in order to limit the increase of the global temperature within 1.5 °C [7, 8]. To prevent further damage to the environment caused by CO_2 emissions, the development of efficient and stable carbon capture technologies has attracted widespread attention [9].

I-2 CO_2 capture technology

I-2-1 CO_2 capture system

The carbon capture can be divided into three systems according to different fuel combustion process: the pre-combustion CO_2 capture system, the oxy-combustion CO_2 capture system, and the post-combustion CO_2 capture system [10-13]. The fossil fuel, water vapor and oxygen (O_2) could react to generate hydrogen (H_2) and CO_2, CO_2 generally accounts for 15-60% of the volume in the mixture. The separation of the CO_2 from this CO_2/H_2 mixture was called pre-combustion CO_2 capture. As for oxy-combustion system, O_2 is used instead of air to support the combustion of the fuel, and the products are the flue gas with water vapor and high concentration of CO_2 (over 80% of the volume). The gas separation in this process is oxy-combustion CO_2 capture. The post-combustion CO_2 capture is that separating the CO_2 from the flue gas produced by the combustion of the primary fuel in air. The flue gas produced in this process is mainly composed of CO_2 (typically 3-15% by volume) and N_2.

I-2-2 CO_2 separation method

At present, the most widely used CO_2 separation methods mainly include absorption method, adsorption method, and membrane separation method [5, 9, 14].

The absorption method realizes the separation of CO_2 due to the different solubility of the CO_2 and other gases in the absorbent. Absorption is currently one of the most mature CO_2 separation methods in industries [9, 15], and can be operated in either physical or chemical way. Physical absorption is generally carried out under high pressure and low temperature conditions, and desorption is carried out by means of decompression or heating. The process does not involve any chemical reactions and is normally governed by Henry's law [16, 17]. Typical physical CO_2 absorbents are pyrrolidone, propylene carbonate, methanol, *N*-methylpyrrolidone, etc [18, 19]. For the chemical absorption method, the absorbed gas could react with the absorbent. The reaction will effectively reduce the partial pressure of the absorbed gas on the surface of the absorbent and generate a strong driving force to promote the absorption of the gas thus improving the absorption efficiency. Typical chemical CO_2 absorbents include monoethanolamine (MEA), diethanolamine (DEA) and potassium carbonate, etc [5, 20]. The absorption method is a well-established separation method with high CO_2 capture efficiency, but the use of absorbents containing amines has serious disadvantages, such as the formation of corrosive by-products from amine degradation and the associated environmental problems caused by the evaporation of volatile amines. The high energy consumption for the solvent regeneration also restricts its development [21-23].

Adsorption is another commonly used CO_2 separation method, and the principle is based on the van der Waals forces between adsorbate and adsorbent molecules [24-26]. Due to the intermolecular van der Waals forces, the gas to be captured can be immobilized on the adsorbent with a porous structure. Commonly used CO_2 adsorbents include calcium oxide, zeolite, carbon-based materials (activated carbon, carbon nanotubes, carbon nanofibers, graphene) and molecular sieves, etc [23, 27, 28]. The practical application of currently developed and proposed adsorption technologies is mainly limited by the problems such as insufficient CO_2 capacity and high cost [29, 30].

Membrane separation is a technology that uses the selective permeability of the gases through the membrane to separate CO_2 from other gases. The separation process is shown by a schematic illustration in Figure I-1. Due to the outstanding advantages such as low energy consumption, low cost,

simple process, small footprint, and less pollution, membrane separation method has attracted extensive attention [31].

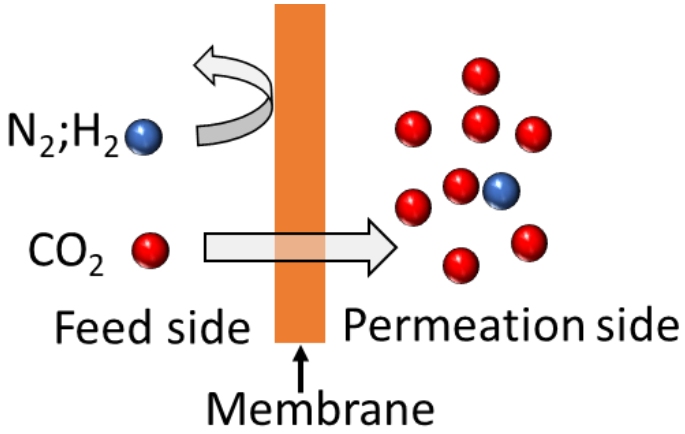

Figure I-1. Schematic illustration of the membrane separation method for CO_2 separation.

I-3 CO_2 separation membrane

Currently, CO_2 capture from the flue gas in cogeneration power plants mainly use chemical absorption such as amine solutions at a cost of about \$40 – \$100/ton CO_2. Merkel et al. estimated the gas separation performance needed for membrane separation methods to replace the existing chemical absorption methods [32]. As shown in Figure I-2, the minimum CO_2 permeance of 1000 GPU (1 GPU = 3.35×10^{-10} mol/($m^2\cdot s\cdot Pa$)) and CO_2/N_2 permselectivity of 20 are needed to reduce the cost to 40 \$/ton CO_2 or less. However, most of the membrane materials currently developed still cannot meet the requirements of industrial applications. Development of high-performance CO_2 separation membrane materials thus is the major focus of the researches in membrane separation field [33].

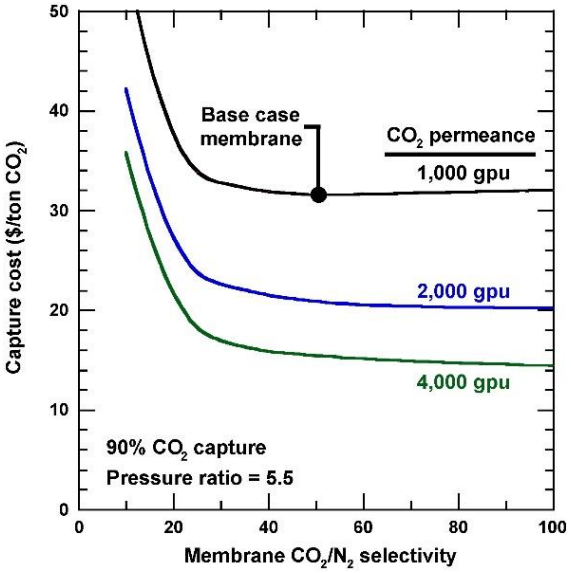

Figure I-2. Effect of the CO_2/N_2 selectivity and the CO_2 permeance of membranes on the cost of capturing 90% of the CO_2 from flue gas using membrane separation method [32].

Based on membrane materials, CO_2 separation membranes usually can be classified as polymeric membranes, inorganic membranes, and polymer-inorganic hybrid membranes.

I-3-1 Polymeric membrane

Polymeric CO_2 separation membranes have the advantages of low cost, easy mass production and good membrane formation performance. Polymeric CO_2 separation membranes include glassy polymer membrane and rubbery polymer membrane. Glassy polymer membranes possess high gas permselectivity and high mechanical strength, but generally exhibit low gas permeability. Additionally, the gas separation performance of glassy polymer membranes is easily limited by plasticization and aging problems. Commonly used glassy polymer membrane materials for gas separation are polyimide (PI), cellulose acetate (CA), polycarbonate (PC), polyacetylene, and polyethersulfone (PES), etc. The properties of the rubbery polymer membrane are opposite to that of the glassy polymer membrane. The rubbery polymer membrane usually has high gas permeability, but its gas permselectivity is generally low. This difference between glassy and rubbery polymeric membranes is related to the flexibility of the polymer segment. The rubbery polymer membrane materials for gas separation include polydimethylsiloxane (PDMS), polyoxyethylene, polyether block amide (Pebax), etc.

However, polymer membranes are constrained by the trade-off restriction between membrane

permeability and selectivity, i.e., increased gas permeability is accompanied by decreasing gas permselectivity, and increased gas permselectivity is accompanied by decreasing gas permeability. The trade-off theory was first proposed by Robeson in 1991 and the Robeson upper bound diagram was developed through extensive statistical analysis as shown in Figure I-3 [34, 35].

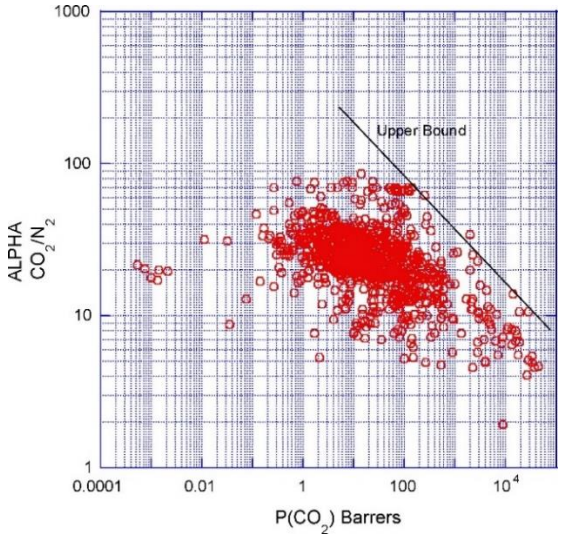

Figure I-3. Robeson upper bound of polymeric membranes for CO_2/N_2 separation in 2008 [34].

I-3-2 Inorganic membrane

Inorganic membranes are prepared using inorganic materials. The widely studied inorganic membrane materials for gas separation include zeolites, ceramics, metal organic frameworks (MOFs), carbon molecular sieves, graphene oxide, etc.

Inorganic membranes have the advantages such as good physical and chemical stability, high mechanical strength, high resistance to acid and alkali, wide operating temperature and pressure range. In addition, the inorganic membrane is not limited by the trade-off effect between the gas permeability and gas permselectivity as the polymeric membranes. Therefore, compared with polymeric membranes, inorganic membranes can be used in harsher environments and usually exhibit higher CO_2 separation performance. However, the inorganic membrane also has some significant disadvantages, such as high brittleness, poor processability and high cost, which make it difficult to be applied in the mass production.

I-3-3 Polymer-inorganic hybrid membrane

The polymer-inorganic hybrid membrane is fabricated by introducing the inorganic fillers into the polymer matrix, also named as mixed matrixed membranes (MMMs). The good processability of polymeric membranes could be maintained in the polymer-inorganic hybrid membrane. In addition, the introduced inorganic fillers could improve the mechanical properties and increase the gas separation performance of the composite membranes. However, some problems of the polymer-inorganic hybrid membranes such as high costs, difficulties in mass production, and interfacial defects between polymer matrix and inorganic fillers still should be addressed before practical application.

I-4 Ionic Liquids (ILs)-based membrane

I-4-1 ILs

ILs are non-volatile and thermally stable liquid salts consisting of organic cation and various kinds of anions (Figure I-4). In 1914, Paul Walden synthesized the earliest ionic liquid, ethyl ammonium nitrate [36]. Since then, the investigations of ionic liquids have grown significantly, with applications in biology, electrochemistry, physical chemistry, engineering, solvents, and catalysis, etc. ILs own the characteristic properties of non-volatility, high thermal and chemical stability, tunable molecular structures and properties. In 1999, Blanchard et al. reported that CO_2 could be effectively dissolved in some ILs [37]. This discovery started the application of ILs in the field of CO_2 separation, and offered a new alternative material for the preparation of high-performance CO_2 separation membranes.

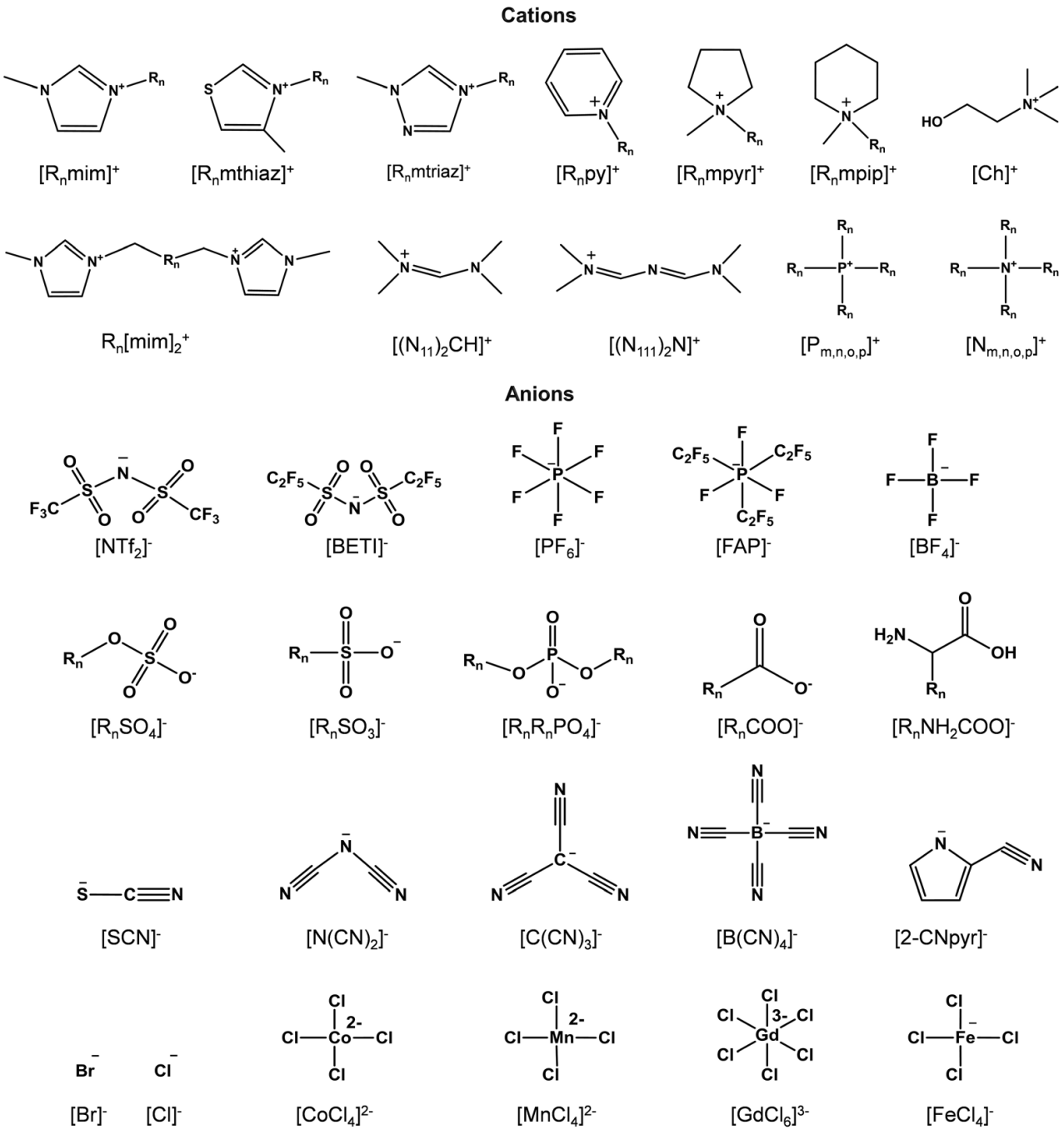

Figure I-4. Cation and anion chemical structures and abbreviations of ILs for CO_2 separation [38].

I-4-2 Supported ionic liquid membranes (SILMs)

SILMs is one of supported liquid membranes, normally fabricated by impregnating the IL into a porous support membrane. Since 2002, Scovazzo et al. had been systematically investigating the SILMs for CO_2 separation, and the prepared SILMs displayed high CO_2 permeability [39-41]. The preparation of SILMs is simple and the CO_2 separation performance of the SILMs could be easily

tuned by changing the type of ILs. But the poor stability is the main problem that restricts the application of SILMs. Especially at high transmembrane pressure, the IL would be pushed out from the pores of the support membrane. Due to this issue, some research efforts have been devoted to other forms of IL-based membranes.

I-4-3 Poly (ionic liquid) (PIL) membrane

In 2005, Tang et al. first reported a new material which was fabricated by the polymerizable IL monomers and showed high CO_2 sorption capacities, named poly (ionic liquids) (PILs) (Figure I-5) [42, 43]. PILs provide a new option to applied the IL for gas separation, and overcome the problem of the poor stability of SILMs. Bara et al. fabricated a series of PILs and fabricated them into membranes for CO_2/N_2 separation and CO_2/CH_4 separation [44, 45]. Early developed PIL membranes have lower CO_2 permeability compared to SILMs. Therefore, based on the neat PIL membrane, the PIL/IL composite membrane [46], PIL copolymer membrane [47] and PIL/IL/inorganic particle mixed matrix membrane [48] are developed to improve the mechanical strength and gas separation performance of PIL membranes.

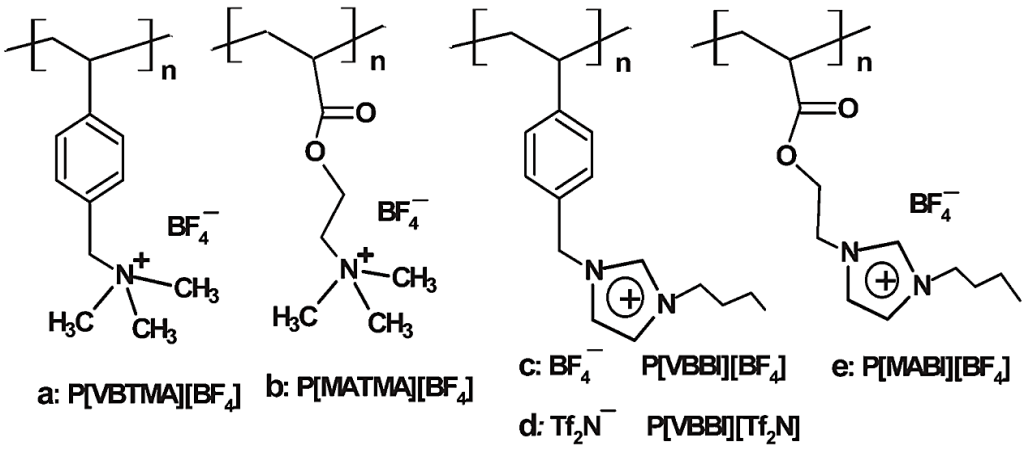

Figure I-5. Chemical structures of some poly (ionic liquids) (PILs) [42].

I-4-4 Ionic liquid gel (ion gel) membrane

Ion gel membrane is normally formed by a small amount of three-dimensional networks and a large amount of an IL (Figure I-6). Due to the high IL content of ion gels, the CO_2 permeability of ion gel

membranes could be comparatable or even higher than that of SILMs. The solid state endows ion gel membranes with the better stability under the high pressure and the long-time operation for CO_2 separation compared with SILMs. In addition, the physicochemical properties and gas separation performance of ion gel membranes could be tuned by changing the type of ILs. Some ion gel membranes containing CO_2-phlic ILs could easily exceed the Robeson upper bound [49, 50].

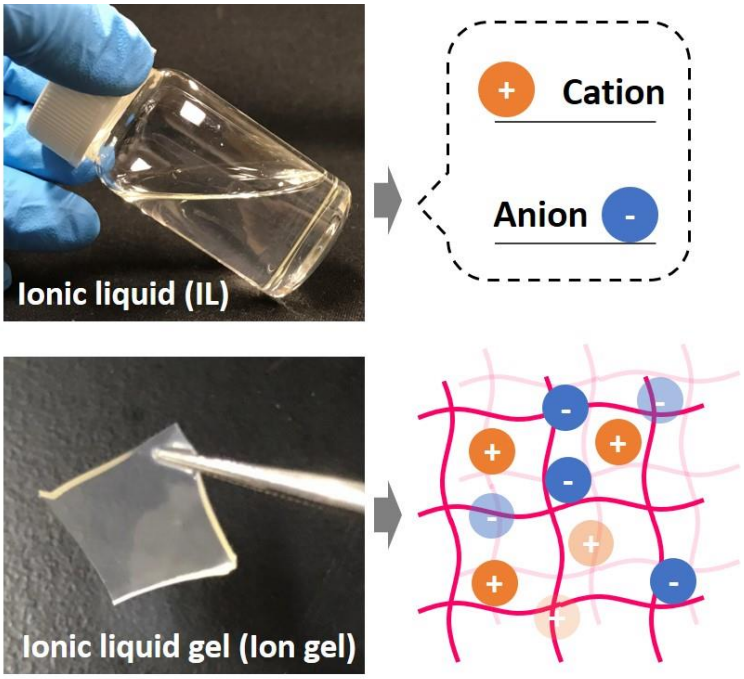

Figure I-6. Photographs and schematics of an ionic liquid and ion gel.

I-5 Challenges of ion gel membrane for CO_2 separation

The ion gel membranes combine the good stability of PIL membranes and the high gas permeability of SILMs. But there are still some challenges that restrict the development of high-performance ion gel membanes.

The poor mechanical property is the major challenge for the application of ion gel membranes in the current stage. Different from polymeric membranes restricted by the trade-off restriction between the gas permeability and gas permselectivity, ion gel membranes show a trade-off between the gas permeability and mechanical strength (Figure I-7). On the one hand, the polymer network could be the resistance for gas transport. Hence, the gas permeability of ion gel membranes could be effectively increased by increasing the IL content. On the other hand, however, the mechanical strength of ion gel

mambrens would dramatically decrease when the IL content increases. Therefore, to obtain high gas separation performance, ion gel membanes with good mechanical properties should be developed. Several strategies has been proposed to improve the mechanical strength of ion gels, whichs will be presented in the next section.

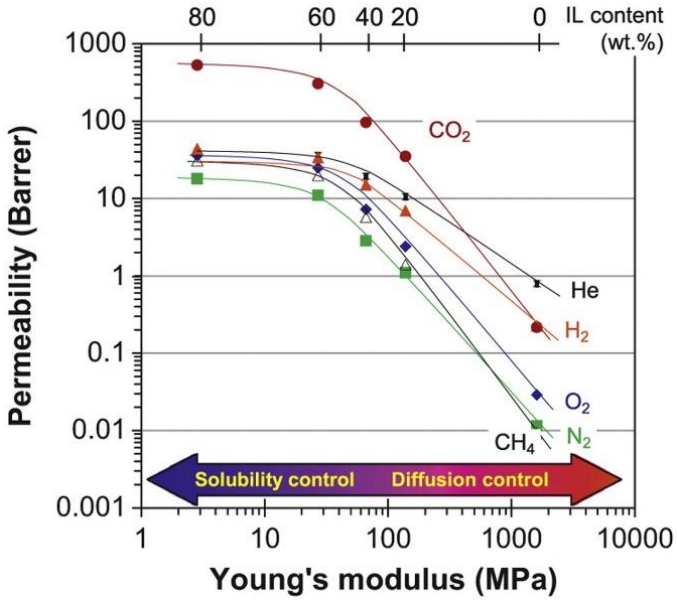

Figure I-7. Correlation of gas permeability and Young's modulus of ion gel membranes containing different IL contents [51].

To reduce the gas transport resistance through ion gel membranes and achieve high gas permeance, ion gel membanes should be made into a thin film. However, preparation of thin ion gel membranes is also restricted by the low mechanical strength of ion gels. It is hard to develop a thin ion gel membrane strong enough to hold a large amount of an IL. In addition, the polymer network of many ion gels are formed from volatile raw materials or the polymerization of monomers that can only be performed in a closed space, making the ion gels can hardly be prepared by conventional thin-film preparation method normally conducted in an open space. Restrected by such difficulties, the thin ion gel membranes has rarely been reported.

I-6 Tough ion gels

As described in last section, the weak mechanical strength is a big challenge for the preparation of high-performance ion gel membranes. Therefore, the development of tough ion gels has drawn lots of attention and been extensively investigated in recent years.

Several strategies have been carried out to fabricate tough ion gels with well-designed polymer networks. Polymer networks of some tough ion gels are shown in Figure I-8. Fujii et al. prepared a tough ion gel consisting of the homogeneous tetra-arm poly(ethylene glycol) (tetra-PEG) cross-linking network as shown in Figure I-8(a) and an IL. The Tetra-PEG ion gel membrane with IL content of 94 wt% showed a high CO_2 permeability of 877 barrer (1 barrer = 3.35×10^{-16} mol·m/(m^2·s·Pa)) [52, 53]. Lodge et al. introduced a self-assembled triblock copolymer network as shown in Figure I-8(b) into an IL and the fabricated ion gel membranes exhibited good toughness and high CO_2 separation performance [47, 54-58]. Some other tough ion gels were developed based on the double-network (DN) principle [59, 60], such as DN ion gels containing organic/organic double network as shown in Figure I-8(c) [49, 50, 61-65] and DN ion gels containing inorganic/organic double network as shown in Figure I-8(d) [66-70]. For example, Kamio et al. developed an inorganic/organic double-network ion gel membrane with excellent mechanical properties, and the CO_2 permeability of the ion gel membrane effectively increased from 146 to 1380 barrer when the IL content was increased from 51 to 95.2 wt% [71]. Overall, tough ion gels have proven to be an excellent membrane material for gas separation.

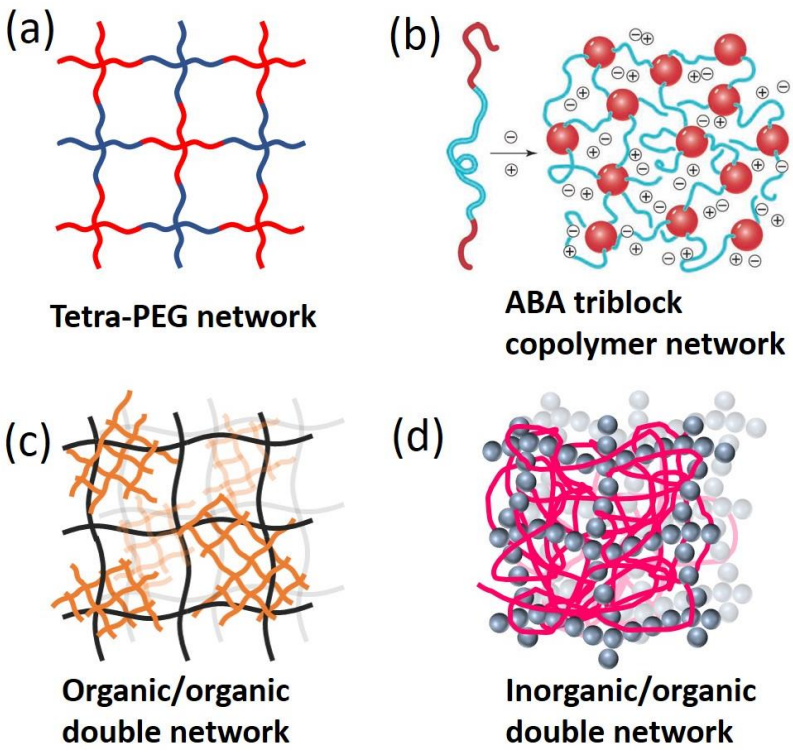

Figure I-8. Schematic illustration of (a) tetra-PEG network, (b) ABA triblock copolymer network [55], (c) organic/organic double network (DN), and (d) inorganic/organic double network (DN) [68].

I-7 Gas transport through an ion gel membrane

I-7-1 Solution-diffusion

In general, gas transport through a dense membranes is mainly dominated by the solution-diffusion mechanism [33]. The gas transport through an ion gel membrane is also governed by the solution-diffusion mechanism [72]. The schematic illustration of gas permeation through an ion gel membrane governed by solution-diffusion mechanism is shown in Figure I-9. The gas is first absorbed by the IL in ion gel membranes from the feed gas side. For the ionic liquid with no functional group which can react with the gas species, the gas absorption isotherm follows the Henry's law [73]. Then the gas diffused through the ion gel membrane to the permeation side under the action of the concentration difference, and desorbed on the membrane surface of the permeation side. The diffusion process of gas in the ion gel membrane follows the Fick's law [74, 75].

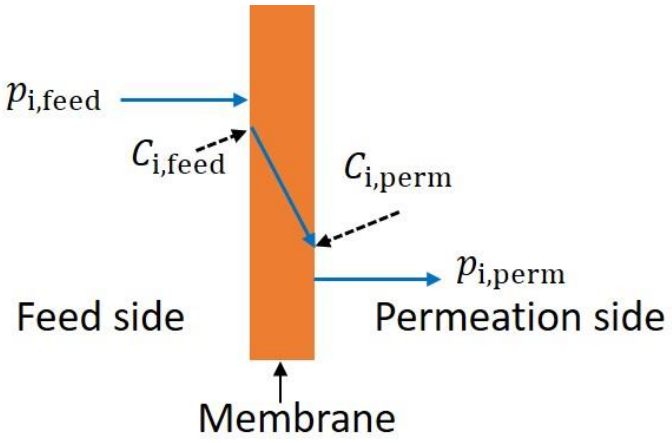

Figure I-9. Schematic illustration of gas permeation through an ion gel membrane governed by solution-diffusion mechanism. $C_{i,feed}, C_{i,perm}$ are the dissolved gas concentrations of gas *i* at the membrane surfaces of the feed side and permeation side, respectively. $p_{i,feed}$, $p_{i,perm}$ are the partial pressures of gas *i* in the feed side and permeation side, respectively.

I-7-2 Permeance, permeability and selectivity

According to Fick's law, the flux (J_i; unit: mol/(s·m^2)) of gas *i* transporting through an ion gel membrane could be expressed by Equation I-1.

$$J_i = D_i \cdot \frac{C_{i,feed} - C_{i,perm}}{\delta} = D_i \cdot \frac{\Delta C_i}{\delta} \qquad (I-1)$$

$C_{i,feed}$, $C_{i,perm}$ are the dissolved gas concentrations (mol/m^3) of gas *i* at the membrane surfaces of the feed side and permeation side, respectively. δ is the membrane thickness. D_i (unit: m^2/s) is the diffusivity coefficient of gas *i* through the ion gel membrane.

Gas permeance (R_i; unit: 1 GPU = 3.35×10^{-10} mol/(m^2·s·Pa)), which indicates the gas permeation rates through a membrane, is defined as the gas flux per unit trans-membrane pressure and could be expressed as Equation I-2.

$$R_i = \frac{D_i}{p_{i,feed} - p_{i,perm}} \cdot \frac{\Delta C_i}{\delta} = \frac{D_i}{\delta} \cdot \frac{\Delta C_i}{\Delta p_i} \qquad (I-2)$$

$p_{i,feed}$ and $p_{i,perm}$ are the partial pressures of gas *i* in the feed side and permeation side, respectively.

Gas permeability (P_i; unit: 1 barrer = 3.35×10^{-16} mol · m/(m^2 · s · Pa)) is the gas permeance normalized by the membrane thickness. Permeability is usually used to indicates the gas permeation ability of membrane materials. The calculation of gas permeability could be expressed by Equation I-3.

$$P_i = R_i \times \delta = D_i \cdot \frac{\Delta C_i}{\Delta P_i} \qquad (I-3)$$

$\Delta C_i/\Delta P_i$ is the gas solubility coefficient (S_i; unit: mol/(m^3 · Pa)), therefore, this equation could be updated to Equation I-4.

$$P_i = D_i \cdot S_i \qquad (I-4)$$

Another important parameter of the gas separation membrane is the gas permselectivity ($\alpha_{i/j}$), which indicates the selective permeability of gas *i* over gas *j*. The gas permselectivity could be calculated by Equation I-5.

$$\alpha_{i/j} = \frac{R_i}{R_j} = \frac{P_i}{P_j} \qquad (I-5)$$

I-7-3 Theoretically estimation about the effect of the IL content on the gas permeability of an ion gel membrane

The gas permeation through an ion gel membrane is governed by the solution-diffusion mechanism. Therefore, the CO_2 permeability (P) of an ion gel membrane can be calculated using the solubility coefficient (S) and the diffusivity coefficient (D) of CO_2 in the ion gel membrane. The diffusivity coefficient of CO_2 in an ion gel membrane can be estimated using Ogston's model (Equation I-6) [76].

$$D = D_0 \times exp\left(-2\pi z L_1 L_s^2 \times \left(\frac{R}{L_s}+1\right)^2 \times \varphi\right) \qquad (I-6)$$

where D_0 is the diffusivity coefficient of the gas molecules (CO_2) in the IL; z is the average number of rods (polymer chains) per unit volume; L_l and L_s are respectively the half-lengths of the rod in the long and short axis directions; d is the radius of the particle (CO_2 molecule); and, φ is the volume fraction of a rod. The z, L_1, L_s, and d are constants; therefore, $2\pi z L_1 L_s^2 \times \left(\frac{d}{L_s}+1\right)^2$ in Equation I-6 can be replaced by a constant K:

$$D = D_0 \times exp(-K \times \varphi) \qquad (I-7)$$

Subsequently, the solubility coefficient (S) can be obtained by dividing the molar amount of the absorbed CO_2 in the ion gel ($n_{CO_2,gel}$) by the volume of the ion gel (V_{gel}). In an ion gel, the IL can absorb while the polymer network can hardly absorb CO_2; hence, S can be described as follows:

$$S = \frac{n_{CO_2,gel}}{V_{gel}} = \frac{S_{IL} \times V_{IL}}{V_{gel}} = \frac{S_{IL} \times \left(V_{gel} \times (1-\varphi)\right)}{V_{gel}} = S_{IL} \times (1-\varphi) \qquad (\mathrm{I}-8)$$

where S_{IL} is the solubility coefficient of CO_2 in the IL, and V_{IL} is the volume of the IL in the ion gel membrane.

According to Equation I-4, Equation I-7, and Equation I-8, the CO_2 permeability (P) of the ion gel membrane can be described as follows:

$$P = D_0 \times exp(-K \times \varphi) \times S_{IL} \times (1-\varphi) \qquad (\mathrm{I}-9)$$

The diffusion coefficient (D_0) and Henry's law constant of CO_2 in pure ILs could be obtained from experiments. The S_{IL} can be calculated from Henry's law constant. When the IL content of the ion gel ($1 - \varphi$) is increased, the theoretical CO_2 permeability of ion gel membranes can be estimated to be increased. When the IL content ($1 - \varphi$) approaches to 100 wt%, the gas permeability of the ion gel membrane would approach to the theoretical maximum CO_2 permeability as $D_0 \times S_{IL}$.

I-7-4 Thin film composite (TFC) membrane with a selective ion gel layer

Ion gel membranes could accommodate a large amount of an IL which usually leads to high CO_2 permeability. However, according to Equation I-2, to obtain high CO_2 permeance for high gas separation efficiency of ion gel membranes, the thickness of the ion gel membrane should be reduced to decrease the gas transport resistance. TFC membrane, normally composed of a porous support membrane, an intermediate layer (gutter layer), and a selective layer, is a good preparation form of thin membrane. The gutter layer is usually an intermediate layer with high gas fluxes and used to prevent the precursor solution from penetrating into the support membrane pores during the preparation of the selective layer.

The gas separation performance of the composite membrane, consisting of a selective ion gel layer (layer 1), a dense gutter layer (layer 2) and a porous support membrane (layer 3), could be estimated by the classical resistance models [69, 77-79]. The structure of the composite membrane was shown

in Figure I-10.

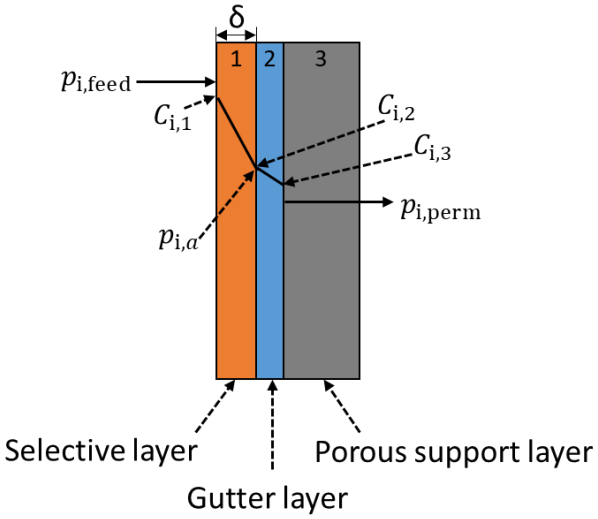

Figure I-10. Structure of composite membrane composed of an ion gel layer, a gutter layer, and a porous support layer. $C_{i,1}$, $C_{i,2}$, and $C_{i,3}$ are the dissolved gas *i* concentrations at respective positions. $p_{i,feed}$, $p_{i,perm}$ are the partial pressures of gas *i* in the feed side and permeation side, respectively. δ is the thickness of the selective layer.

The gas transport resistance of the porous support membrane could be ignored. When the gas transport through this composite membrane become stable, the gas flux through the ion gel layer and the gutter should be the same. The flux of gas *i* could be expressed as followed (Equation I-10). $R_{i,1}$ and $R_{i,2}$ are respectively the permeance of gas *i* through the IPN ion gel layer and the PDMS gutter layer. $p_{i,feed}$ and $p_{i,perm}$ are the partial pressures of gas *i* on the feed and permeation sides of the composite membrane. $p_{i,a}$ is partial pressure of gas *i* at the interface between the ion gel layer and the gutter layer.

$$J_i = R_{i,1} \times (p_{i,feed} - p_{i,a}) = R_{i,2} \times (p_{i,a} - p_{i,perm}) \quad (I-10)$$

Equation I-11 could be obtained by eliminating $p_{i,a}$ from Equation I-10.

$$J_i = \frac{1}{\left(\frac{1}{R_{i,1}} + \frac{1}{R_{i,2}}\right)} (p_{i,feed} - p_{i,perm}) \quad (I-11)$$

The total gas *i* permeance of the composite membrane could be expressed as Equation I-12.

$$R_{\mathrm{i,total}} = \frac{J_i}{\left(p_{\mathrm{i,feed}} - p_{\mathrm{i,perm}}\right)} = \frac{1}{\left(\frac{1}{R_{\mathrm{i},1}} + \frac{1}{R_{\mathrm{i},2}}\right)} \qquad (\mathrm{I}-12)$$

Replacing $R_{\mathrm{i},1}$ with the gas permeability $P_{\mathrm{i},1}$ and thickness δ_1 of the ion gel layer using Equation I-3, Equation I-13 was obtained.

$$R_{\mathrm{i,total}} = \frac{1}{\left(\frac{\delta_1}{P_{\mathrm{i},1}} + \frac{1}{R_{\mathrm{i},2}}\right)} \qquad (\mathrm{I}-13)$$

Then, if the membrane is used for CO_2/N_2 separation. The CO_2/N_2 permselectivity of the composite membrane (α_{total}) could be calculated as follows.

$$\alpha_{\mathrm{total}} = \frac{R_{\mathrm{CO_2,total}}}{R_{\mathrm{N_2,total}}} = \frac{\left(\frac{\delta_1}{P_{\mathrm{N_2},1}} + \frac{1}{R_{\mathrm{N_2},2}}\right)}{\left(\frac{\delta_1}{P_{\mathrm{CO_2},1}} + \frac{1}{R_{\mathrm{CO_2},2}}\right)} \qquad (\mathrm{I}-14)$$

Therefore, the CO_2 permeance and CO_2/N_2 permselectivity of the composite membrane could be estimated using Equation I-13 and Equation I-14, respectively.

I-8 Purpose of this study

Ion gel membrane is one of the promising forms of high-performance CO_2 separation membrane due to the high CO_2 permeability. To obtain the high separation efficiency of ion gel membranes, the ion gel membrane with high CO_2 permeance should be developed. From Equation I-3, high CO_2 permeability and low thickness of ion gel membranes can lead to high CO_2 permeance. Increasing IL content of ion gel membranes could effectively increase the CO_2 permeability. However, ion gels are generally weak material. It is hard to develop a thin ion gel membrane strong enough to hold a large amount of an IL. Therefore, in this dissertation, targeting on the development of high-performance ion gel membrane for CO_2 separation. Some fundamental investigations on the development of tough and thin ion gel membranes were performed in this dissertation.

I-9 Scope of this thesis

This thesis includes 6 chapters as follows.

Chapter I This chapter introduces the background of the CO_2 separation membranes and the development of ionic liquid-based CO_2 separation membranes. The advantages and challenges of ion gel membranes are introduced. The purpose and scope of this thesis are also given.

Chapter II A micro-double-network (μ-DN) ion gel membrane was fabricated using non-volatile network precursors consisting of a pre-synthesized cross-linkable polymer as the organic part, silica nanoparticles as the inorganic part, and 80 wt% of an IL. To examine the potential of the μ-DN ion gel as a base material for developing CO_2 separation membranes, the mechanical properties and CO_2 separation performance of the μ-DN ion gel membrane were investigated. The effect of the μ-DN structure on the mechanical properties of the μ-DN ion gel membrane was investigated. The CO_2 permeability and CO_2/N_2 permselectivity of the μ-DN ion gel membrane under different temperatures, different trans-membrane pressures, and different operation time were evaluated to confirm the durability and stability of the μ-DN ion gel membrane.

Chapter III In this chapter, a composite membrane with a μ-DN ion gel selective layer was developed. The mechanical properties and surface roughness of the μ-DN ion gel fabricated in an open space were optimized for the preparation of thin μ-DN ion gel layer. The effect of the organic/inorganic network ratios on the CO_2 permeance and CO_2/N_2 permselectivity of the μ-DN ion gel membranes were evaluated. Using the optimized condition, the composite membrane consisting of a thin μ-DN ion gel layer, a porous support membrane and a dense intermediate layer was fabricated by spin coating. The CO_2 permeamce and CO_2/N_2 permselectivity of the composite membrane were evaluated. The long-term stability of the composite membrane for CO_2 separation was confirmed.

Chapter IV A novel tough ion gel with an interpenetrating polymer network (IPN), named IPN ion gel, was developed in this chapter. The IPN structure is composed of semi-crystalline and cross-linkable polymers. The low surface roughness of the IPN ion gel thin layer was confirmed. The polymer network compositions and preparation temperatures of the IPN ion gels were adjusted to optimize their mechanical properties and IL holding properties. Based on the optimized preparation conditions, the IPN ion gels with increasing IL contents were prepared. The CO_2 permeability and CO_2/N_2 permselectivity of IPN ion gel membranes prepared with different polymer network compositions, different preparation temperatures, and different IL contents were measured to investigate the gas separation performance of the IPN ion gel membranes.

Chapter V The composite membrane with thin IPN ion gel layer was prepared in this chapter. The IPN ion gel layer was fabricated on a poly(dimethylsiloxane) (PDMS) gutter layer by the spin coating method. To increase the gas permeance of the composite membrane, the thickness of the IPN ion gel layer was reduced by increasing the dilution degree of the IPN ion gel precursor solution. In addition, the IL content of the IPN ion gel layer was increased to increase the CO_2 permeability of the ion gel layer and thereby improve the CO_2 permeance of the composite membrane. Theoretical estimation of the gas permeation performance was also performed to indicate that the IPN ion gel is a good material as a selective layer of a composite membranes for efficient CO_2 separation.

Chapter VI The conclusions of this thesis are summarized in this chapter.

Chapter II
Development of a tough ion-gel-based CO_2 separation membrane with the micro-double-network formed from non-volatile network precursors

II-1 Introduction

Ion gels are generally weak material. It is hard to develop a thin ion gel membrane strong enough to hold a large amount of an IL. To overcome the weak mechanical strength of ion gels, an inorganic/organic double-network (DN) ion gel was developed by our group and exhibited high mechanical strength [68, 71]. The DN ion gel was prepared using volatile network precursors in a closed space. However, conventional thin-film preparation methods such as dip coating, casting, roll-to-roll, and spin coating are normally performed in an open space. Therefore, it is hard to prepare thin DN ion gel membranes using such thin-film preparation methods.

Recently, an inorganic/organic double-network (DN) tough ion gel was developed by our group, designated as micro-double-network (μ-DN) ion gels [66]. μ-DN ion gel was prepared from non-volatile network precursors using silica nanoparticles and the pre-synthesized cross-linkable polymer poly(dimethylacrylamine-*co*-*N*-succinimidyl acrylate) (poly(DMAAm-*co*-NSA)) as the inorganic network precursor and the organic network precursor, respectively. The μ-DN ion gel provided the possibility of controlling the mechanical properties and CO_2 permeability via the network structure using pre-synthesized network precursors as building blocks. Importantly, the μ-DN ion gel shows a potential to be prepared into a thin film using the conventional thin-film preparation methods performed in an open space. However, before the preparation of thin μ-DN ion gel membrane, the CO_2 separation performance of the μ-DN ion gel should be checked.

In this chapter, the potential of the μ-DN ion gel as a membrane material for CO_2 separation was examined. To optimize the mechanical strength of μ-DN ion gel membranes, the mechanical properties of the μ-DN ion gel were firstly investigated. The effects of the molecular weight (M_n) of

poly(DMAAm-*co*-NSA) and organic/inorganic network compositions on the mechanical properties of the μ-DN ion gel membrane were studied. The CO_2/N_2 separation performance of the μ-DN ion gel membrane under different temperatures and different trans-membrane pressures was evaluated. The long-term gas separation test was performed under the trans-membrane pressure of 600 kPa at 70 °C to confirm the durability and stability of the μ-DN ion gel membrane.

II-2 Experimental Section

II-2-1 Materials

The IL 1-butyl-3-methylimidazolium bis(trifluoromethylsulfonyl)imide ($[C_4mim][Tf_2N]$) was purchased from Sigma-Aldrich Co. and used for the ion gel preparation. The SiO_2 nanoparticles (Aerosil 200; particle diameter of 12 nm) were supplied by Nippon Aerosil Co., Ltd., Japan. *N,N*-dimethylacrylamide (DMAAm), *N*-succinimidyl acrylate (NSA) and diethylene glycol bis(3-aminopropyl)ether (DGBE) were purchased from Tokyo Chemical Industry Co., Ltd., and the polymerization inhibitor in DMAAm was removed by activated alumina before using. 2-(dodecylthiocarbonothioylthio)-2-methylpropionic acid (Sigma-Aldrich Co.) and 2,2'-azobis(2,4-dimethylvaleronitrile) (ADVN) (FUJIFILM Wako Pure Chemical Co., Japan) were the chain transfer agent (CTA) and initiator for the polymerization, respectively. Tetrahydrofuran (THF), super dehydrated 1,4-dioxane, ethanol, dimethyl sulfoxide-d_6 (d_6DMSO), n-hexane and maleic acid were purchased from FUJIFILM Wako Pure Chemical Co.. DMAAm, tetraethyl orthosilicate (TEOS) (Sigma-Aldrich Co.) and formic acid (FUJIFILM Wako Pure Chemical Co.) were used to fabricate the DN ion gel membrane.

II-2-2 Synthesis and characterization of poly(DMAAm-*co*-NSA)

Poly(DMAAm-*co*-NSA), a cross-linkable polymer with different molecular weights (M_n) and different NSA molar ratios, was synthesized by the reversible addition-fragmentation chain-transfer (RAFT) polymerization, in which the NSA is the cross-linking point for crosslinkers. Here, we controlled the molecular weight of the polymer by changing the amount of ADVN and CTA used in the polymerization reaction. First, a sealed three-necked flask was purged with N_2 for 10 min five times. Then, a certain amount of ADVN (0.032, 0.016, 0.012, 0.0080, 0.0053, 0.0040 mmol) was dissolved in 20.0 g of 1,4-dioxane. The solution was injected into a three-necked flask using a syringe. In another

vessel, a mixture of 100 mmol DMAAm, 5.30 mmol NSA, and a certain amount of CTA (0.32, 0.16, 0.12, 0.080, 0.053, 0.040 mmol) was prepared. The mixture was injected into a three-necked flask using a syringe. The obtained solution was purged with N_2 bubbling for 30 min under magnetic stirring. Subsequently, the three-necked flask with the solution was heated in an oil bath at 333 K and continuously agitated by magnetic stirring for 24 h. The reaction product was dissolved in 100 g of THF and transferred into a 200 mL eggplant flask for evaporation at 333 K for 2 h. The white precipitate was purified 2 times by reprecipitation using THF and hexane as the good and poor solvents, respectively. After drying for 24 h at 373 K in a vacuum oven, the synthesized cross-linkable copolymer was obtained. Poly(DMAAm-*co*-NSA) samples with different NSA molar ratios were synthesized by controlling the NSA/DMAAm molar ratios. The purities of all the polymer samples were determined by ^{1}H NMR measurements (ECZ-400S, JEOL) [66]. The purity results are presented in Table II-1.

The synthesized poly(DMAAm-*co*-NSA) (20 mg) was dissolved in 5 mL THF to prepare the sample for SEC (GPCmax, TDA305, Malvern Panalytical Ltd.) measurement. The measurement was carried out at 313 K with a mobile phase flow rate of 1.0 mL/min. A refractometer (Abbemat-550, Anton Paar) was used to determine the refractive index increment (d*n*/d*c*) of the sample under a wavelength of 598 nm at 313 K. The obtained molecular weights of poly(DMAAm-*co*-NSA) are shown in Table II-1. The NSA molar ratio in poly(DMAAm-*co*-NSA) was determined using a method described in the literature [66]. The determined NSA ratios for each polymer are also shown in Table II-1.

Table II-1. Characterization results of poly(DMAAm-*co*-NSA)

	Molar ratio of NSA (mol%)	Purity (wt%)	Molecular weight (kg/mol)		
			M_n	M_w	M_w/M_n
Sample 1	4.99	95.3	32	41	1.3
Sample 2	4.76	94.9	54	71	1.3
Sample 3	4.31	98.2	65	93	1.4
Sample 4	4.99	97.9	92	133	1.5
Sample 5	5.21	95.2	116	185	1.6
Sample 6	5.08	93.5	126	248	2.0
Sample 7	3.84	95.5	102	131	1.3
Sample 8	2.91	95.4	121	186	1.5
Sample 9	2.08	95.5	140	239	1.5
Sample 10	1.18	97.1	127	220	1.7

II-2-3 Fabrication of μ-DN and single network (SN) ion gel membranes using non-volatile network precursors

In this study, we prepared a series of μ-DN ion gel membranes using poly(DMAAm-*co*-NSA) with different M_n and with different organic/inorganic network compositions. The μ-DN ion gel membranes were also fabricated using poly(DMAAm-*co*-NSA) with different NSA molar ratios to endow the micro-double-network with different cross-linking degrees. The IL content of the μ-DN ion gels was adjusted to be 80 wt%. In addition, single-network (SN) ion gels containing 80 wt% IL were fabricated by crosslinked poly(DMAAm-*co*-NSA) network without silica nanoparticles.

The μ-DN and SN ion gel membranes were prepared using the following three solutions. The first one was the IL/ethanol solution with silica nanoparticles (μ-DN ion gel) or without silica nanoparticles (SN ion gel). In 3.2 g of ethanol, 5.12 g of [C_4mim][Tf_2N] was dissolved, and then a certain amount of Aerosil 200 was suspended by vortex mixing for 1 min followed by ultrasonication for 20 min. The second solution was a polymer solution, which was prepared by dissolving a certain amount of poly(DMAAm-*co*-NSA) in 3.84 g of ethanol by magnetic stirring for 30 min. The third solution was a cross-linker solution. A certain amount of the cross-linker was dissolved in 3.2 g of ethanol by magnetic stirring for 30 min.

To prepare the precursor solutions of the ion gels, first, the cross-linker solution was added to the [C_4mim][Tf_2N]/ethanol solution and mixed up by vortex for 1min and ultrasonication for 3 min. The mixture was added to a poly(DMAAm-*co*-NSA) solution under agitation for 1 min. The prepared precursor solution was poured into a closed mold. The mold containing the precursor solution was put in an oven at 333 K for 24 h. After 24 h, the ion gel was obtained and was dried at 333 K for 24 h. More detailed preparation conditions are provided in Table II-2.

Table II-2. Preparation conditions of μ-DN and SN ion gel membranes.

(a) μ-DN ion gel membranes fabricated with cross-linkable poly(DMAAm-*co*-NSA) with different molecular weights

	Sample 1	Sample 2	Sample 3	Sample 4	Sample 5	Sample 6
[C_4mim][Tf_2N] (g)	5.12	5.12	5.12	5.12	5.12	5.12
Aerosil 200 (g)	0.32	0.32	0.32	0.32	0.32	0.32
Organic network (g)	0.96	0.96	0.96	0.96	0.96	0.96
Poly(DMAAm-*co*-NSA) (g)	0.91	0.91	0.92	0.91	0.91	0.91
M_n (kg/mol)	32	54	65	92	116	126
NSA ratio (mol%)	4.99	4.76	4.31	4.99	5.21	5.08
Cross-linker; DGBE (g)	0.049	0.046	0.042	0.049	0.050	0.050
Ethanol (g)	10.24	10.24	10.24	10.24	10.24	10.24

(b) μ-DN ion gel membranes fabricated with different organic/inorganic network precursor weight ratios

	Sample 1	Sample 2	Sample 3	Sample 4	Sample 5	Sample 6
Organic/inorganic ratios	1.0	1.5	2.0	3.0	5.0	7.0
[C_4mim][Tf_2N] (g)	5.12	5.12	5.12	5.12	5.12	5.12
Aerosil 200 (g)	0.64	0.51	0.43	0.32	0.21	0.16
Organic network (g)	0.64	0.77	0.85	0.96	1.07	1.12
Poly(DMAAm-*co*-NSA) (g)	0.61	0.73	0.81	0.91	1.01	1.06
M_n (kg/mol)	126	126	126	126	126	126
NSA ratio (mol%)	5.08	5.08	5.08	5.08	5.08	5.08
Cross-linker; DGBE (g)	0.033	0.037	0.044	0.050	0.055	0.058
Ethanol (g)	10.24	10.24	10.24	10.24	10.24	10.24

(c) SN ion gel membranes fabricated with cross-linkable poly(DMAAm-*co*-NSA) with different molecular weights

	Sample 1	Sample 2	Sample 3	Sample 4	Sample 5
[C_4mim][Tf_2N] (g)	5.12	5.12	5.12	5.12	5.12
Aerosil 200 (g)	0	0	0	0	0
Organic network (g)	1.28	1.28	1.28	1.28	1.28
Poly(DMAAm-*co*-NSA) (g)	1.22	1.22	1.22	1.22	1.21
M_n (kg/mol)	54	65	92	116	126
NSA ratio (mol%)	4.76	4.31	4.99	5.21	5.08
Cross-linker; DGBE (g)	0.062	0.057	0.065	0.068	0.050
Ethanol (g)	10.24	10.24	10.24	10.24	10.24

(d) μ-DN ion gel membranes fabricated with cross-linkable poly(DMAAm-*co*-NSA) with different NSA molar ratios.

	Sample 1	Sample 2	Sample 3	Sample 4	Sample 5
[Bmim][Tf_2N] (g)	5.12	5.12	5.12	5.12	5.12
Aerosil 200 (g)	0.425	0.425	0.425	0.425	0.425
Organic network (g)	0.85	0.85	0.85	0.85	0.85
Poly(DMAAm-co-NSA) (g)	0.84	0.83	0.82	0.82	0.81
M_n (kg/mol)	127	140	121	102	126
NSA ratio (mol%)	1.18	2.08	2.91	3.84	5.08
Cross-linker; DGBE (g)	0.011	0.019	0.026	0.034	0.044
Ethanol (g)	10.24	10.24	10.24	10.24	10.24

II-2-4 Fabrication of DN ion gel membranes using volatile network precursors

To compare the CO_2 permeabilities between ion gel membranes fabricated using non-volatile and volatile inorganic/organic network precursors, the DN ion gel membrane was prepared using DMAAm and TEOS as the volatile network precursors. The DN ion gel membranes were prepared according to the one-pot/two-step method described in our previous work [68, 71]. Herein, the TEOS/DMAAm ratio and the IL content of the DN ion gel were fixed at 0.35 mol/mol and 80 wt%, respectively.

II-2-5 Fabrication of supported ionic liquid membrane

A hydrophilic PTFE membrane (Toyo Roshi Kaisha, Ltd. (Japan)) with pore size of 0.1 μm and thickness of 30 μm was immersed in [C_4mim][Tf_2N] for 1 h. Then, the obtained membrane was taken out of the IL, and the excess IL on the membrane surface was wiped off.

II-2-6 Mechanical property test of the ion gel membranes

The mechanical properties of the fabricated ion gels were measured by a universal testing instrument (EZ-LX, Shimadzu Co., Japan) at ambient temperature (~ 298 K). The sample was made into a dumbbell-shaped specimen with a length of 17.0 mm and a width of 2.0 mm. The thickness of each ion gel membrane was determined from the average of at least 10 different spots by a micrometer (IP65, Mitsutoyo Co., Japan). The sample was uniaxially stretched at a fixed strain rate of 100 mm/min. The measurements were taken at least three times.

The cyclic stretching test was conducted to investigate the hysteresis and energy dissipation of the samples. The cyclic stretching operations are performed by gradually increasing the tensile strain in steps of 0.5 until the ion gel was broken.

II-2-7 Swelling ratio measurements

The cross-linkage degree of the ion gel membranes was characterized by their swelling ratio in pure water. The experimental procedures for the swelling ratio measurement are as follows:

Approximately 0.1 g of the ion gel was placed in a vial with a lid. Ethanol (40 g) was added to the vial and shaken at room temperature for 1 day to extract the IL from the ion gel. Ethanol was then removed from the vial, and Milli-Q water (40 g) was added. The mixture was shaken at room temperature for 24 h to form a hydrogel. The weight of the hydrogels formed from the SN ion gel (W_{h1}) and the μ-DN ion gel (W_{h2}) were measured after gently wiping away the excess water on the surface. The hydrogels were dried in an oven, first at 80 °C for 3 h, and then at 100 °C under vacuum for 1 h. The weight of the dried hydrogel network skeletons formed from the SN ion gel (W_{d1}) and the μ-DN ion gel (W_{d2}) were measured after cooling at room temperature for more than 30 min. The swelling ratios of the SN ion gel (Q_{SN}) and μ-DN ion gel ($Q_{(\mu\text{-DN})}$) were calculated using Equations II-1 and II-2, respectively. W_{water} in the equations is the weight of the Milli-Q water in the hydrogel and $W_{polymer}$ is the weight of the organic network in the hydrogel. $C_{organic}$ in Equations II-1 and II-2 implies the organic network weight ratio in the organic/inorganic network skeleton of the μ-DN ion gel.

$$Q_{SN}\ (\mathrm{g/g}) = \frac{W_{water}}{W_{polymer}} = \frac{W_{h1} - W_{d1}}{W_{d1}} \qquad (\mathrm{II}-1)$$

$$Q_{(\mu-DN)}\ (\mathrm{g/g}) = \frac{W_{water}}{W_{polymer}} = \frac{W_{h2} - W_{d2}}{C_{organic} * W_{d2}} \qquad (\mathrm{II}-2)$$

II-2-8 Evaluation of CO_2 permeation performance of the ion gel membranes

The sweep method was taken to evaluate the gas separation performance of the ion gel membranes [71]. A schematic illustration of the gas permeation apparatus used in this experiment is shown in Figure II-1. The effective permeation surface area of the permeation cell is 12.5 cm^2. A thermostat oven (Yamato Scientific Co., Japan) is used to control the temperature of the gas permeation process. The feed gas consists of 50 vol% CO_2 and 50 vol% N_2. The flow rates of CO_2 and N_2 were 100 mL/min. The total pressure on the feed side can be adjusted from 100 kPa to 700 kPa by controlling a backpressure valve. Pure helium was used as the sweep gas. The flow rate and pressure of the sweep gas were 40 mL/min and the atmospheric pressure, respectively. The mass flow controllers (Hemmi

Slide Rule Co., Ltd., Japan) were used to control the flow rates of all gases. A gas chromatograph (GC-8A, Shimadzu Co.) was used to measure the composition of the sweep gases containing the permeated gases from the membrane. The attainment of the steady state was confirmed by having less than 1% of the peak area difference between adjacent measurements.

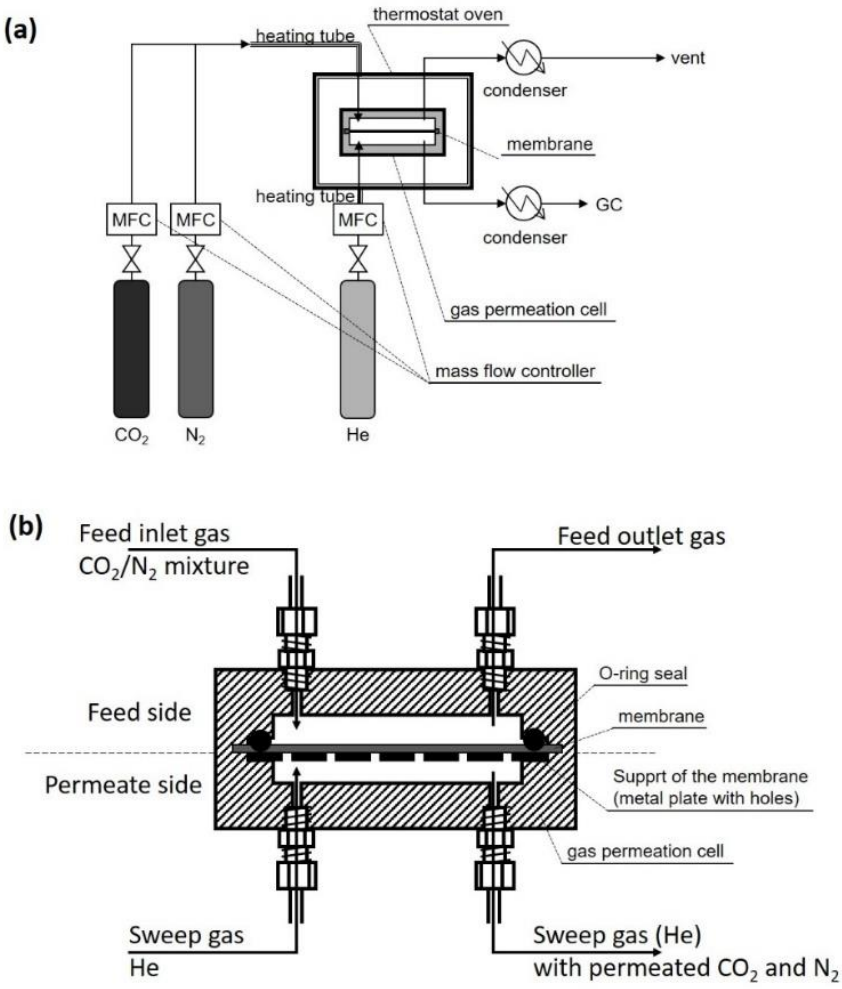

Figure II-1. Schematic illustrations of (a) the gas permeation measurement apparatus and (b) the membrane cell used in this study [71].

II-3 Results and discussion

II-3-1 Optimization of the mechanical properties of the μ-DN ion gel membranes prepared using non-volatile network precursors

The μ-DN ion gel membranes consists of brittle silica nanoparticle clusters as the first network and a loosely cross-linked polymer network as the second network [66]. The mechanical strength of the

classic DN ion gel membranes prepared from volatile network precursors were reported to be dependent on the molecular weight of the polymer network. That means a higher molecular weight of the polymer network tended to yield higher mechanical strength [71]. In this study, the pre-synthesized polymer was used as the organic network precursor to prepare the μ-DN ion gel membranes, hence, the molecular weight of the polymer network can be easily controlled. Therefore, we investigated the mechanical properties of the μ-DN ion gel membranes and the corresponding SN ion gel membranes as a function of the M_n values of the cross-linkable poly(DMAAm-*co*-NSA). The results of the uniaxial tensile tests of the μ-DN and SN ion gel membranes are presented in Figure II-2, indicating that the mechanical strength of the μ-DN ion gel membranes is significantly affected by the M_n of the cross-linkable polymers.

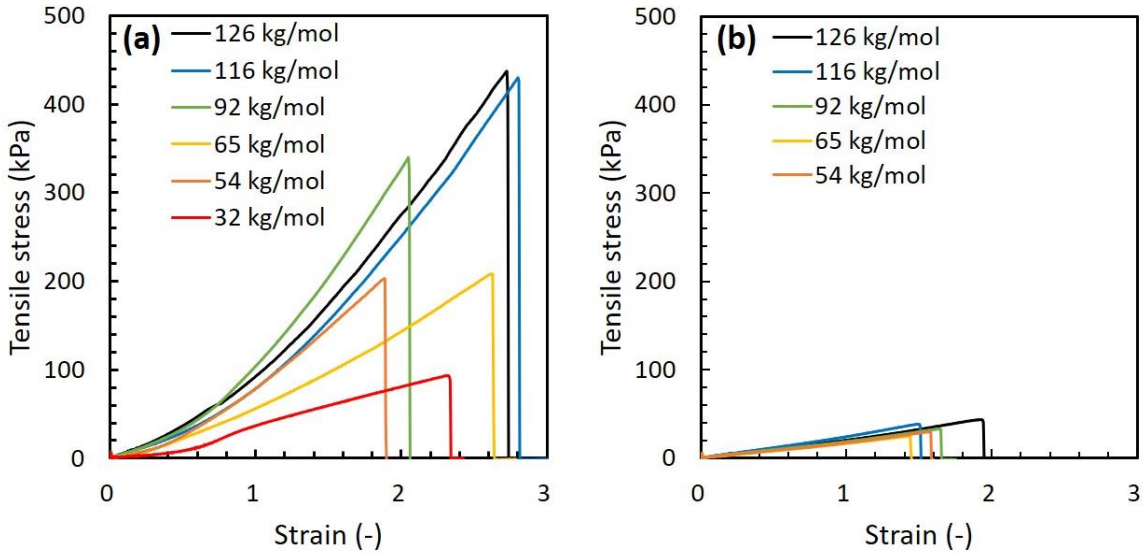

Figure II-2. Uniaxial tensile stress-strain curves of the (a) μ-DN and (b) SN ion gel membranes prepared by poly(DMAAm-*co*-NSA) with different M_n. The μ-DN ion gel membranes were prepared using the precursor solution with organic/inorganic network precursor ratio of 3 g/g.

The specific mechanical properties of the ion gel membranes were determined from the uniaxial stress-strain curves in Figure II-2, and the results are presented in Figure II-3. When the M_n of the poly(DMAAm-*co*-NSA) increased, the Young's modulus, fracture stress, and fracture energy of the SN ion gel membranes only slightly increased. However, the mechanical properties of the μ-DN ion gel membranes are largely depended on the M_n of the cross-linkable polymer. This could be due to the

contribution of the inorganic network in the μ-DN ion gel membranes. A further explanation is that the silica nanoparticle clusters could entangle with the polymer network and sustain the load applied to the μ-DN ion gel membrane. The detailed mechanism would be introduced in the following content.

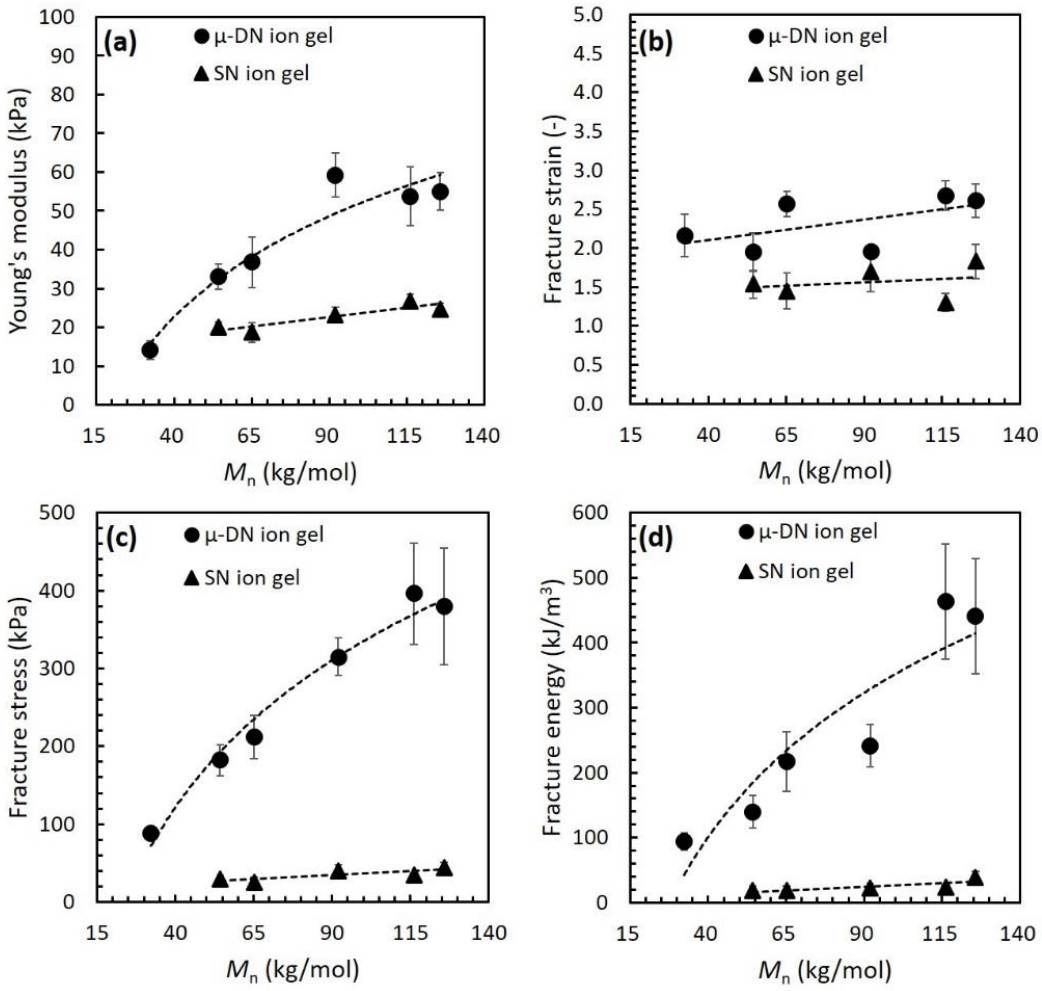

Figure II-3. (a) Young's modulus (b) fracture strain (c) fracture stress (d) fracture energy of the μ-DN and SN ion gel membranes prepared by poly(DMAAm-*co*-NSA) with different M_n. The μ-DN ion gel membranes were prepared using the precursor solution with organic/inorganic network precursor ratio of 3 g/g.

The cyclic tensile stress-strain curves were used to investigate how the inorganic network contributes to the mechanical strength of the μ-DN ion gel membranes [66-68]. The resulting cyclic tensile stress-strain curves for the μ-DN and SN ion gel membranes are presented in Figure II-4 and II-5, respectively. Typical examples are shown in Figure II-6(a). As shown in these figures, clear

hysteresis could be found for the μ-DN ion gel membranes. However, no hysteresis was observed for the SN ion gel membranes. The hysteresis indicates an energy dissipation of the μ-DN ion gel membranes by the internal rupture of the inorganic network during the stretching process. Therefore, it can be said that the inorganic network acted as a sacrificial bond to dissipate the load energy applied to the μ-DN ion gel membranes.

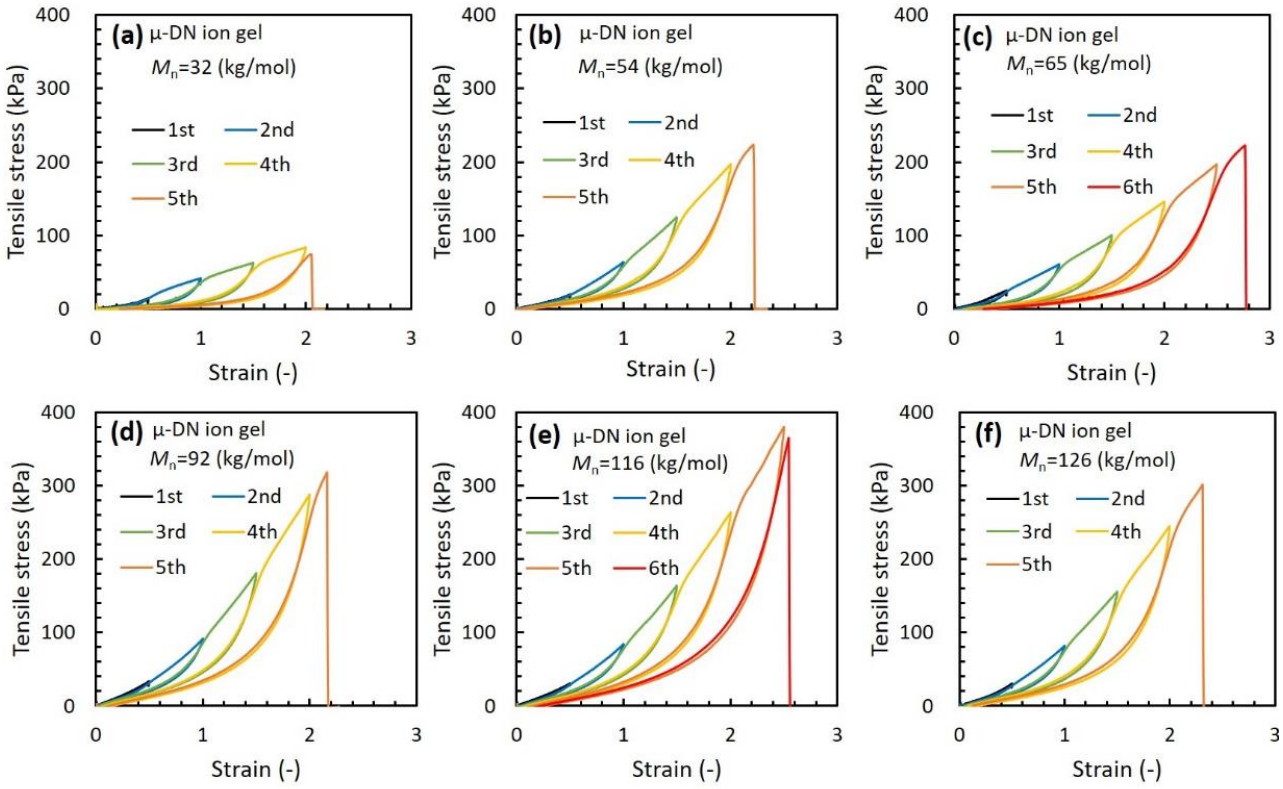

Figure II-4. Cyclic stress–strain curves of the μ-DN ion gel membranes prepared using poly(DMAAm-*co*-NSA) with different M_n. The ion gel membranes were prepared using the precursor solution with organic/inorganic network precursor ratio of 3 g/g.

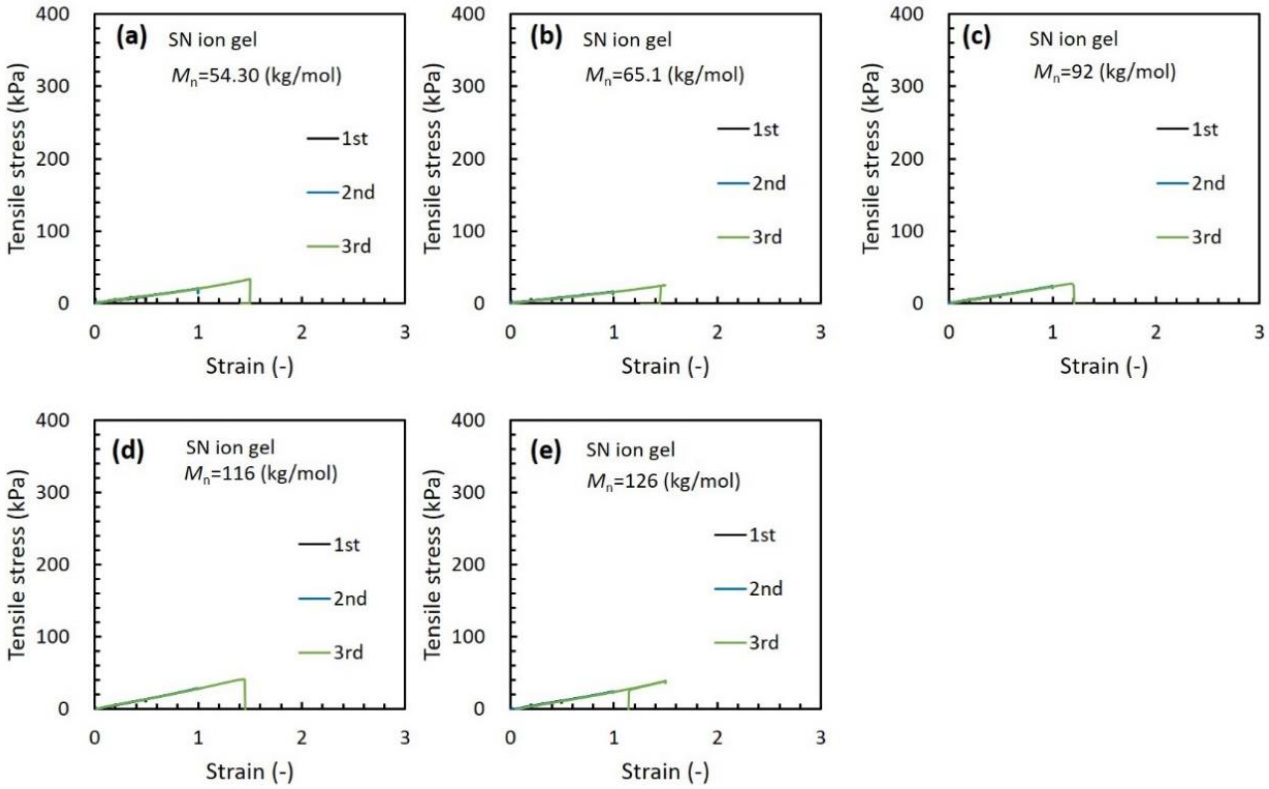

Figure II-5. Cyclic stress–strain curves of the SN ion gel membranes prepared using poly(DMAAm-*co*-NSA) with different M_n.

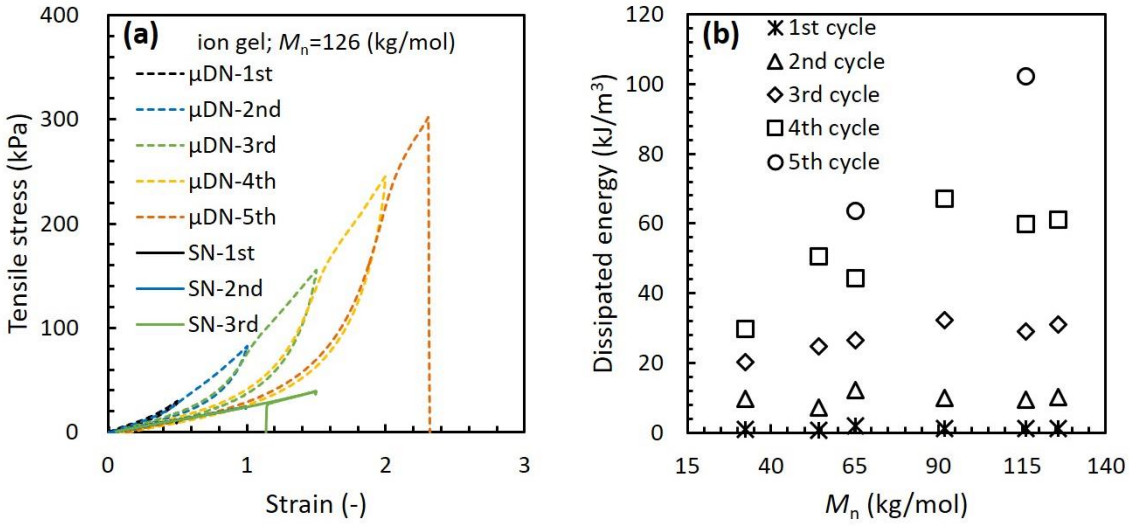

Figure II-6. (a) Cyclic tensile stress-strain curves of the μ-DN ion gel membrane and SN ion gel membrane fabricated using poly(DMAAm-*co*-NSA) with M_n of 126 kg/mol, and (b) the dissipated energy of the μ-DN ion gel membranes fabricated by poly(DMAAm-*co*-NSA) with different M_n. The μ-DN ion gel membranes were fabricated using the precursor solution with organic/inorganic network precursor ratio of 3 g/g.

To further investigate how the inorganic part contributed to toughening the μ-DN ion gel membrane fabricated by cross-linkable polymers with different M_n, the cross-linking degree of the μ-DN network formed in the μ-DN ion gel and the organic network formed in the SN ion gel were compared. The cross-linking degree of the networks can be evaluated by the swelling ratio of the cross-linking network skeleton in pure water, that is, a higher swelling ratio indicates a lower cross-linking degree. Therefore, the cross-linking structures of the network formed in the μ-DN and SN ion gel membranes were evaluated from the swelling ratios of the network skeletons of the μ-DN and SN ion gel membranes in pure water. As shown in Figure II-7, both the swelling ratios of the μ-DN and SN ion gel membranes decreased slightly with the increasing molecular weight of the poly(DMAAm-*co*-NSA). This implies that the poly(DMAAm-*co*-NSA) with a higher M_n tends to form a polymer network with a higher crosslinking degree. When the crosslinking degree of the polymer network increases, many inorganic clusters get caught by the highly cross-linked polymer network. Therefore, the inorganic cluster formed in the highly cross-linked polymer network could better sustain the applied load during the stretching process. As a result, the Young's modulus and fracture stress of the μ-DN ion gel membranes increased dramatically as the molecular weight of the cross-linkable polymer increased, whereas those of the SN ion gel hardly increased (Figure II-3 (a) and (c)).

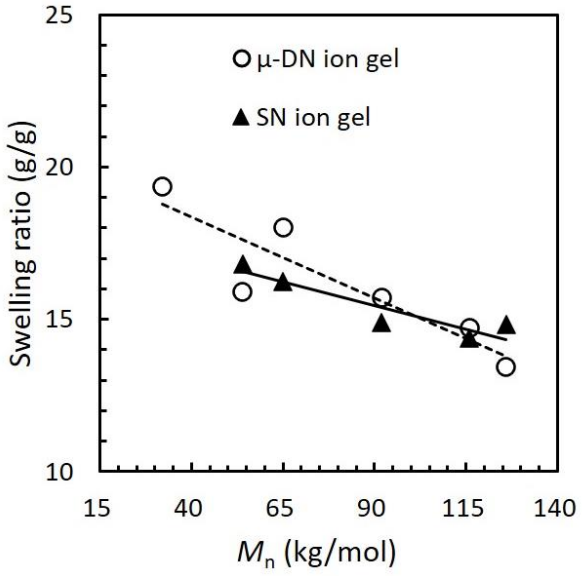

Figure II-7. Swelling ratios of the network skeletons of the μ-DN and SN ion gel membranes in pure water. Effect of molecular weight of poly(DMAAm-*co*-NSA). The μ-DN ion gel membranes were prepared with organic/inorganic network precursor ratio of 3 g/g.

The fracture strains of the ion gels can hardly be changed by changing the M_n of poly(DMAAm-*co*-NSA), as shown in Figure 2(b). The fracture strains of the SN ion gel membranes were lower than those of the μ-DN ion gel membranes. This might be due to the multifunctional cross-linking effect of the inorganic part. The silica nanoparticle clusters could entangle with the cross-linkable polymer and acted as multifunctional cross-linkers, resulting in a higher fracture strain (Figure II-3(b)) [66]. That indicates the inorganic network has a positive effect not only on the Young's modulus and fracture stress but also on the fracture strain.

The origin of energy dissipation of the μ-DN ion gel during the tensile test was the destruction of inorganic networks; however, the polymer networks had a significant influence on the amount of dissipated energy as well. Figure II-6(b) shows the dissipated energy of the μ-DN ion gel membranes at each elongation cycle. In particular, the dissipated energy increases significantly with increasing M_n of poly(DMAAm-*co*-NSA) in larger stretching cycles. This reveals that the poly(DMAAm-*co*-NSA) with higher M_n could rupture larger numbers of silica nanoparticle network clusters under a highly stretched state because the cross-linking degree could be increased with increasing molecular weight. Therefore, the fracture energy of the μ-DN ion gel membranes was improved by increasing the M_n of poly(DMAAm-*co*-NSA).

The results above indicate that the high toughness of the μ-DN ion gel prepared with the cross-linkable polymer having a high M_n is due to the large contribution of the inorganic network. In the μ-DN ion gel, the polymer network acted as the hidden length to sustain large deformations and triggered the destruction of the inorganic network cluster. Therefore, it can be expected that the mechanical properties of the μ-DN ion gel membranes can be further improved by optimizing the organic/inorganic network composition of the μ-DN ion gel membrane fabricated using poly(DMAAm-*co*-NSA) with a high M_n.

Subsequently, the organic/inorganic network ratio was investigated to optimize the mechanical properties of the μ-DN ion gel membranes. In this investigation, for the preparation of the μ-DN ion gel membranes, the M_n of poly(DMAAm-*co*-NSA) was fixed at 126 kg/mol. The μ-DN ion gel membranes with different organic/inorganic network ratios were fabricated, the uniaxial tensile stress-strain curves of the fabricated ion gel membranes are presented in Figure II-8. The cyclic tensile stress-strain curves of the μ-DN ion gel membranes were measured and presented in Figure II-9. A larger

hysteresis circle was obtained when the inorganic network content of the ion gel membranes is higher, indicating the positive effect of the inorganic network on strengthening the prepared μ-DN ion gel membranes by energy dissipation. The mechanical properties of the μ-DN ion gel membranes determined from the uniaxial stretching tests are shown in Figure II-10. As expected, the mechanical strength strongly depended on the ratio of organic/inorganic networks.

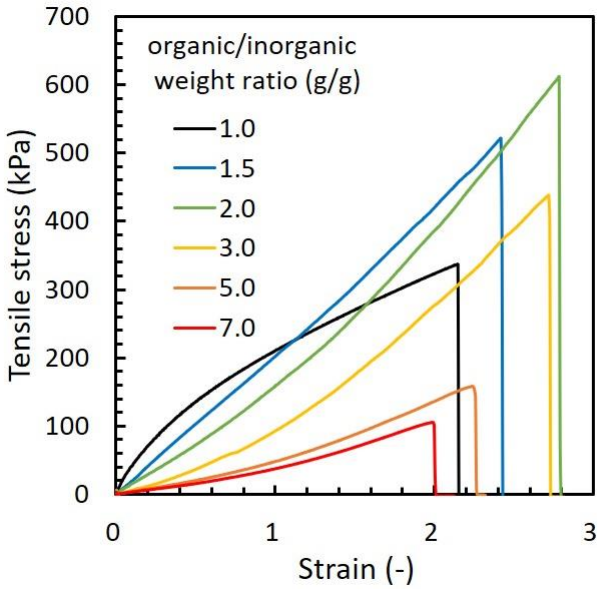

Figure II-8. Uniaxial tensile stress-strain curves of the μ-DN ion gel membranes prepared with different organic/inorganic network precursor ratios. The ion gel membranes were fabricated using poly(DMAAm-*co*-NSA) with M_n = 126 kg/mol.

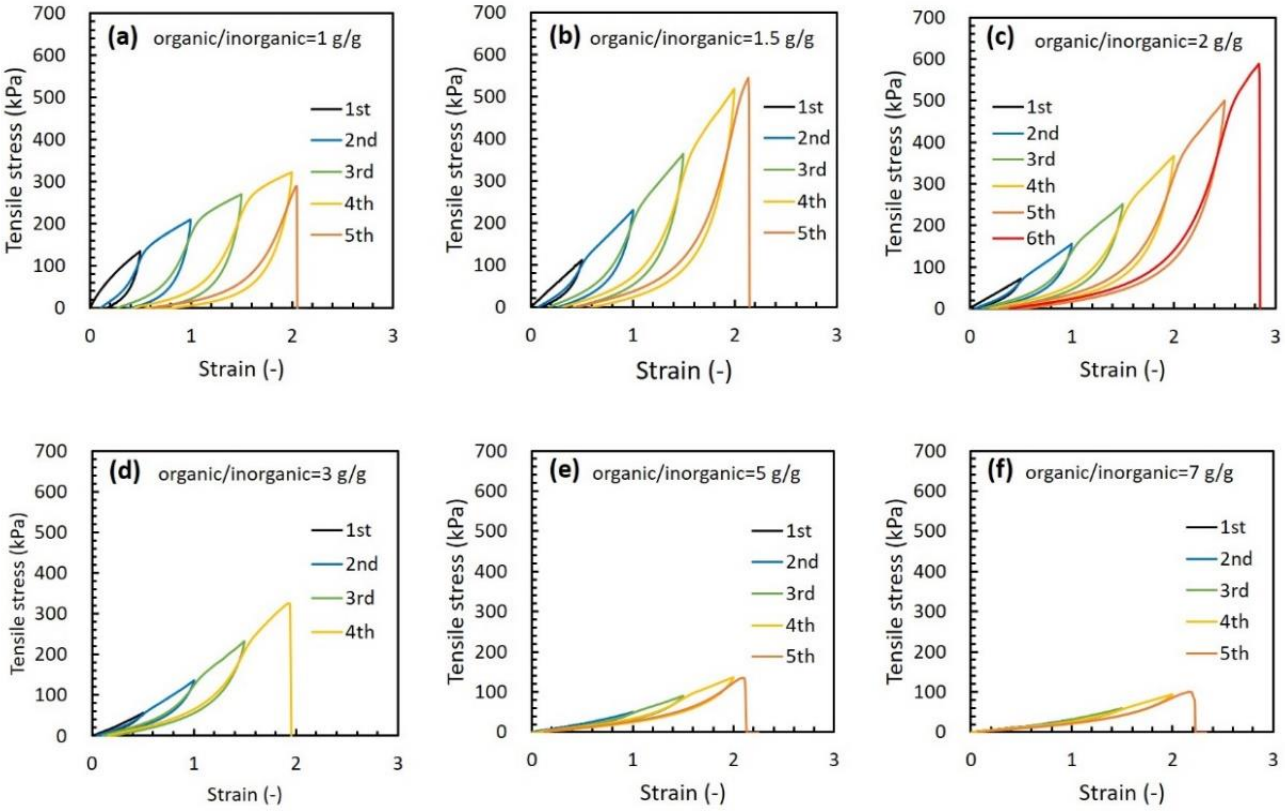

Figure II-9. Cyclic stress–strain curves of the μ-DN ion gel membranes prepared with different organic/inorganic network precursor ratios (a-f; organic/inorganic = 1, 1.5, 2, 3, 5 and 7 g/g). The ion gel membranes were all prepared in a closed mold by poly(DMAAm-*co*-NSA) with M_n=126 kg/mol.

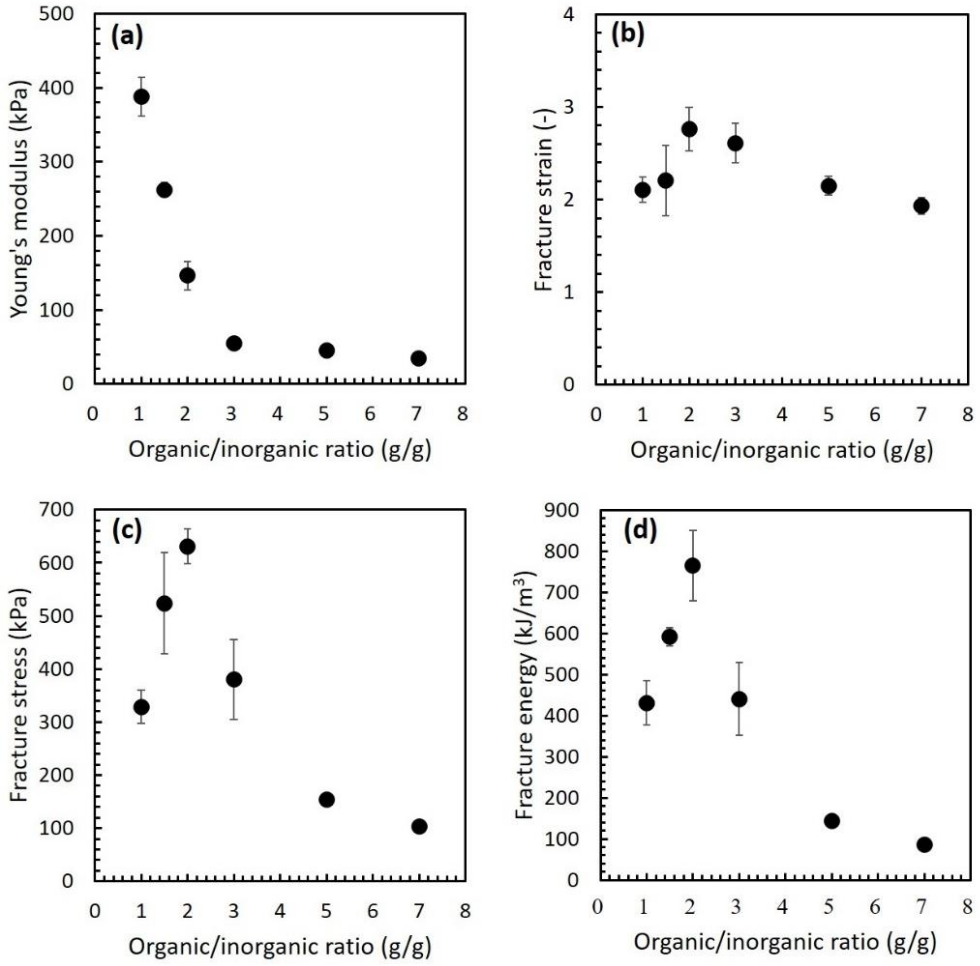

Figure II-10. Mechanical properties of the μ-DN ion gel membranes as a function of the organic/inorganic network precursor ratios, (a) Young's modulus (b) fracture strain (c) fracture stress and (d) fracture energy. The ion gel membranes were fabricated using poly(DMAAm-*co*-NSA) with M_n = 126 kg/mol.

As shown in Figure II-10(a), the Young's modulus monotonically increases with the decreasing organic/inorganic network ratios. This is because the inorganic network sustained most of the load applied to the μ-DN ion gel membrane. On the other hand, as indicated in Figures II-10 (b), (c), and (d), the fracture strain, fracture stress, and fracture energy show the maximum value at an organic/inorganic network ratio of 2 g/g. As for the fracture strain and fracture stress, because the content of silica nanoparticles decreased with an increase in the organic/inorganic network ratio, the multi-functional cross-linking effect of the inorganic network also decreased. This is the reason for the decrease in the fracture strain and fracture stress from the network ratio of 2 g/g to 7 g/g. In contrast,

at a low organic/inorganic network ratio (less than 2 g/g), the fracture strain and fracture stress tend to decrease. This is because when the organic/inorganic network ratio is less than 2 g/g, the amount of the organic network in the μ-DN ion gel is small. The organic network acted as a hidden length to sustain a large deformation, the μ-DN ion gel could not sustain a high load when the polymer network content was very low. As a result, the fracture strain and fracture stress showed maximum values at an organic/inorganic network ratio of 2 g/g. Because of the maximum fracture strain and stress, the dissipated energy and fracture energy of the μ-DN ion gel membranes also reached a maximum at 2 g/g organic/inorganic network ratio. Therefore, it can be concluded that 2 g/g organic/inorganic network ratio using a high-molecular-weight organic network is the optimal condition for strengthening the μ-DN ion gel membranes.

II-3-2 CO_2/N_2 permeability of the ion gel membranes prepared using non-volatile network precursors

The inorganic/organic DN ion gel membrane prepared using volatile network precursors had high CO_2 permeability due to the low network content [71]. It is expected that the μ-DN ion gel membrane prepared using non-volatile network precursors could also have high CO_2 permeability. The CO_2 separation performance and separation stability of the μ-DN ion gel membrane prepared using non-volatile network precursors were investigated in this section. The μ-DN ion gel membrane used for the gas separation test was fabricated under the optimized conditions obtained in the former section, and the gas separation test results are presented in Figure II-11.

First, the durability of the μ-DN ion gel membrane for CO_2 separation was evaluated by increasing the trans-membrane pressure differences. As shown in Figure II-11(a), the CO_2 separation performance of the μ-DN ion gel membrane did not depend on the trans-membrane pressure difference. Even under a transmembrane pressure difference of 600 kPa, the CO_2/N_2 selectivity was maintained the same as that measured under the trans-membrane pressure difference of 0 kPa. Additionally, the CO_2 separation performance of the μ-DN ion gel membrane showed good reversibility when the trans-membrane pressure decreases from 600 kPa to 0 kPa as shown in Figure II-12(a).

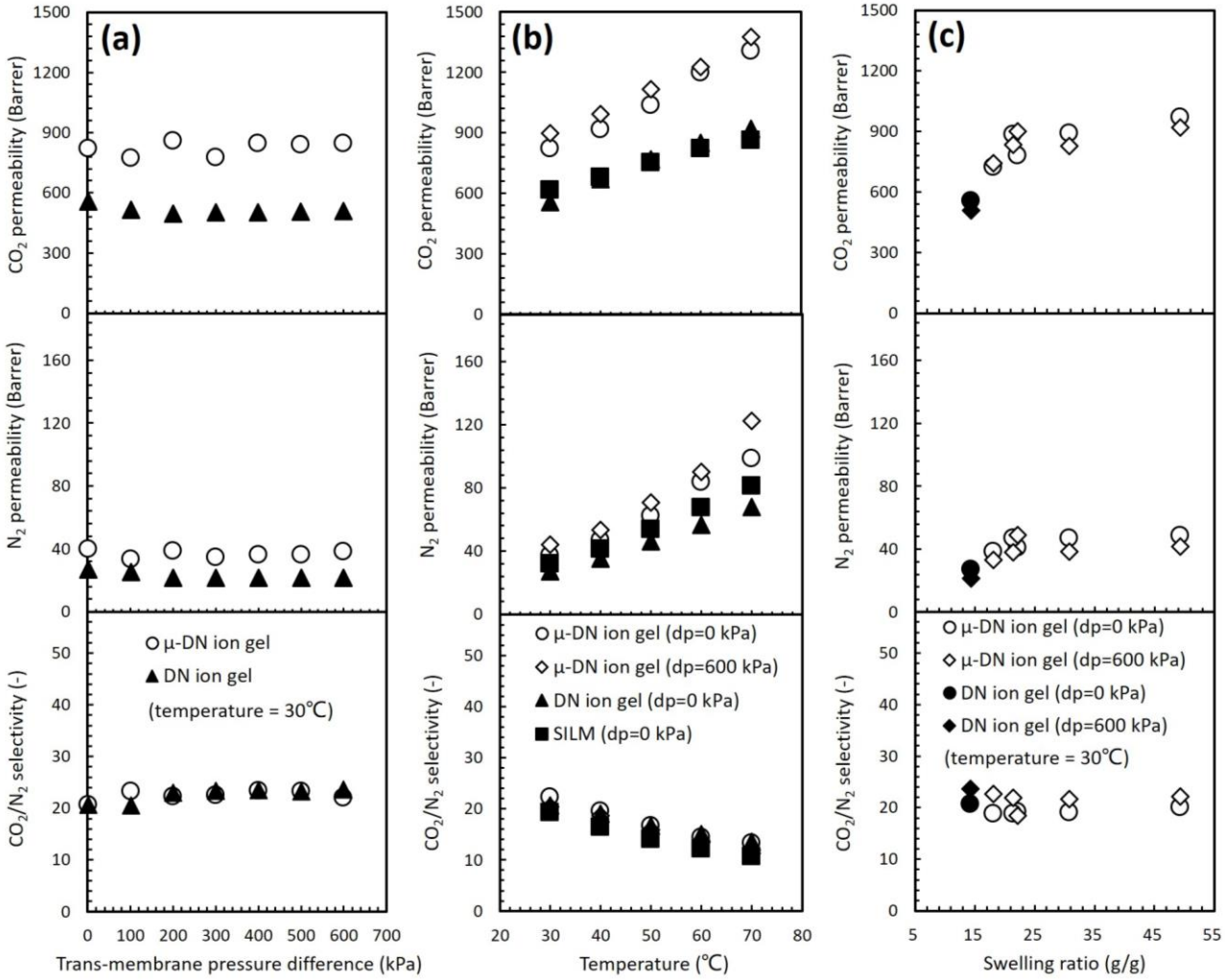

Figure II-11. Effects of (a) trans-membrane pressure differences, (b) temperatures, and (c) swelling ratios on the CO_2/N_2 separation performance of ion gel membranes and the SILM. The μ-DN ion gel membrane was prepared under the optimized condition of the organic/inorganic network precursor ratio of 2 g/g using poly(DMAAm-*co*-NSA) with M_n of 126 kg/mol. The DN ion gel membrane was fabricated from the precursor solution with the optimized TEOS/DMAAm ratio of 0.35 mol/mol [71]. The IL content in the μ-DN and DN ion gel membrane was the same (80 wt%). The SILM was formed by the same IL ([C_4mim][Tf_2N]). "dp" in the plots represents trans-membrane pressure difference. The gas permeation was measured with 50 vol%/50 vol% of CO_2/N_2 and the permeate side was under atmospheric pressure.

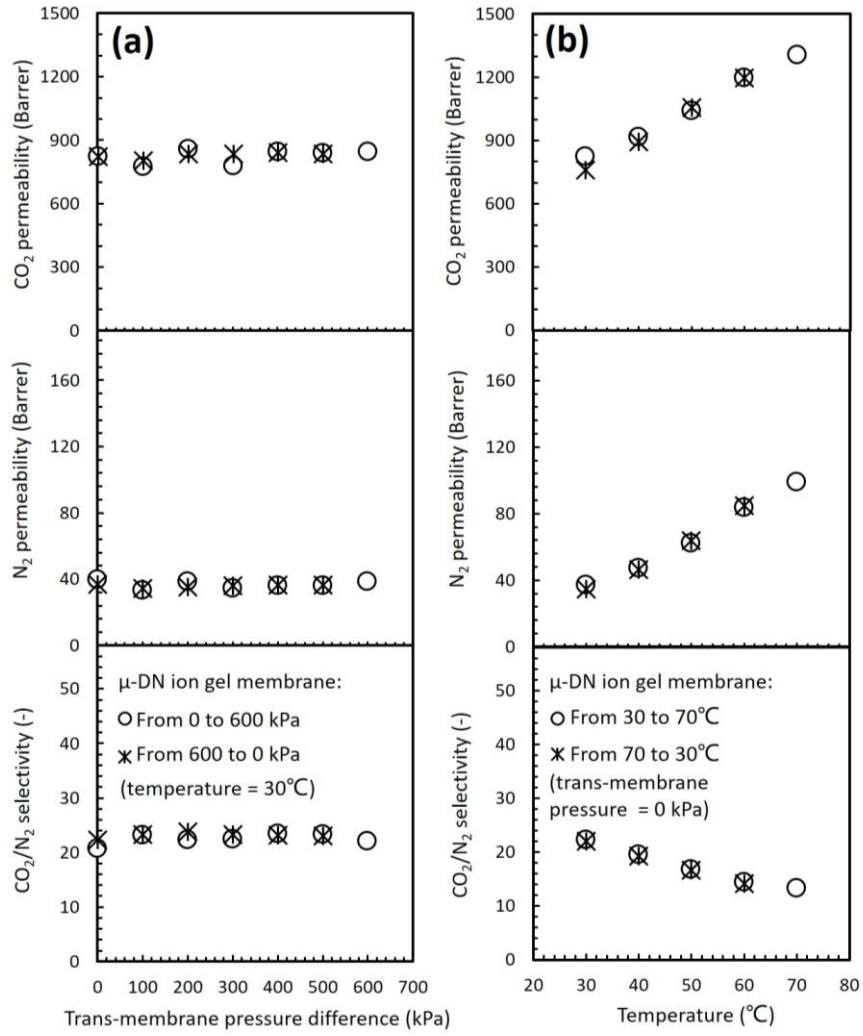

Figure II-12. Reversibility of the CO_2/N_2 separation performance of the μ-DN ion gel membrane under different (a) transmembrane pressure differences, (b) temperatures. The μ-DN ion gel membrane was prepared under the optimized condition of the organic/inorganic network precursor ratio of 2 g/g using the cross-linkable polymer with M_n of 126 kg/mol. The gas permeation was measured with 50 vol%/50 vol% of CO_2/N_2 and the permeate side pressure was maintained at atmospheric pressure.

The long-term stability of the membrane separation was also performed to evaluate the high mechanical strength and good IL holding property of the μ-DN ion gel membrane. The result is presented in Figure II-13(a). The test was performed at 30 °C under a pressure difference of 600 kPa for 100 h. Both CO_2 permeability and CO_2/N_2 selectivity were maintained at constant levels, indicating the good stability of the μ-DN ion gel membrane for CO_2 separation.

To further prove the good durability of the μ-DN ion gel membrane resulted from the non-volatility and high thermal stability of the IL, the CO_2 separation performance of the μ-DN ion gel membrane

was evaluated at elevated temperatures. As shown in Figure II-11(b), the CO_2 and N_2 permeabilities of the ion gel membrane monotonically increased with increasing temperature. When the temperature decreases from 70 °C to 30 °C at the trans-membrane pressure of 0 kPa, the gas permeability and permselectivity of the μ-DN ion gel membrane showed good reversibility as shown in Figure II-12(b). Furthermore, even at elevated temperatures, the CO_2/N_2 selectivity of the μ-DN ion gel membrane under the transmembrane pressure difference of 600 kPa was almost the same as that of the SILM measured under no transmembrane pressure difference. This result indicated that the μ-DN structure was not broken, no IL brew out from the μ-DN ion gel, and no defects were formed in the μ-DN ion gel membrane at elevated temperatures. In addition, the CO_2 permeability of the μ-DN ion gel membrane was higher than that of the SILM at all temperatures investigated here. The long-term stability measured under the conditions of trans-membrane pressure of 600 kPa at 70 °C was shown in Figure II-13(b). These results highlight the good thermal stability of the μ-DN ion gel membrane. The good thermal stability of the μ-DN ion gel membrane is important for practical applications such as CO_2 capture in flue gas at approximately 70 °C from thermal power plants [80].

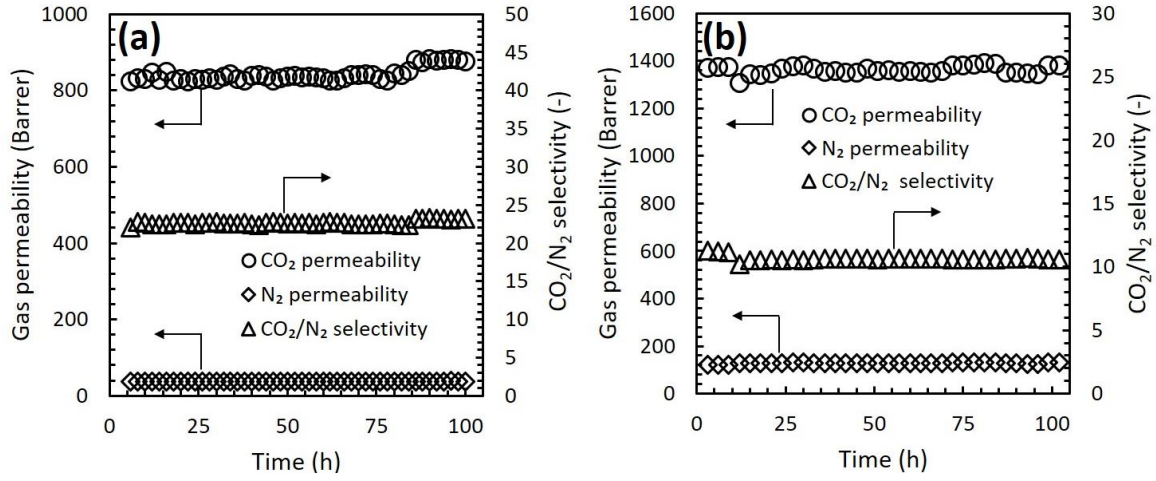

Figure II-13. Long-term stability of the μ-DN ion gel membrane prepared using non-volatile network precursors. (a) Trans-membrane pressure difference was 600 kPa and temperature was 30°C. (b) Trans-membrane pressure difference was 600 kPa and temperature was 70°C. The organic/inorganic network ratio of the membrane was 2 g/g. The M_n of poly(DMAAm-*co*-NSA) used was 126 kg/mol. The gas permeation was measured with 50 vol%/50 vol% of CO_2/N_2 and the permeate side pressure was maintained at atmospheric pressure.

Subsequently, we compared the CO_2 separation performance of the μ-DN ion gel membrane with that of the DN ion gel membrane prepared using volatile network precursors. As shown in Figure II-11(a) and (b), the μ-DN ion gel membrane showed much higher CO_2 and N_2 permeabilities than those of the DN ion gel membrane. Because the IL in these μ-DN and DN ion gel membranes was the same, the differences in the CO_2 and N_2 permeabilities were solely due to the different diffusivities of the dissolved gas molecules in these gel membranes. In general, the solute diffusivity in gels strongly depends on the liquid content of the gel and the cross-linking degree of the gel network [81]. Thus, to investigate the higher CO_2 permeability of the μ-DN ion gel membrane, the swelling ratios of the μ-DN and DN ion gel membranes were compared. The IL contents of these ion gel membranes were the same (ca. 80 wt%), but the swelling ratio of the μ-DN ion gel membrane was higher than that of the DN ion gel membrane (Table II-3). This indicates that the organic network in the μ-DN ion gel membrane was cross-linked more loosely than that in the DN ion gel membrane, which might be the reason for the higher CO_2 and N_2 permeabilities of the μ-DN ion gel membrane.

Table II-3. Swelling ratios of the crosslinking network skeletons of the DN and the μ-DN ion gel membranes.

Membranes	NSA ratio of cross-linkable polymer (mol%)	Swelling ratio (g/g)
DN ion gel	-	14.3
μ-DN ion gel	5.08	21.4
μ-DN ion gel	3.84	18.1
μ-DN ion gel	2.91	22.1
μ-DN ion gel	2.08	30.7
μ-DN ion gel	1.18	49.2

μ-DN ion gel membranes with the cross-linking networks having different swelling ratios were successfully fabricated to investigate the effect of the cross-linking degree on the gas permeability. NSA is the cross-linking point in the cross-linkable polymer for the crosslinkers, so that poly(DMAAm-*co*-NSA) with different NSA molar ratios (1–5 mol%) were synthesized and used for the ion gel preparation to achieve the different crosslinking degrees of the crosslinking networks. The swelling ratios of the crosslinking network of the ion gels are listed in Table II-3. The gas separation performance of the membrane formed by poly(DMAAm-*co*-NSA) with different NSA molar ratios was measured, as shown in Figure II-11(c). The CO_2 and N_2 gas permeabilities tended to increase with

an increase in the swelling ratio, and the CO_2/N_2 permselectivity was nearly constant. This indicates that the gas permeability of the ion gel membranes significantly depended on the cross-linking degree of the gel network, that is, the lower cross-linkage degree tended to have a higher gas permeability. The μ-DN ion gel membrane fabricated using poly(DMAAm-*co*-NSA) with an NSA ratio of 1.18 mol% showed the highest CO_2 permeability of approximately 920 Barrer.

In our previous research, we demonstrated that the toughness of the μ-DN ion gels increased using a cross-linkable polymer with a lower NSA ratio [66]. Therefore, poly(DMAAm-*co*-NSA) with a low NSA ratio is preferable for fabricating μ-DN ion gel membranes with both high CO_2 permeability and high mechanical strength. As a result, the preparation conditions of the μ-DN ion gel membrane could be optimized. It was also confirmed that the μ-DN ion gel prepared under optimized conditions has great potential as a base material for high-performance CO_2 separation membranes. It can be said that the μ-DN ion gel membrane is a promising material to develop IL-based CO_2 separation membranes for practical applications.

II-4 Conclusion

In this study, a μ-DN ion gel-based CO_2 separation membrane fabricated using non-volatile network precursors was developed. The network structure of the μ-DN ion gel was optimized via adjusting the M_n of the cross-linkable polymer and the organic/inorganic network compositions. The μ-DN ion gel membrane prepared under the optimized condition showed excellent mechanical properties with a fracture energy of 765 kJ/m^3, Young's modulus of 146 kPa, and fracture stress of 631 kPa. As for the gas separation performance, the μ-DN ion gel membrane fabricated using the poly(DMAAm-*co*-NSA) with the NSA ratio of 1.18 mol% exhibited the CO_2 permeability of approximately 920 barrer, which was much higher than that of the classic DN membrane fabricated using volatile network precursors and the SILM. In addition, the μ-DN ion gel membrane showed good durability under high-pressure conditions and elevated temperatures. Due to such good mechanical properties and high CO_2 separation performance, the μ-DN ion gel displayed the great potential to be used as the base material of high-performance CO_2 separation membranes.

Chapter III
Preparation of a composite membrane with an inorganic/organic micro-double-network ion gel layer

III-1 Introduction

Preparing thin ion gel membranes with high CO_2 permeance is difficult due to the poor mechanical properties of ion gels. The μ-DN ion gel membrane developed in Chapter II displayed good mechanical properties and high CO_2 separation performance. Additionally, the μ-DN ion gel membrane showed good durability under high-pressure conditions at elevated temperatures. Importantly, the μ-DN ion gel was fabricated using non-volatile network precursors, which make it possible to prepare thin μ-DN ion gel membrane using thin-film preparation methods normally performed in an open space. Therefore, the μ-DN ion gel has the good potential as a base material for developing high-permeance thin ion gel membranes. The next target is to fabricate thin μ-DN ion gel membrane with high CO_2 permeance.

In this study, first, we fabricated the μ-DN ion gel membrane in an open space and investigated the effects of the specific inorganic/organic μ-DN network on the mechanical properties and surface roughness of the μ-DN ion gel thin layer. The preparation condition for high mechanical properties, suitable surface roughness and high gas permeability was optimized for thin ion gel membrane preparation. Based on the optimized conditions, a composite membrane consisting of a thin μ-DN ion gel layer and a support membrane with an intermediate layer was developed by spin coating. The structure of the composite membrane is as illustrated in Scheme III-1. The CO_2 permeance and CO_2/N_2 selectivity of the prepared composite membranes were evaluated. The long-term stability of the composite membrane for CO_2 separation was confirmed.

Scheme III-1. Schematic illustrations of the composite membrane and the μ-DN ion gel layer, and the composition of the μ-DN ion gel layer

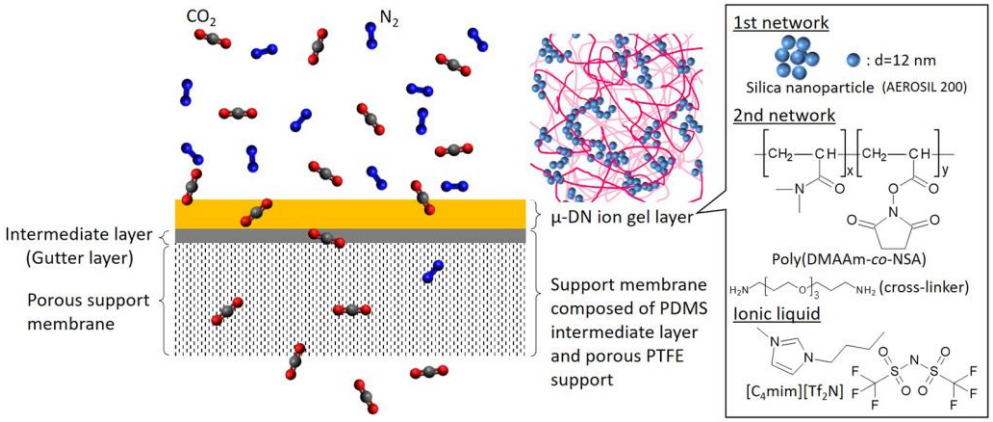

III-2 Experimental section

III-2-1 Materials

The materials used in this chapter to prepare the μ-DN ion gel membrane is the same as those described in Chapter II.

III-2-2 Synthesis and characterization of the poly(DMAAm-*co*-NSA)

The cross-linkable polymer poly(DMAAm-*co*-NSA) was synthesized by the RAFT polymerization. NSA is the crosslinking point of poly(DMAAm-*co*-NSA). The synthesis procedures and materials were the same as those described in Chapter II. The preparation conditions are listed in Table III-1. Poly(DMAAm-*co*-NSA) with different molecular weights (M_n) and different NSA molar ratios were successfully synthesized. The M_n and NSA ratio of poly(DMAAm-*co*-NSA) were measured using size exclusion chromatography (SEC) and nuclear magnetic resonance spectroscopy (NMR) following the procedures from a reported work [66]. The results of the M_n and NSA ratio are presented in Table III-2.

Table III-1. Amount of reagents used for the synthesis of poly(DMAAm-*co*-NSA).

	CTA (mmol)	DMAAm (mmol)	NSA (mmol)	ADVN (mmol)	1,4 dioxane (g)
Sample 1	0.32	100	5.30	0.032	20
Sample 2	0.16	100	5.30	0.016	20
Sample 3	0.12	100	5.30	0.012	20
Sample 4	0.08	100	5.30	0.008	20
Sample 5	0.053	100	5.30	0.0053	20
Sample 6	0.040	100	5.30	0.0040	20
Sample 7	0.040	100	4.20	0.0040	20
Sample 8	0.040	100	3.12	0.0040	20
Sample 9	0.040	100	2.06	0.0040	20
Sample 10	0.040	100	1.02	0.0040	20

Table III-2. Characterization results of poly(DMAAm-*co*-NSA)

	Molar ratio of NSA (mol%)	Purity (wt%)	Molecular weight (kg/mol)		
			M_n	M_w	M_w/M_n
Sample 1	4.99	95.3	32	41	1.3
Sample 2	4.76	94.9	54	71	1.3
Sample 3	4.31	98.2	65	93	1.4
Sample 4	4.99	97.9	92	133	1.5
Sample 5	5.21	95.2	116	185	1.6
Sample 6	5.08	93.5	126	248	2.0
Sample 7	3.84	95.5	102	131	1.3
Sample 8	2.91	95.4	121	186	1.5
Sample 9	2.08	95.5	140	239	1.5
Sample 10	1.18	97.1	127	220	1.7

III-2-3 Fabrication of the μ-DN ion gel membrane in open space

The inorganic/organic μ-DN ion gel membrane was fabricated by a one-pot/one-step method in open space under mild conditions. The IL content of the μ-DN ion gel membrane used in this study was fixed at 80 wt%. For the preparation of the μ-DN ion gel membrane, poly(DMAAm-*co*-NSA) with different M_n and NSA molar ratios were used. μ-DN ion gels with different organic/inorganic network compositions were also prepared. The preparation conditions are listed in Table III-3. The preparation procedures of the precursor solution are the same as those of the μ-DN ion gel membrane described in Chapter II. The ion gel membrane precursor solution was added to an open mold. The mold with the precursor solution was placed in an oven at 60 °C for 24 h, and the obtained ion gel membrane was dried on a hot plate at 60 °C for 24 h.

Table III-3. Reagents used for the preparation of the μ-DN ion gel membrane.

(a) μ-DN ion gel membranes formed by poly(DMAAm-*co*-NSA) with different molecular weights

	Sample 1	Sample 2	Sample 3	Sample 4	Sample 5	Sample 6
[C_4mim][Tf_2N] (g)	5.12	5.12	5.12	5.12	5.12	5.12
Aerosil 200 (g)	0.32	0.32	0.32	0.32	0.32	0.32
Organic network (g)	0.96	0.96	0.96	0.96	0.96	0.96
Poly(DMAAm-*co*-NSA) (g)	0.91	0.91	0.92	0.91	0.91	0.91
M_n (kg/mol)	32	54	65	92	116	126
NSA ratio (mol%)	4.99	4.76	4.31	4.99	5.21	5.08
Cross-linker; DGBE (g)	0.049	0.046	0.042	0.049	0.050	0.050
Ethanol (g)	10.24	10.24	10.24	10.24	10.24	10.24

(b) μ-DN ion gel membranes formed with different organic/inorganic network weight ratios.

	Sample 1	Sample 2	Sample 3	Sample 4	Sample 5	Sample 6
Organic/inorganic ratios	1.0	1.5	2.0	3.0	5.0	7.0
[C_4mim][Tf_2N] (g)	5.12	5.12	5.12	5.12	5.12	5.12
Aerosil 200 (g)	0.64	0.51	0.43	0.32	0.21	0.16
Organic network (g)	0.64	0.77	0.85	0.96	1.07	1.12
Poly(DMAAm-*co*-NSA) (g)	0.61	0.73	0.81	0.91	1.01	1.06
M_n (kg/mol)	126	126	126	126	126	126
NSA ratio (mol%)	5.08	5.08	5.08	5.08	5.08	5.08
Cross-linker; DGBE (g)	0.033	0.037	0.044	0.050	0.055	0.058
Ethanol (g)	10.24	10.24	10.24	10.24	10.24	10.24

(c) μ-DN ion gel membrane formed by poly(DMAAm-*co*-NSA) with different NSA molar ratios

	Sample 1	Sample 2	Sample 3	Sample 4	Sample 5
[Bmim][Tf_2N] (g)	5.12	5.12	5.12	5.12	5.12
Aerosil 200 (g)	0.32	0.32	0.32	0.32	0.32
Organic network (g)	0.96	0.96	0.96	0.96	0.96
Poly(DMAAm-co-NSA) (g)	0.948	0.939	0.931	0.922	0.913
M_n (kg/mol)	127	140	121	102	126
NSA ratio (mol%)	1.18	2.08	2.91	3.84	5.08
Cross-linker; DGBE (g)	0.012	0.021	0.029	0.038	0.050
Ethanol (g)	10.24	10.24	10.24	10.24	10.24

III-2-4 Fabrication of μ-DN ion gel-based composite membrane

The composite membrane was fabricated by spin-coating the μ-DN ion gel precursor solution on a support membrane with dimethylpolysiloxane (PDMS)-based intermediate layer (*Nitto Denko Corporation*). The precursor solution was prepared according to the conditions shown in Table III-3(c)

("Sample 1"). A poly(DMAAm-*co*-NSA) with an NSA ratio of 1.18 mol% and M_n of 127 kg/mol was used, and the organic/inorganic network ratio was set to 3 g/g. The spin-coater (MS-A100, Mikasa Co., Ltd.) was used to fabricate the composite membrane. The rotation speed was changed from 500 to 1000, 1500, 2000, 3000, 5000, or 7000 rpm for the preparation of ion gel layers with different thicknesses. After spin coating, the composite membrane was dried in an oven at 60 °C for 24 h.

III-2-5 Mechanical strength measurements

For mechanical strength measurement, self-standing μ-DN ion gel membranes were prepared and used. The measurement method is the same as that described in Chapter II.

III-2-6 CO_2/N_2 separation performance evaluation

The CO_2/N_2 separation performance of the μ-DN ion gel membranes was measured by the sweep method. The feed gases were CO_2 (100 mL/min) and N_2 (100 mL/min). The sweep gas was pure helium with a flow rate of 40 mL/min, and the sweep-side absolute pressure was fixed at atmospheric pressure. The flow rates of the gases were controlled using mass flow controllers (Hemmi Slide Rule Co., Ltd., Japan). The ion gel membrane was sandwiched between two porous PTFE support membranes (pore size, 0.1 μm) (Toyo Roshi Kaisha, Ltd., Japan) and fixed in the membrane cell for gas separation measurements. The composition of the gases was measured using a gas chromatograph (GC-8A, Shimadzu Co., Japan) at a steady state. The data were selected when the peak area difference between adjacent measurements was less than 1%. The gas permeation measurement apparatus used in this chapter is the same as that used in Chapter II.

III-3 Results and discussion

For the preparation of the composite membrane, the high mechanical strength of the ion gel would facilitates the preparation of the much thinner and more stable μ-DN ion gel layer. Therefore, the mechanical properties of the μ-DN ion gel formed in open space were investigated and optimized by first.

III-3-1 Mechanical properties of the μ-DN ion gel membrane prepared in open space

The μ-DN ion gel membrane was developed based on the DN principle. When the μ-DN ion gel

membrane was subjected to tensile stress, the cluster formed by SiO_2 nanoparticles acted as a sacrificial bond to dissipate the energy, and the polymeric network formed by cross-linked poly(DMAAm-*co*-NSA) acted as the hidden length to toughen the ion gel [67, 68, 82]. Therefore, the cross-linking network structure and network proportion are crucial factors for improving the mechanical properties of the μ-DN ion gel membrane.

First, the effect of the cross-linkable polymer M_n on the mechanical properties of the μ-DN ion gel membrane was investigated. The uniaxial tensile stress-strain curves of the μ-DN ion gel membrane prepared in an open space are presented in Figure III-1(a). The μ-DN ion gel membranes were fabricated using poly(DMAAm-*co*-NSA) with different M_n while the organic/inorganic network ratio is fixed at 3 g/g and the NSA ratio of poly(DMAAm-*co*-NSA) is fixed 5 mol%. As shown in Figure III-1(a), the mechanical strength of the μ-DN ion gel membranes is nearly the same at a poor level. The detailed mechanical properties of the μ-DN ion gel membranes obtained from Figure III-1(a) are presented in Figure III-2. In Figure III-2, it can be found that the Young's modulus, fracture stress, fracture strain, and fracture energy of the μ-DN ion gel membranes are nearly constant when the M_n of the polymer poly(DMAAm-*co*-NSA) changes. This implies that for the μ-DN ion gel membrane prepared in open space, the mechanical properties don't depend on the M_n of the cross-linkable polymer. The cross-linking degree of the μ-DN structure was characterized by the swelling ratio of the μ-DN ion gel network skeleton in pure water. The measurement procedures for the swelling ratio were the same as described in Chapter II. A lower swelling ratio usually indicates a higher degree of the cross-linking. As shown in Figure III-1(d), the swelling ratio of the μ-DN ion gel network skeleton fabricated by the cross-linkable polymer with different M_n in an open space is constant at a low level. The low swelling ratio indicates the high cross-linking degree of the network which results in a high Young's modulus of more than 250 kPa (Figure III-2(a)) and a low fracture strain of approximately 0.9 (Figure III-2(b)). Owing to the constant Young's modulus and fracture strain, the fracture stress is also nearly constant, as shown in Figure III-2(c). In Figure III-2 (d), the μ-DN ion gel membrane shows a low fracture energy (ca. 100 kJ/m^3), which indicates a low mechanical strength.

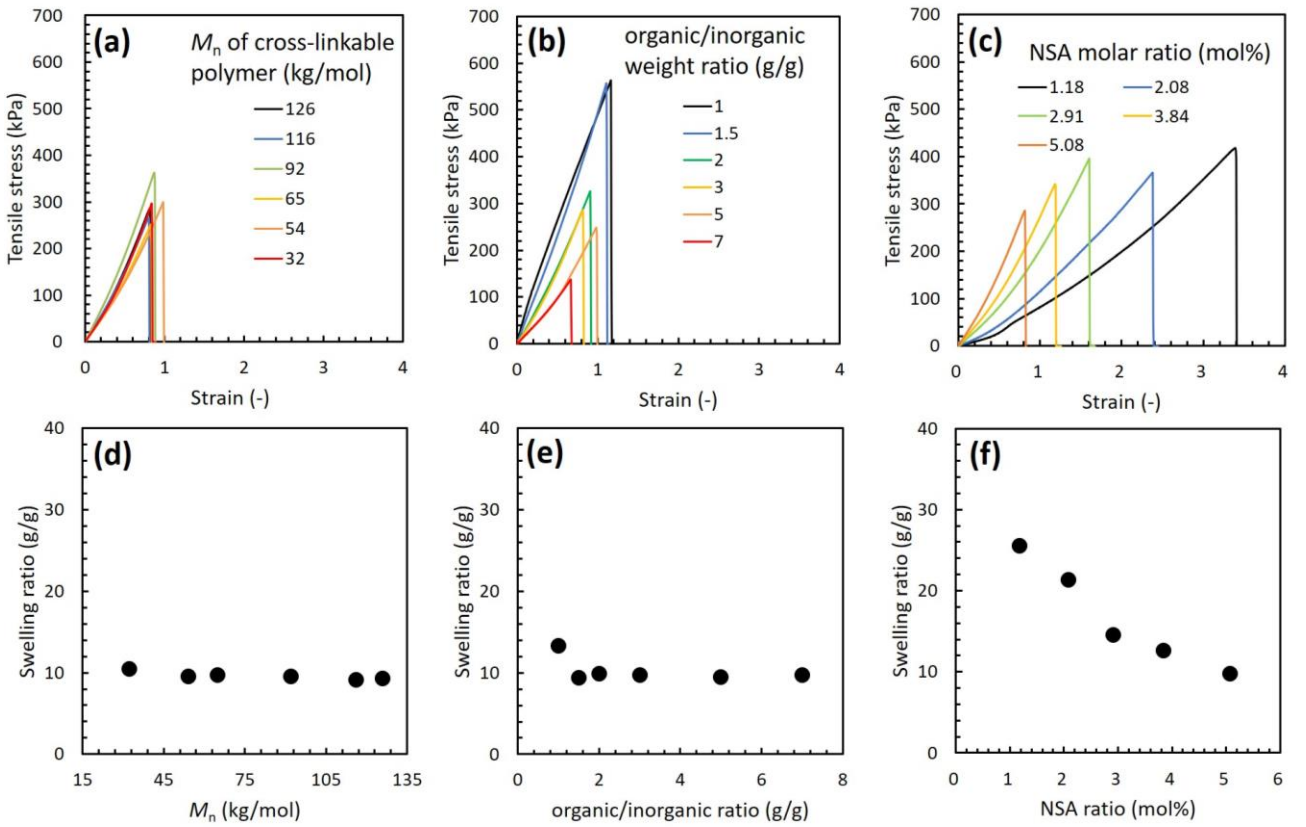

Figure III-1. Uniaxial tensile stress-strain curves (a-c) and swelling ratio (d-f) of the μ-DN ion gel membranes prepared in an open system. (a, d) effect of molecular weight of poly(DMAAm-*co*-NSA), (b, e) effect of organic/inorganic network ratio, and (c, f) effect of cross-linkable NSA ratio in the poly(DMAAm-*co*-NSA). Preparation conditions of the μ-DN ion gel membranes: (a, d) NSA ratio of the poly(DMAAm-*co*-NSA) was 5 mol% and the organic/inorganic network ratio was 3 g/g, (b, e) M_n and the NSA ratio of the poly(DMAAm-*co*-NSA) were 126 kg/mol and 5 mol%, respectively, and (c, f) M_n of the poly(DMAAm-*co*-NSA) was 126 kg/mol and the organic/inorganic network ratio was 3 g/g.

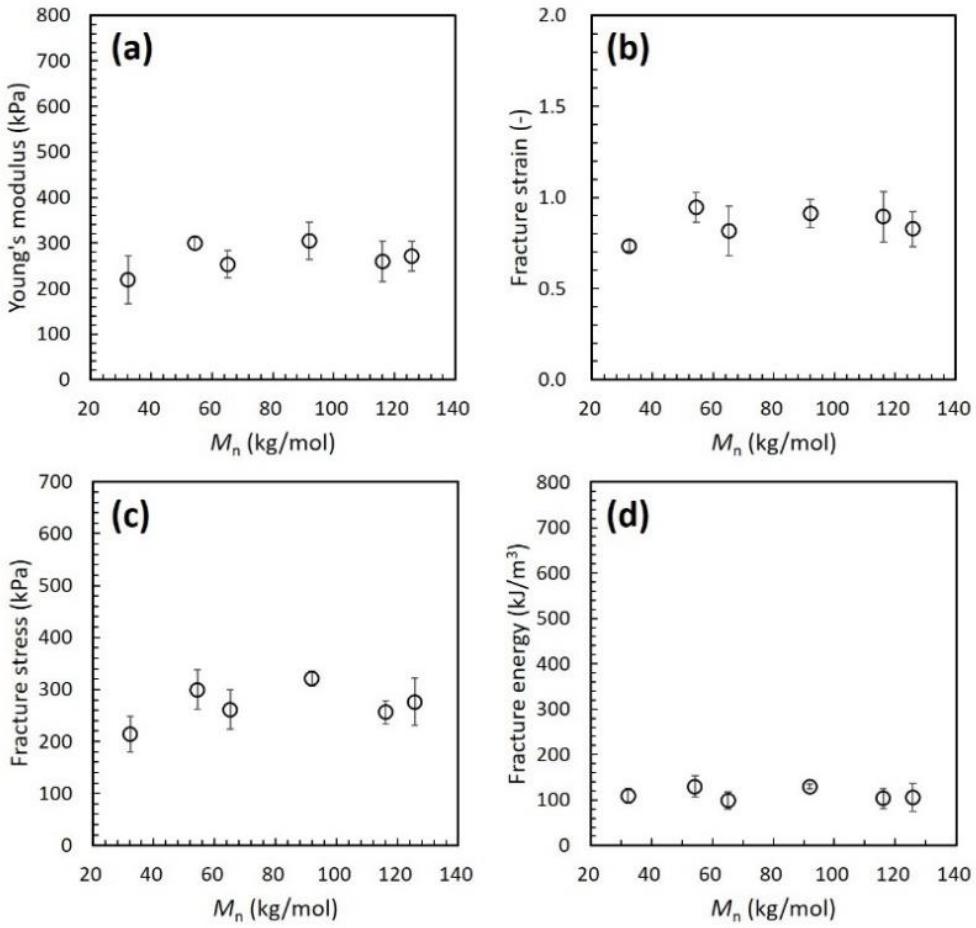

Figure III-2. (a) Young's modulus, (b) fracture strain, (c) fracture stress, and (d) fracture energy of the μ-DN ion gel membranes prepared in open space by poly(DMAAm-*co*-NSA) (NSA=5.08 mol%) with different M_n and an organic/inorganic network ratio of 3 g/g.

The fracture energy of the μ-DN ion gel membrane was strongly dependent on the energy dissipation of the inorganic part. Therefore, the organic/inorganic network ratio of the μ-DN ion gel membrane was adjusted and was expected to improve the fracture energy. As shown in Figure III-1(b), the mechanical properties were significantly changed by changing the network ratios. The Young's modulus, fracture strain, fracture stress, and fracture energy effectively increase as the organic/inorganic network ratio decreases (Figure III-3). The load applied to the μ-DN ion gel membrane was mainly sustained by the inorganic network, so that the Young's modulus of the ion gel dramatically decreased as the inorganic content decreased (Figure III-3(a)). It is worthy to mention that the fracture strain of the μ-DN ion gel membrane increases with the decrease of the organic/inorganic network ratio (Figure III-3(b)). In the double-network system, it has been reported

that the 1st network cluster acts as a multi-functional cross-linking point to connect the 2nd networks and suppresses macro-destruction of the DN gel [59]. In our inorganic/organic μ-DN ion gel, silica nanoparticle network cluster plays a similar role as the 1st network cluster of the double-network hydrogel. Therefore, if the amount of the inorganic network cluster decreases as the organic/inorganic network ratio increases, the multi-functional cross-linking point of the organic network would decrease. As a result, the fracture strain of μ-DN ion gel decreased as the organic/inorganic network ratio increased. The decreased fracture stress (Figure III-3(c)) is attributed to the decreased Young's modulus and fracture strain. Figure III-4 shows the cyclic tensile stress-strain curves of the μ-DN ion gel membranes, the result shows that the area of the hysteresis, which represents the dissipated energy of the inorganic network, decreases significantly as the inorganic content decreases. This indicates that the decrease in the inorganic content would decrease the energy dissipation of the inorganic network, which results in a decrease in the fracture energy (Figure III-3(d)). The μ-DN ion gel shows a much higher mechanical strength (fracture energy of 327 kJ/m^3) at an organic/inorganic network ratio of 1 g/g than that at 3g/g.

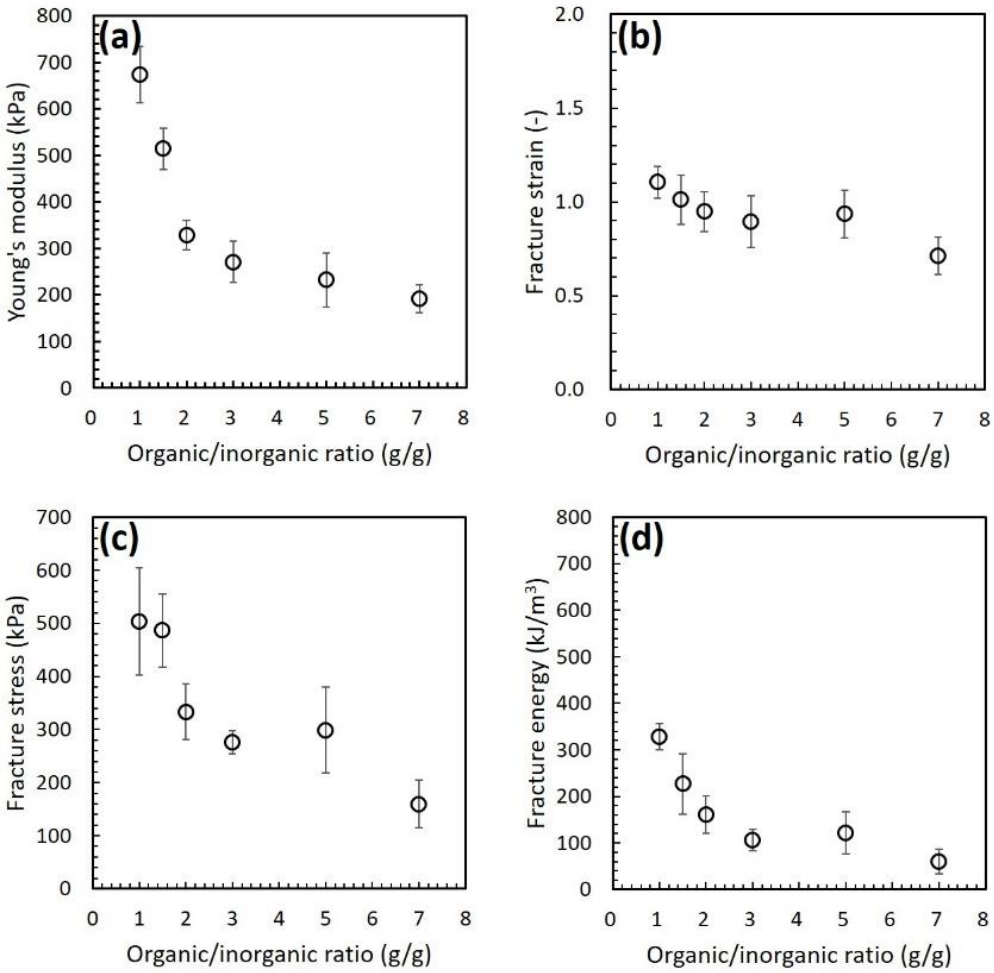

Figure III-3. (a) Young's modulus, (b) fracture strain, (c) fracture stress, and (d) fracture energy of the μ-DN ion gel membranes prepared in open space with different organic/inorganic network mass ratios. The μ-DN ion gel was prepared by poly(DMAAm-*co*-NSA) (NSA = 5.08 mol%) with a molecular weight (M_n) of 126 kg/mol.

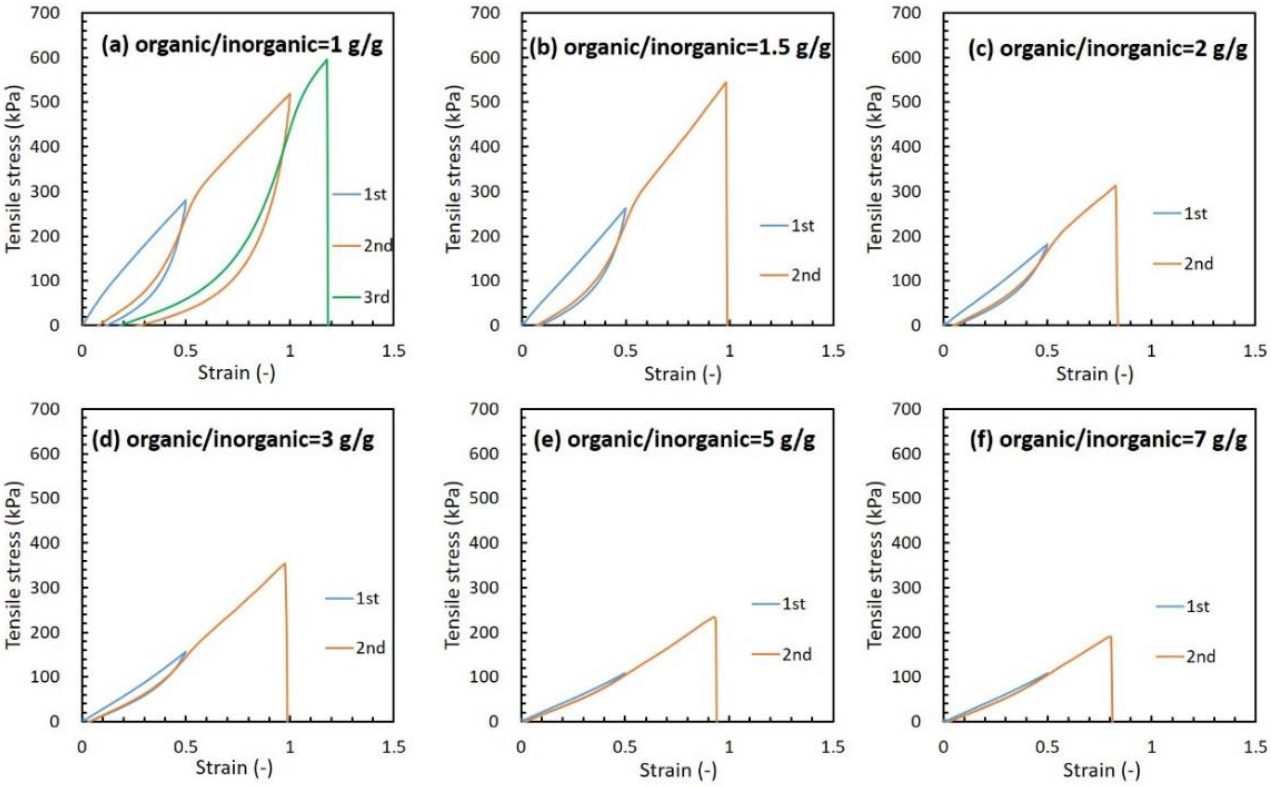

Figure III-4. Cyclic tensile stress–strain curves of the μ-DN ion gel membranes prepared with different organic/inorganic network mass ratios: (a) 1 g/g, (b) 1.5 g/g, (c) 2 g/g, (d) 3 g/g, (e) 5 g/g and (f) 7 g/g. The μ-DN ion gel was prepared by poly(DMAAm-co-NSA) (NSA=5.08 mol%) with M_n of 126 kg/mol.

As well as high mechanical strength, low surface roughness is also vital for thin μ-DN ion gel layer preparation. The surface roughness strongly affects to the mechanical strength of the gel membrane because the applied force concentrates to the thin part of the gel membrane and make the thin part easily broken. The μ-DN ion gel membrane with smooth surface had much higher mechanical strength [83]. Thus, it can be said that the surface roughness is important to give high mechanical strength to the μ-DN ion gel membrane.

The inorganic content in the μ-DN ion gel strongly affects the surface roughness. Hence, thin μ-DN ion gel layers with different organic/inorganic network ratios were fabricated by spin coating at the rotation speed of 1000 rpm for 20 s on the glass plate, and their roughness was measured using a laser microscope (KEYENCE, VK-X3000); the results are shown in Figure III-5. From Figure III-5, the arithmetic mean height (S_a) of the μ-DN ion gel surface decreases dramatically with decreasing

inorganic content, which indicates a decreased surface roughness, and remains constant at organic/inorganic ratios greater than 3 g/g. Figure III-6 shows the surface morphology of the samples. The surface roughness of the μ-DN ion gel layer with an organic/inorganic ratio of 3 g/g was much smoother than that with a ratio of 1 g/g. Therefore, considering both the surface roughness and mechanical properties, the suitable organic/inorganic network ratio for thin membrane preparation is 3 g/g. However, it worth noting that even when the organic/inorganic network ratio is higher than 3 g/g, the surface of the μ-DN ion gel layer is not highly smooth. This should be due to the micron-sized particles formed on the surface of the μ-DN ion gel layer as shown in Figure III-6. These micron-sized particles might be formed from the aggregation of the inorganic nanoparticles during spin-coating, which should be the disadvantage of the μ-DN ion gel for thin ion gel membrane preparation.

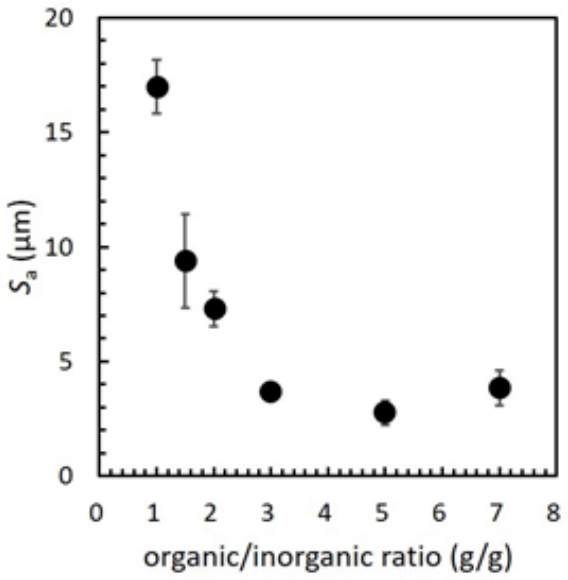

Figure III-5. Arithmetic mean height S_a the μ-DN ion gel prepared by spin coating with different organic/inorganic network ratios.

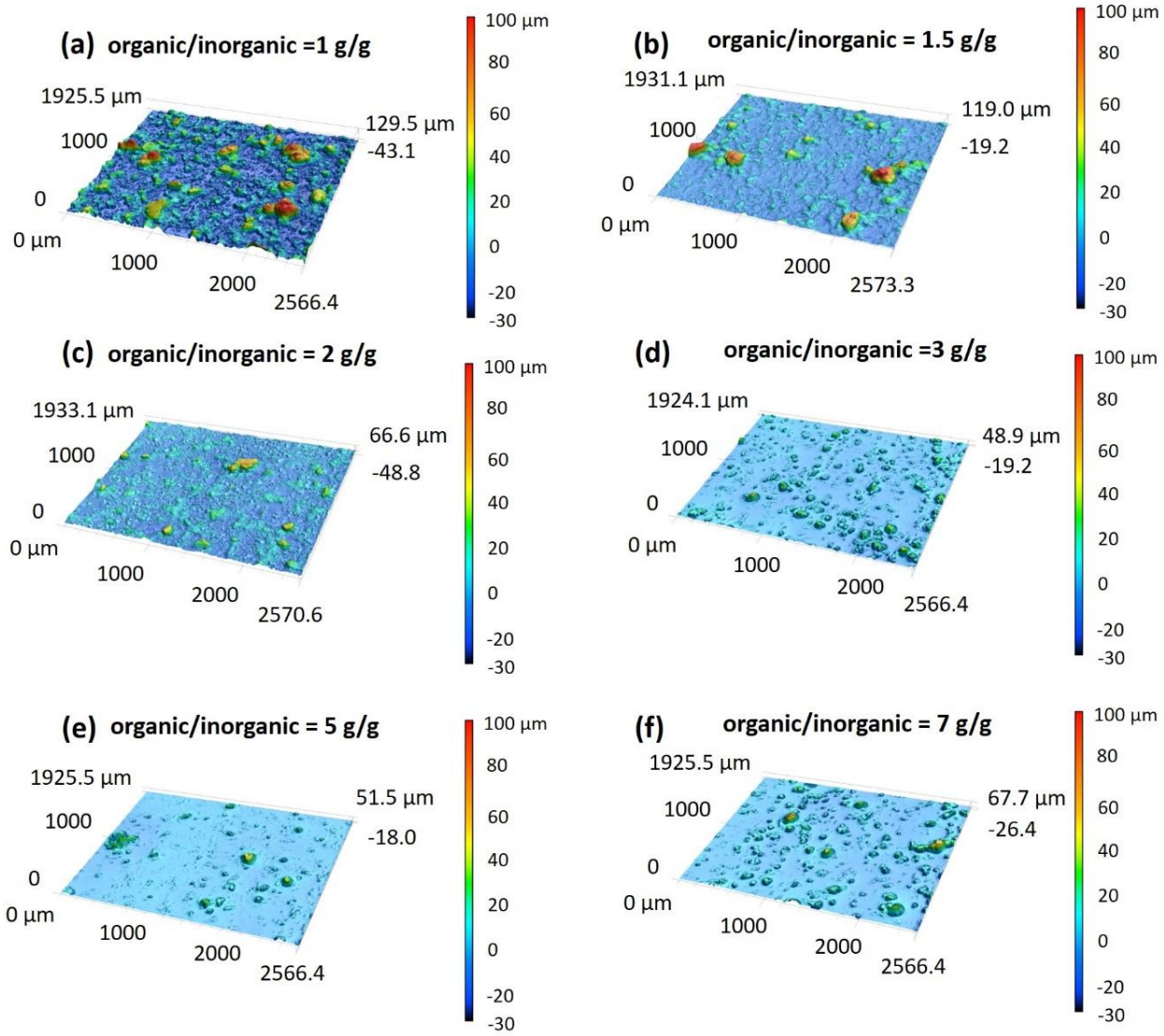

Figure III-6. Surface morphology of the µ-DN ion gel layer prepared by spin coating with different organic/inorganic network ratios: (a) 1 g/g, (b) 1.5 g/g, (c) 2 g/g, (d) 3 g/g, (e) 5 g/g, and (f) 7 g/g.

Therefore, restricted by the surface roughness, the organic/inorganic network ratio of the µ-DN ion gel membrane cannot be decreased to improve the mechanical strength. Another factor that restricted the mechanical strength of the µ-DN ion gel membrane is the low fracture strain, which attributes to the very high cross-linking degree indicated by the low swelling ratio (Figure III-1(d) and (e)). The excessively high cross-linking degree reduces the stretchability, and under a small deformation the amount of the ruptured inorganic network for energy dissipation is low so that the mechanical strength would be restricted. To decrease the cross-linking degree, a more ductile organic network should be formed.

NSA is the cross-linking point of the organic network; thus, decreasing the NSA molar ratio could be expected to form a more ductile and loosely cross-linked network. We fabricated μ-DN ion gel membranes by cross-linkable polymers with NSA molar ratios from 1.18% to 5.08%, and the mechanical property was strongly affected by the NSA molar ratio (Figure III-1(c)). The swelling ratio was also measured (Figure III-1(f)) to show the crosslinking degree. As the NSA molar ratio decreased, the swelling ratio was effectively increased from approximately 10 to 25 g/g, which indicates that the cross-linking degree of the μ-DN structure is significantly decreased. As a result, with the NSA molar ratio decreased, the Young's modulus decreased (Figure III-7(a)) while the fracture strain significantly increased (Figure III-7(b)). With the increased fracture strain, more inorganic clusters were ruptured to dissipate more energy during the stretching process. Therefore, the fracture energy of the μ-DN ion gel increased from 105 to 636 kJ/m^3 as the NSA ratio of the cross-linkable polymer was changed from 5 to 1.18 mol% (Figure III-7(d)). This indicates that a sufficiently high fracture strain was achieved by decreasing the NSA molar ratio of poly(DMAAm-*co*-NSA). With the improved mechanical property under the optimized preparation conditions, a thin μ-DN ion gel layer-based composite membrane was expected to be fabricated by spin coating.

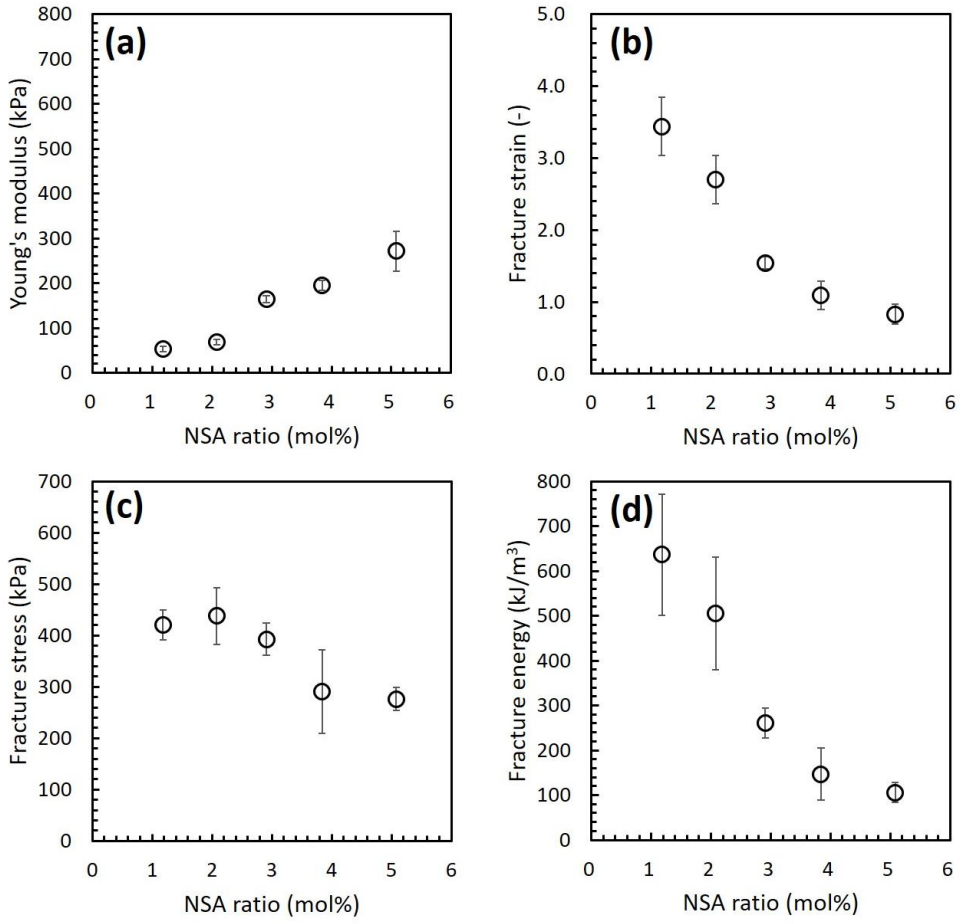

Figure III-7. (a) Young's modulus, (b) fracture strain, (c) fracture stress, and (d) fracture energy of the μ-DN ion gels prepared in open space by poly(DMAAm-*co*-NSA) with different NSA molar ratios, molecular weight (M_n) of approximately 126 kg/mol, and organic/inorganic network ratio of 3 g/g.

III-3-2 Effect of the inorganic ratio on the gas separation performance of the μ-DN ion gel membrane

Before preparing the μ-DN ion gel-based composite membrane by spin coating on a support membrane, the gas permeabilities of the self-standing μ-DN ion gel membranes fabricated with different organic/inorganic network weight ratios were evaluated to investigate whether the inorganic part would be resistant to gas transport in the membrane. The results are presented in Figure III-8. The results displays a constant trend of the gas permeabilities under different organic/inorganic network ratios, which indicates the inorganic part has no significant resistance to the gas transport in the μ-DN ion gel membrane at the organic/inorganic ratio from 2 g/g to 7 g/g.

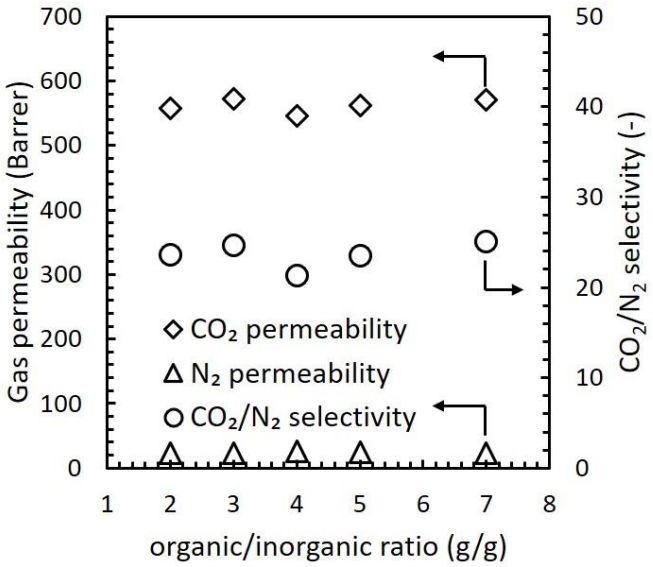

Figure III-8. Gas separation performance of the self-standing μ-DN ion gel membranes fabricated with different organic/inorganic network weight ratios. The NSA ratio of the used poly(DMAAm-*co*-NSA) is 1.18 mol% and the IL contents are fixed at 80 wt%. The gas separation performance was evaluated using 50/50 mol/mol CO_2/N_2 mixed gas at 30 °C under dry and atmospheric pressure conditions.

III-3-3 Ion-gel-based composite membrane

Subsequently, the μ-DN ion gel precursor solution prepared using the optimized condition was spin coated on a support membrane composed of a porous support and a dense intermediate layer, and formed the composite membrane [84]. The thickness of the μ-DN ion gel layer of the composite membrane was decreased by increasing the rotation speed of the spin coater. The CO_2/N_2 separation performances of the composite membranes with μ-DN ion gel layers having different thicknesses were measured and the results were shown in Figures III-9(a) and (b). The CO_2 permeance significantly increased with a decrease in the ion gel layer thickness. The maximum value of the CO_2 permeance obtained was 119 GPU, which is 53 times higher than that of the DN ion gel membrane formed by conventional volatile network precursors. The estimated curves in Figures III-9 were calculated using Equations I-13 and I-14. For the calculations, the CO_2 permeance ($R_{CO_2,2}$, 750 GPU) and N_2 permeance ($R_{N_2,2}$, 68 GPU) of the intermediate layer were measured from the support membrane, and the CO_2 permeability ($P_{CO_2,1}$, 564 barrer) and N_2 permeability ($P_{N_2,1}$, 24 barrer) of the μ-DN ion gel layer were measured from the self-standing μ-DN ion gel membrane. It was confirmed that the CO_2/N_2 separation

performance of the composite membrane was in good agreement with the estimated values. The performance of the self-standing μ-DN ion gel membrane with high thickness are also in good agreement with the estimated curve of the composite membrane. This indicates that when the ion gel layer thickness is high, the permeation resistance of the intermediate layer can be ignored.

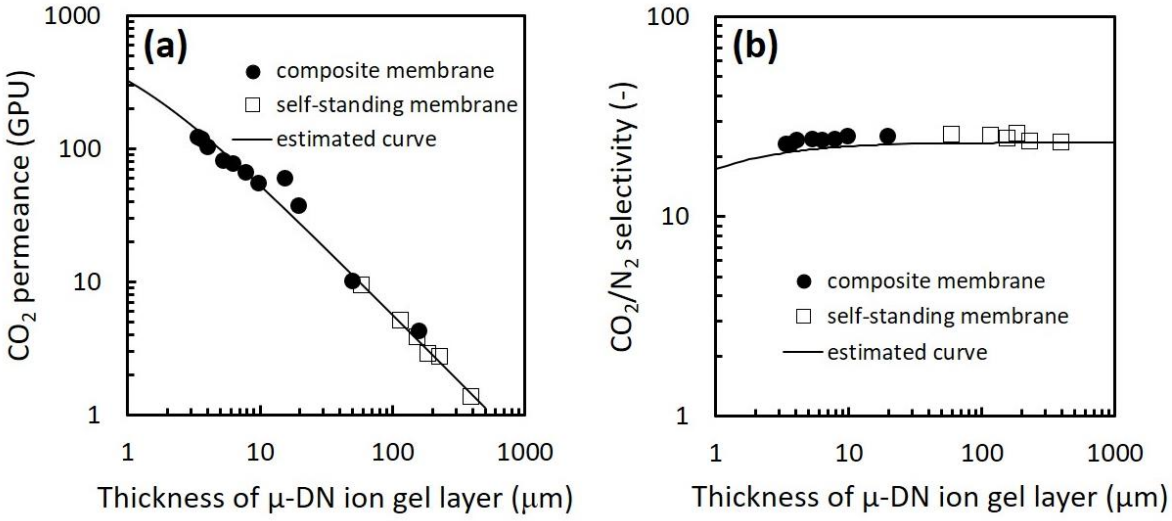

Figure III-9. CO_2 permeation performance of the composite membrane with thin μ-DN ion gel layer and self-standing μ-DN ion gel membranes: (a) CO_2 permeance and (b) CO_2/N_2 selectivity. The estimated curves were calculated by Equations I-13 and I-14 with CO_2 and N_2 permeabilities of μ-DN ion gel layer fixed at 564 barrer and 24 barrer, respectively, and CO_2 and N_2 permeance of the support membrane fixed at 750 GPU and 68 GPU, respectively. The gas separation performance of the composite membranes was from a published work [84] and used with permission. The gas separation performance was evaluated using 50/50 mol/mol CO_2/N_2 mixed gas at 30 °C under dry and atmospheric pressure conditions.

In addition, as shown in Figures III-10, the long-term stability of the μ-DN ion gel-based composite membrane at 30 °C under dry and atmospheric pressure conditions was also evaluated. The constant gas permeance and permselectivity within 100 h indicates a good long-term stability of the composite membrane with the μ-DN ion gel layer.

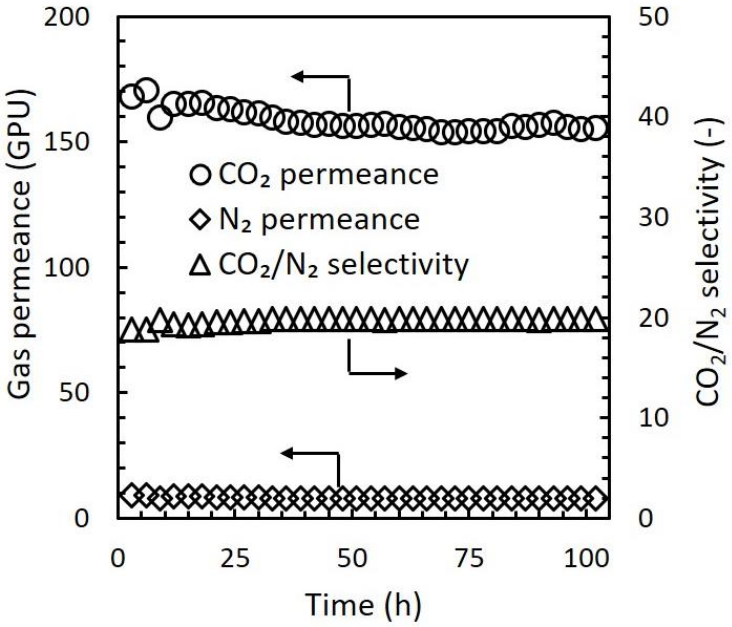

Figure III-10. Long-term stability of the μ-DN ion gel-based composite membrane. The μ-DN ion gel layer with 80 wt% of IL content formed on the support membrane by spin-coating at the rotation speed of 7000 rpm. The organic/inorganic network ratio of the μ-DN ion gel layer was 3 g/g. The poly(DMAAm-co-NSA) with 1 mol% of NSA ratio was used to form the organic network in the μ-DN ion gel layer. The gas separation performance was evaluated using 50/50 mol/mol CO_2/N_2 mixed gas at 30 °C under dry and atmospheric pressure conditions.

III-4 Conclusion

We optimized the preparation conditions of the μ-DN ion gel prepared in an open space. The high mechanical properties and good surface morphology was obtained by investigating the network materials and network compositions. The spin-coating method was used to fabricate a composite membrane with a μ-DN ion gel layer. The composite membrane prepared using the optimized conditions presents the highly improved CO_2 permeance. However, micron-sized particles found on the surface of the μ-DN ion gel layer, which contribute mostly to the high roughness of the surface of the μ-DN ion gel layer, is the disadvantage of the μ-DN ion gel for thin ion gel membrane preparation.

Chapter IV
Novel tough ion-gel-based CO_2 separation membrane with interpenetrating polymer network composed of semi-crystalline and cross-linkable polymers

IV-1 Introduction

The composite membrane with a μ-DN ion gel layer developed in Chapter III displayed the high CO_2 permeance of 119 GPU and remained CO_2/N_2 selectivity of 23. However, some micron-sized particles were found on the surface of the μ-DN ion gel layer (Figure III-6). The micron-sized particles caused the high roughness of surface of the μ-DN ion gel layer, which will result in poor mechanical properties of the ion gel layer [83]. This is detrimental to the thin ion gel membrane preparation. It was considered that the micron-sized particles were formed from the agglomeration of the inorganic silica nanoparticles during spin-coating. Therefore, replacing the inorganic network with an organic network and developing a new tough ion gel was considered as a strategy to solve this problem.

Poly(vinylidene fluoride-*co*-hexafluoropropylene) (PVDF–HFP), a semi-crystalline polymer, is a material which has attracted extensive attention due to its high chemical and thermal stabilities [85-87]. The PVDF–HFP could be physically cross-linked by the crystallization of the VDF segments, and it was widely utilized as the network material for tough ion gel preparation. In this chapter, a novel tough ion gel constructed from an interpenetrating polymer network (IPN) and high IL content was developed using a one-pot/one-step method in an open space. The IPN structure was composed of the physically cross-linked PVDF–HFP network and the chemically cross-linked poly(DMAAm-*co*-NSA) network (Scheme IV-1). The polymer network compositions and preparation temperatures of the IPN ion gels were optimized for better mechanical properties and IL holding properties. Using the optimized preparation conditions, the IPN ion gels with increasing IL contents were prepared. The CO_2 permeabilities and CO_2/N_2 permselectivities of IPN ion gel membranes prepared with different polymer network compositions, different preparation temperatures, and different IL contents were measured to investigate the gas separation performance of the IPN ion gel membranes.

Scheme IV-1. Schematic illustrations of the structure of the PVDF-HFP/poly(DMAAm-*co*-NSA) interpenetrating polymer network (IPN) ion gel membrane.

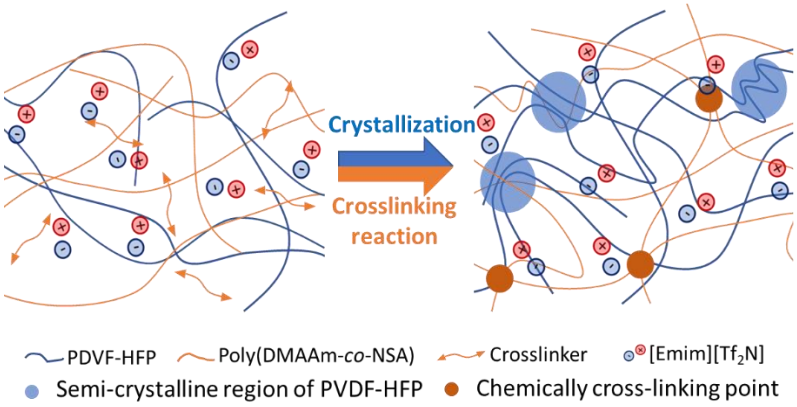

IV-2 Experimental section

IV-2-1 Materials

PVDF–HFP purchased from Sigma-Aldrich (M_w ~ 400000 g/mol, M_n ~ 130000 g/mol, pellets) was used as received. Poly(DMAAm-*co*-NSA) with an NSA molar ratio of 2.91 mol%, a molecular weight of approximately 121 kg/mol and purity of 91.13 wt% was synthesized following the method described elsewhere [66, 70]. Diethylene glycol bis(3-aminopropyl) ether (DGBE) and 1-ethyl-3-methylimidazolium bis(trifluoromethanesulfonyl)imide ([Emim][Tf_2N]) were purchased from Tokyo Chemical Industry Co., Ltd. DGBE was used as the cross-linker of poly(DMAAm-*co*-NSA). In this study, we selected [Emim][Tf_2N] because of the following reasons; (1) [Emim][Tf_2N] could be gelled by PVDF-HFP, and the gel had high mechanical strength [51, 61, 88], and (2) [Emim][Tf_2N] is one of the widely used ILs for the CO_2 separation membrane [89]. All ion gels, in this study, were fabricated using [Emim][Tf_2N] as the IL. Acetone (99.5 wt%, FUJIFILM Wako Pure Chemical Co.) was used as the diluent of the IPN ion gel precursor solution. The chemical structures of the [Emim][Tf_2N] and network precursors used for the IPN ion gel preparation are shown in Figure IV-1(a).

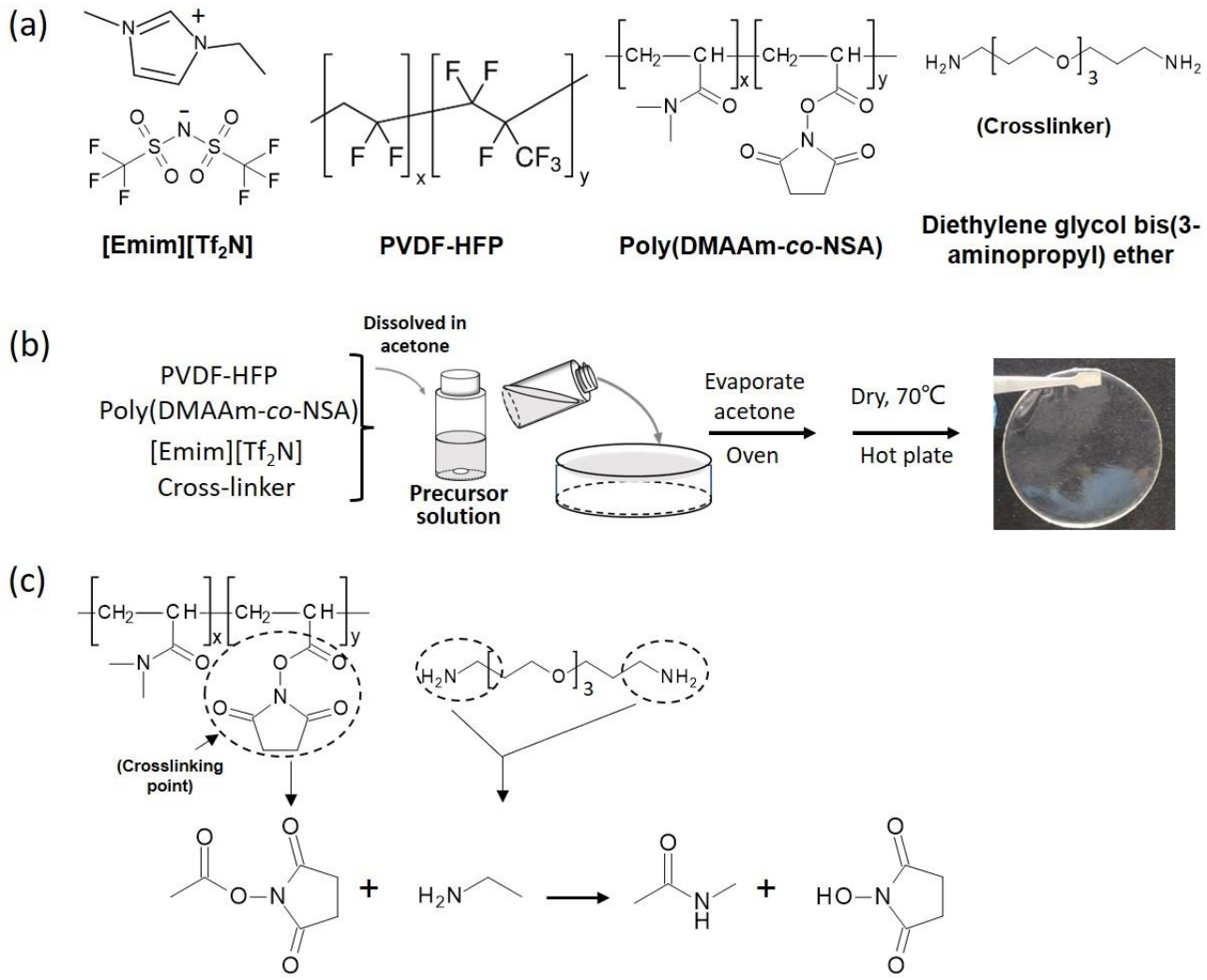

Figure IV-1. Illustrations of (a) the chemical structures of the IL and network precursors used for IPN ion gel preparation, (b) the preparation procedures of IPN ion gels, and (c) the cross-linking reaction of the poly(DMAAm-*co*-NSA) network.

IV-2-2 Ion gel preparation

The preparation procedure for the PVDF–HFP/poly(DMAAm-*co*-NSA) IPN ion gel is shown in Figure IV-1(b). A certain amount of PVDF–HFP was first added into 9.24 g of acetone and stirred for 3 h until completely dissolved. Then, a certain amount of poly(DMAAm-*co*-NSA) was added to the PVDF–HFP solution and stirred for 1 h to completely dissolve the poly(DMAAm-*co*-NSA). For the preparation of the IPN ion gel with 80 wt% IL content, the total weight of the polymer networks was fixed at 1.28 g, and each polymer weight was determined by the PVDF–HFP/poly(DMAAm-*co*-NSA) network weight ratio. Subsequently, 5.12 g of IL was added and stirred for 30 min. Finally, the cross-

linker solution, which was composed of DGBE and acetone (1.0 g), was added to the mixture. After stirring for 3 min, the IPN ion gel precursor solution was prepared. As shown in Figure IV-2, PVDF-HFP and poly(DMAAm-*co*-NSA) could be dissolved in the precursor solution and formed a transparent and homogeneous solution, which indicates the good miscibility of these two polymers in the solution. Therefore, PVDF-HFP and poly(DMAAm-*co*-NSA) polymer chains could be easily entangled in the precursor solution. In the precursor solution, the DGBE/NSA molar ratio was fixed at 0.5 mol/mol. By one minute of sonication, the air bubbles in the precursor solution were removed and the bubble-free solution was poured into a mold. The acetone in the precursor solution was evaporated in an oven for 24 h at a temperature described hereafter as the "evaporation temperature". During this heating process, an amide crosslinking reaction between *N*-hydroxysuccinimide (NHS) ester from the poly(DMAAm-*co*-NSA) and a primary amine from DGBE took place (Figure IV-1(c)). The obtained ion gel was completely dried by a hot plate at 70 °C for 24 h.

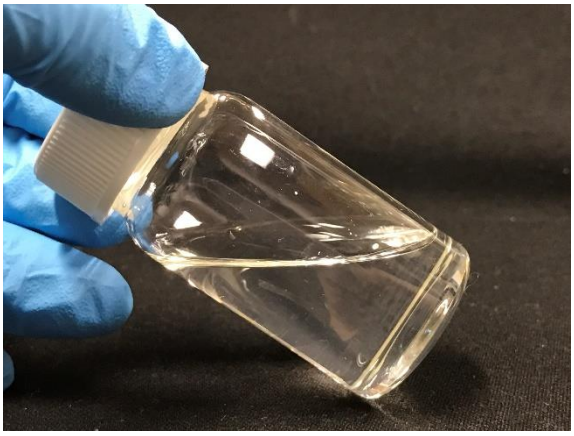

Figure IV-2. The IPN ion gel precursor solution composed of PVDF-HFP, poly(DMAAm-*co*-NSA), DGBE, [Emin][Tf_2N], and acetone.

The single-network (SN) ion gel with the poly(DMAAm-*co*-NSA) network was prepared in the same way as IPN ion gels, except for the use of PVDF–HFP. In 9.24 g of acetone, 1.24 g of poly(DMAAm-*co*-NSA) and 5.12 g of IL were dissolved sequentially as described above. Acetone DGBE solution (0.04 g of DGBE dissolved in 1.0 g of acetone) was then added into the solution and stirred for 3 min to prepare the precursor solution. For the SN ion gel with PVDF–HFP network, 1.28 g of PVDF–HFP was dissolved in 10.24 g of acetone; then, 5.12 g of IL was added, and the solution

was stirred for 30 min to form the precursor solution. Both precursor solutions of the SN ion gels were degassed by ultrasonication for 1 min, poured into a mold, and heated in an oven at evaporation temperature for 24 h. The obtained SN ion gels (poly(DMAAm-*co*-NSA) SN ion gel and PVDF–HFP SN ion gel) were completely dried on a hot plate at 70 °C for 24 h.

In this study, IPN ion gels with different polymer network compositions were fabricated at 50 °C by changing the PVDF–HFP weight ratios in the IPN (0, 0.25, 0.5, 0.75, and 1 g/g) so that a PVDF–HFP/IPN ratio of 0.25 g/g indicates that the IPN structure is composed of 25 wt% of the PVDF–HFP network and 75 wt% of the poly(DMAAm-*co*-NSA) network. Therefore, the ion gel with the PVDF–HFP/IPN weight ratio of 0 g/g corresponds to the poly(DMAAm-*co*-NSA) SN ion gel, while the PVDF–HFP/IPN weight ratio of 1.0 g/g corresponds to the PVDF–HFP SN ion gel. The IL contents of the IPN and SN ion gels were fixed at 80 wt%.

To evaluate the effect of evaporation temperature on the mechanical strength of the IPN and PVDF–HFP SN ion gels, the IPN ion gels with PVDF–HFP/IPN weight ratios of 0.5 g/g and PVDF–HFP SN ion gels were prepared at different evaporation temperatures (30, 50, 70, 90, and 110 °C).

To explore the effect of the IL content on the mechanical properties and gas separation performance of the IPN ion gel membranes, IPN ion gel membranes containing different contents of the IL were fabricated. The PVDF–HFP/IPN weight ratio of the IPN ion gel was fixed at 0.5 g/g, and the DGBE/NSA molar ratio was fixed at 0.5 mol/mol. The weight ratio of acetone to the mixture of IL and polymer networks was fixed at 1.6 g/g.

IV-2-3 Mechanical property test

The ion gels were made into dumbbell-shaped samples for mechanical property measurement using a universal testing instrument (EZ-LX, Shimadzu Co., Japan). The sample thickness was measured using a digital microscope system (Leica DMS300). For the uniaxial tensile test, the tensile strain rate was 100 mm/min. The loading–unloading cyclic tensile test was conducted with the tensile strain increased by 50% after each cycle.

IV-2-4 IL holding property test

The IL holding property was examined by checking the IL leakage from the ion gel under compression using a universal testing instrument (EZ-LX, Shimadzu Co., Japan). The ion gel was

compressed under the initial pressure of 1.16 MPa and kept at the constant compression strain for 2 min. After compression, the ion gel was removed from the apparatus, and the surface of the ion gel sample was wiped to remove the leaked IL. The weights of the ion gel before and after compression were measured to determine the leaked IL weight. The IL leakage was calculated using Equation IV-1.

$$\text{IL leakage} = (m_0\text{-}m_1)/m_0 \times 100\% \quad \text{(IV-1)}$$

where m_0 and m_1 are the weights of the ion gel samples before and after compression, respectively.

IV-2-5 Extent of the crosslinking reaction between *N*-hydroxysuccinimide (NHS) ester group and DGBE

The crosslinker DGBE could reacted with NHS ester and give the product NHS as shown in Figure VI-1(c). Therefore, the extent of the crosslinking reaction between NHS ester group and DGBE can be determined as the molar ratio of the released NHS (n_{NHS}) to the total NSA ($n_{NSA,0}$) in poly(DMAAm-*co*-NSA). It was determined in the same manner as reported elsewhere [66].

The IPN ion gel was immersed in DMSO-d_6 and shaken at 30 ℃ for 20 h to completely extract the IL and NHS released via the crosslinking reaction. The obtained solution was analyzed by ^{1}H-NMR to determine the molar ratio of the released NHS to the IL (n_{NHS}/n_{IL}). On the other hand, the total amount of NHS ester group in the poly(DMAAm-*co*-NSA) used to prepare the ion gel ($n_{NSA,0}$) can be calculated from the weight of used poly(DMAAm-*co*-NSA), the weight ratio of NSA in poly(DMAAm-*co*-NSA), and the molecular weight of NSA. Here, the weight ratio of NSA in poly(DMAAm-co-NSA) was calculated from the molar ratio of NSA in poly(DMAAm-*co*-NSA) (2.91 mol%) and the polymer purity (91.13 wt%). In addition, the molar amount of the IL used for the preparation of the ion gel ($n_{IL,0}$) can be calculated from the amount of the IL used and the molecular weight of the IL. Then, the $n_{NSA,0}/n_{IL,0}$ ratio could be obtained.

Because it was considered the IL was completely incorporated in the ion gel, $n_{IL} = n_{IL,0}$. Therefore, the $(n_{NHS}/n_{IL})/(n_{NSA,0}/n_{IL,0})$ equals $n_{NHS}/n_{NSA,0}$, which is the extent of the crosslinking reaction between NHS ester group and DGBE. The $n_{NHS}/n_{NSA,0}$ ratios of the IPN ion gels prepared under different conditions were determined in this study.

IV-2-6 IL content measurement of the ion gels

The ion gel (0.2 g) was placed in a vial with a lid. EtOH (40 g) was added to the vial and shaken at ambient temperature for 24 h to extract the IL in the ion gel. The EtOH was removed, and the residues were dried at 90 °C under vacuum. The dried polymers were weighed (m_1 g). The IL content was calculated using Equation IV-2.

$$\text{IL content} = (0.2\text{-}m_1)/0.2 \times 100\% \quad \text{(IV-2)}$$

IV-2-7 X-ray diffraction

Using an X-ray diffractometer (D2 PHASER Specifications, BRUKER), the X-ray diffraction (XRD) patterns of the ion gels in the 2θ range from 10° to 40° were detected. The measurement was conducted at 30 kV and 10 mA using a Cu Kα radiation with λ of 1.54 Å.

IV-2-8 Gas separation performance evaluation

The sweep method was adopted in this study to evaluated the gas separation performance of the membranes. The thicknesses of the IPN ion gel membranes, which were detected via a digital microscope (Leica DMS300, Leica Microsystems Inc.), were approximately 400 ~ 500 μm. The gas permeation apparatus and the membrane cell were the same as those used in our previously reported work [70, 71]. A mixed gas composed of 50/50 mol/mol of CO_2 and N_2, of which the total flow rate was 200 mL/min, was used as the feed gas. The sweep gas was pure helium with the flow rate of 40 mL/min. For gas flow rate controlling, mass flow controllers (Hemmi Slide Rule Co., Ltd., Japan) were used. The absolute pressures at the feed and sweep sides were set as the atmospheric pressure. The gas permeation tests were conducted at 30 °C.

The compositions of the permeated CO_2 and N_2 were measured using a gas chromatograph (GC-8A, Shimadzu Co., Japan) to calculate the permeances of CO_2 and N_2. The steady-state of the gas permeation test was confirmed from the GC peak area difference, and steady data was obtained when the difference in the adjacent peak areas was less than 1%. The gas permeation measurement apparatus used in this chapter is the same as that used in Chapter II.

IV-3 Results and discussion

IV-3-1 Surface morphology, mechanical properties and IL holding property of the IPN ion gel

The ion gel composed of the PVDF–HFP/poly(DMAAm-*co*-NSA) IPN and a high content of the IL [Emim][Tf_2N] was successfully fabricated. The IPN was formed by the physically crosslinked PVDF-HFP network and the chemically crosslinked poly(DMAAm-*co*-NSA) network. First, the mechanical properties and IL holding property of the IPN ion gel were optimized by varying the polymer network ratios and evaporation temperatures.

To confirm the formation of IPN structure in the ion gel, crosslinking of each PVDF-HFP and poly(DMAAm-co-NSA) network was evaluated. Regarding the crosslinking of the PVDF-HFP network, it was reported that PVDF–HFP formed a semi-crystalline structure in an IL [61, 90]. To confirm the formation of the semi-crystalline structure in the developed ion gel, we measured the XRD patterns of the ion gels with different PVDF–HFP/IPN weight ratios. The results are shown in Figure IV-3(a). The PVDF–HFP SN ion gel and IPN ion gel showed a peak at $2\theta = 20.0°$, which corresponds to the (110) reflection of the α crystal phase in PVDF [90, 91]. The ion gels also showed another peak at $2\theta = 12.5°$, which corresponds to the structured [Emim][Tf_2N]. From the peak at $2\theta = 20.0°$, the physical crosslinking structure formation of the PVDF–HFP network by the formation of the PVDF crystalline part in the ion gel was evidenced. On the other hand, regarding the crosslinking of the poly(DMAAm-*co*-NSA) network, the extent of the crosslinking reaction of the poly(DMAAm-*co*-NSA) network was determined by ^{1}H-NMR measurement. The extents of the crosslinking reaction in the ion gels with different PVDF–HFP/IPN weight ratios are shown in Figure IV-4(a). The results indicated the formation of the chemically crosslinked poly(DMAAm-*co*-NSA) network in the ion gel. Because the PVDF-HFP and poly(DMAAm-*co*-NSA) showed good miscibility (Figure IV-2), these polymers could be entangled with each other in the precursor solution. The entangled structure could be kept in the ion gel. In addition, the entangled each network was cross-linked separately. Therefore, it can be considered that the IPN structure was formed in the ion gel.

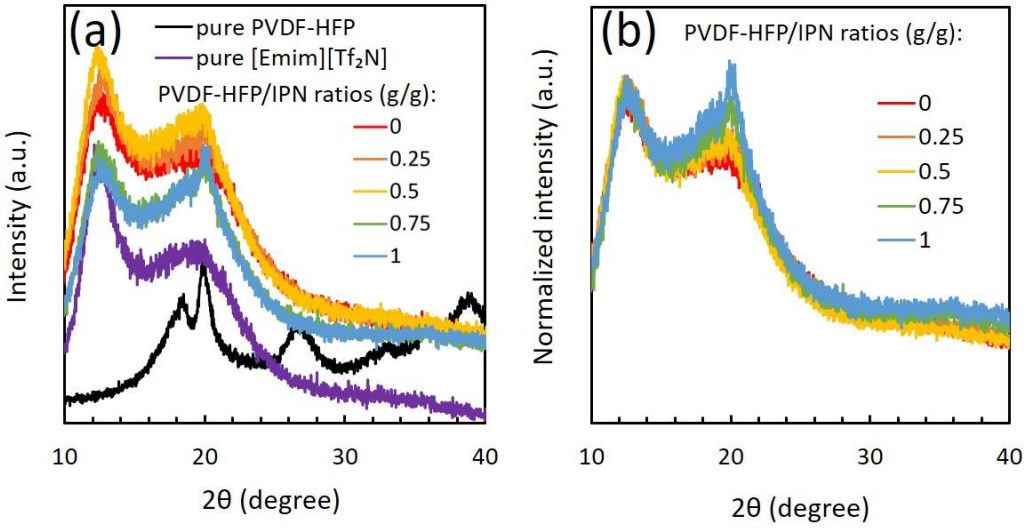

Figure IV-3. XRD patterns of the pure PVDF–HFP, pure [Emim][Tf_2N], and ion gels fabricated with different PVDF–HFP/IPN weight ratios at the evaporation temperature of 50 °C. (a) The original XRD patterns and (b) the XRD patterns normalized by the structured [Emim][Tf_2N] peak at $2\theta = 12.5°$.

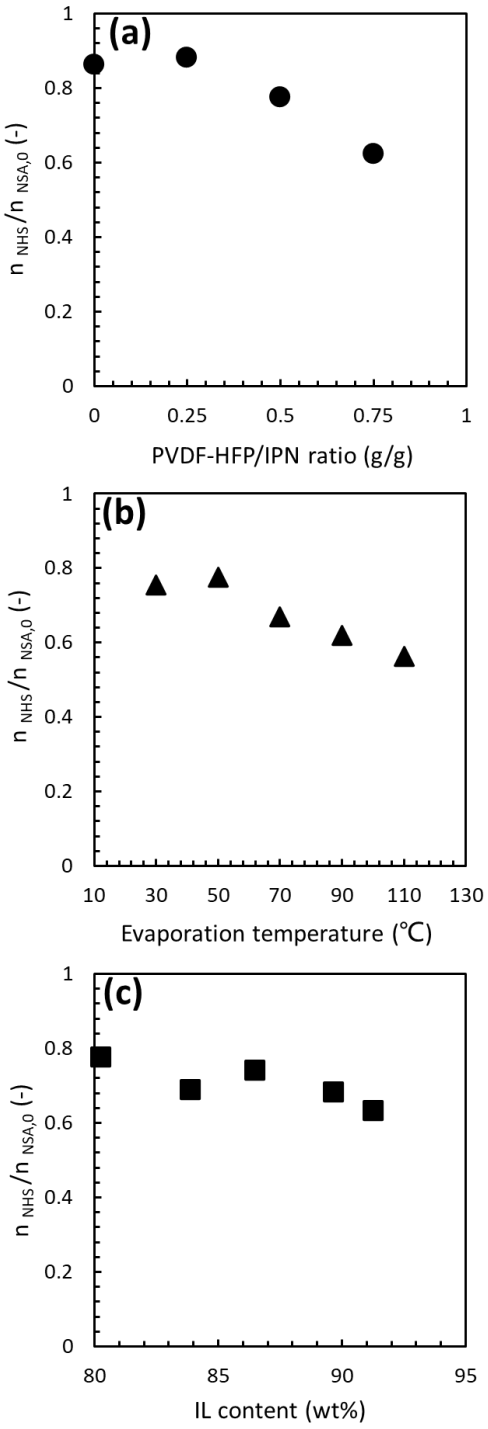

Figure IV-4. Extent of the crosslinking reaction between *N*-hydroxysuccinimide (NHS) ester group and DGBE during the formation of poly(DMAAm-*co*-NSA) network. The IPN ion gels were prepared under the conditions of (a) evaporation temperature of 50 ℃, IL content of 80 wt% and different PVDF–HFP/IPN weight ratios, (b) PVDF–HFP/IPN ratio of 0.5 g/g, IL content of 80 wt% and different evaporation temperatures, and (c) PVDF–HFP/IPN ratio of 0.5 g/g, evaporation temperature of 50 ℃ and different IL contents.

Then, the IPN ion gel layer was fabricated by spin-coating at the rotation speed of 1000 rpm for 20 s on a glass plate, and the roughness was measured using a laser microscope (KEYENCE, VK-X3000). The result is presented in Figure IV-5. The IPN ion gel layer shows a highly smooth surface morphology without the any micron-sized particles found in the μ-DN ion gel layer. The arithmetic mean height (S_a) of the IPN ion gel layer surface is 1.6 μm, which is much lower than that of the μ-DN ion gel layer described in Chapter III. This result indicates that the IPN ion gel overcame the problem of the micro-sized particles formed on the μ-DN ion gel surface. The smooth surface of the IPN ion gel layer is preferred for thin ion gel layer preparation.

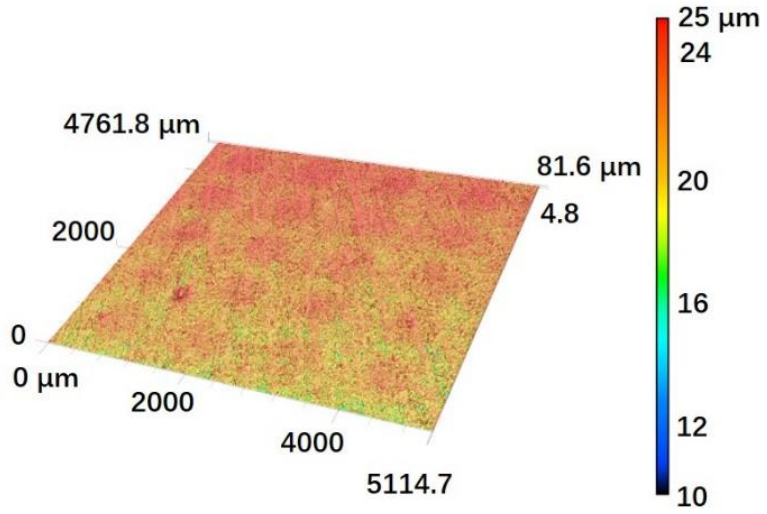

Figure IV-5. Surface morphology of the IPN ion gel layer prepared by spin coating on a glass plate.

Subsequently, to investigate the effect of the PVDF–HFP/poly(DMAAm-*co*-NSA) network compositions on the IPN ion gel mechanical properties, ion gels with different PVDF–HFP/IPN ratios were prepared. The PVDF–HFP ratio in the PVDF–HFP/poly(DMAAm-*co*-NSA) IPN varied from 0 to 1 g/g. The IPN and IL contents of the IPN ion gels were fixed at 20 wt% and 80 wt%, respectively. The ion gel mechanical properties were evaluated using uniaxial tensile tests. The obtained tensile stress–strain curves are shown in Figure IV-6(a). The mechanical strength of the ion gels dramatically increased with increasing PVDF–HFP weight ratio in the IPN. The mechanical properties of the ion gels, such as Young's modulus, fracture stress, fracture strain, and fracture energy, were determined from the stress–strain curves. These are summarized in Figure IV-7. From the results, it was found that

the mechanical properties tended to increase with increasing the PVDF–HFP ratio. These results indicate that the PVDF–HFP network greatly enhances the mechanical strength of the IPN ion gel.

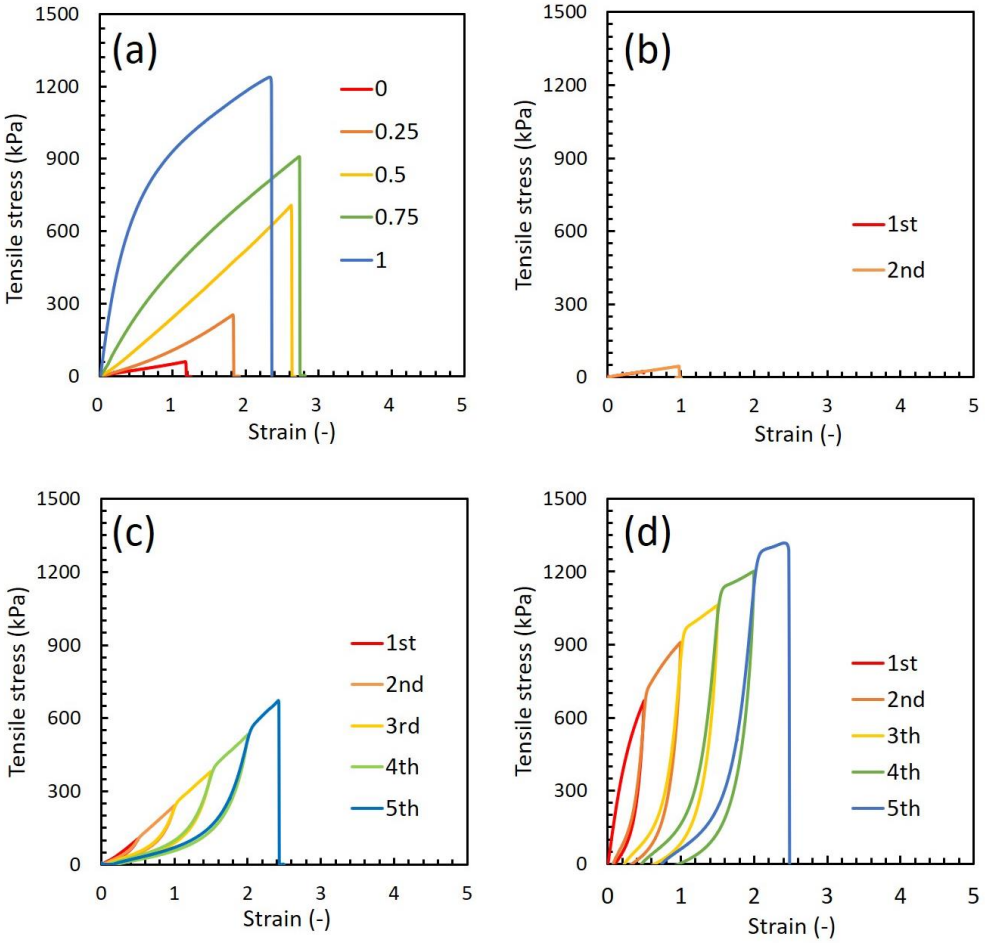

Figure IV-6. (a) Stress–strain curves measured by the uniaxial tensile test of the ion gels fabricated with different PVDF–HFP/IPN weight ratios. (b–d) Stress–strain curves measured by the cyclic tensile test of ion gels with PVDF–HFP/IPN ratios of (b) 0 g/g (poly(DMAAm-*co*-NSA) SN ion gel); (c) 0.5 g/g (IPN ion gel); and (d) 1 g/g (PVDF–HFP SN ion gel). The ion gels were formed at an evaporation temperature of 50 °C.

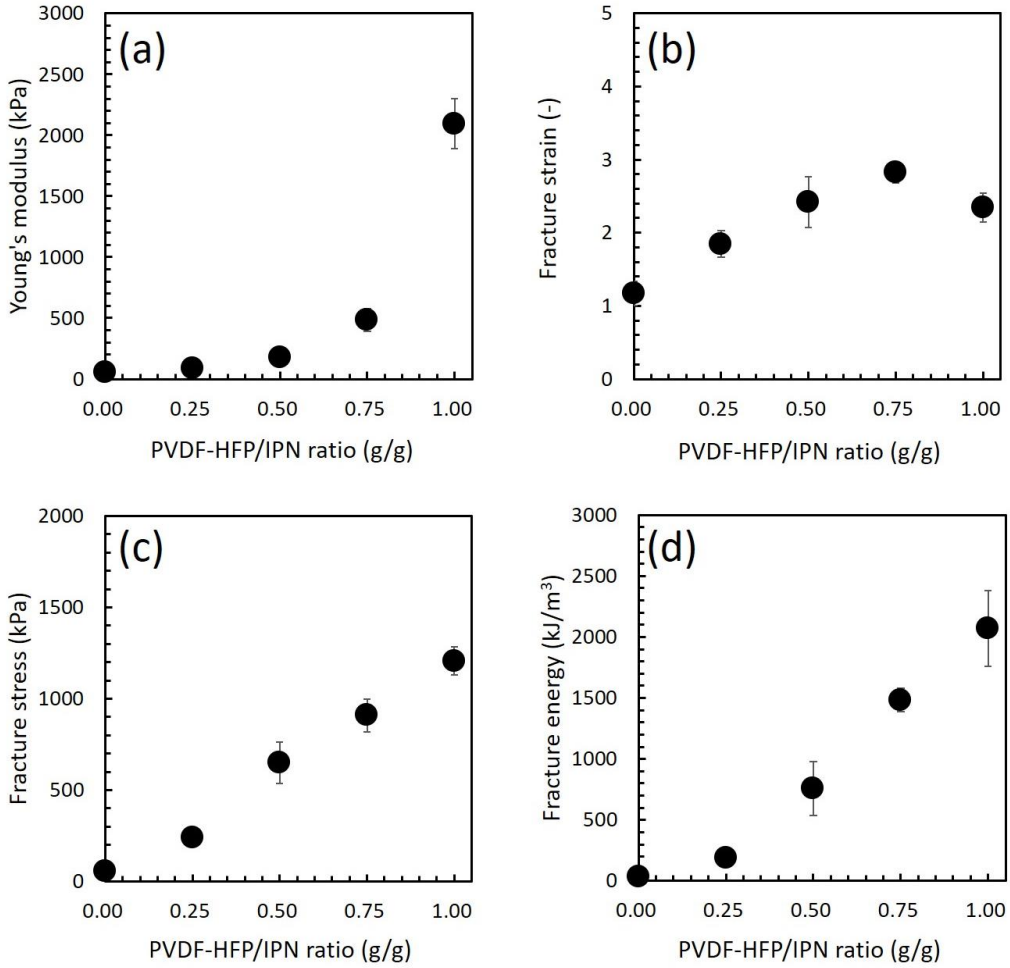

Figure IV-7. (a) Young's modulus; (b) fracture strain; (c) fracture stress; and (d) fracture energy of the ion gels fabricated with different PVDF–HFP/IPN weight ratios. The ion gels were prepared at the evaporation temperature of 50 °C.

Furthermore, to clarify the effect of the PVDF–HFP network on the high mechanical strength, the results of the cyclic tensile test of the ion gels with PVDF–HFP/IPN ratios of 0, 0.5, and 1.0 g/g were measured as shown in Figure IV-6(b), (c), and (d), respectively. The cyclic tensile stress–strain curves of the ion gels with PVDF–HFP/IPN ratio of 0.5 g/g (IPN ion gel) and 1 g/g (PVDF–HFP SN ion gel) showed clear hysteresis, while that of the poly(DMAAm-*co*-NSA) SN ion gel showed no hysteresis. These results indicate that the PVDF–HFP network dissipated the energy loaded to the ion gels.

To compare the amounts of crystalline PVDF in the IPN ion gels, the XRD patterns were normalized using the structured [Emim][Tf_2N] peak. The normalized IPN ion gel XRD patterns are shown in Figure IV-3(b). As shown in this figure, the crystalline part of PVDF in the IPN ion gels increased with

the increase in the PVDF–HFP/IPN weight ratio. Regarding the mechanical properties, as mentioned above, the ion gels with the PVDF–HFP network dissipated the loaded energy. As indicated in Figures IV-6(c) and (d), the dissipated energy, which corresponds to the area of the hysteresis loop, became large with increasing the PVDF–HFP/IPN ratio in the ion gel. From these results of the amount of the PVDF crystalline part and the mechanical property of the IPN ion gel, it was considered that the destruction of the PVDF crystalline region in PVDF–HFP network dissipated the loaded energy during the stretching process.

To further confirm the effect of the PVDF crystalline part on the enhancement of the mechanical strength of the IPN ion gels, the mechanical properties of the IPN ion gels with different crystallinity of the PVDF network were measured. In general, the temperature is a vital factor that affects the crystallization process [92, 93]. The crystallinity of the PVDF networks in this study was found to be controlled by the evaporation temperature, defined as the temperature of the acetone removal process during the ion gel preparation. The uniaxial tensile stress–strain curves of ion gels prepared at different evaporation temperatures are shown in Figure IV-8. The ion gel mechanical properties determined from the stress–strain curves are summarized in Figure IV-9. As can be seen in these figures, the mechanical properties of the PVDF–HFP SN ion gels were strongly dependent on the evaporation temperature. As shown in Figure IV-10, the dissipated energy of the PVDF–HFP SN ion gels increased with increasing evaporation temperature. Furthermore, the SN ion gel XRD patterns normalized by the structured [Emim][Tf_2N] peak ($2\theta = 12.5°$) are shown in Figure IV-11(a); the intensity of the XRD peak at $2\theta = 20.0°$, which results from the PVDF crystalline structure in the PVDF–HFP SN ion gel, increased with increasing evaporation temperature. These results further suggest that energy dissipation was caused by the destruction of the crystalline part of the PVDF segment.

On the other hand, as shown in Figures IV-8 and IV-9, the mechanical properties of the IPN ion gels changed only slightly with increasing evaporation temperatures. As show in Figure IV-4(b), the crosslinking reaction extent of the poly(DMAAm-*co*-NSA) network was decreased with increasing evaporation temperatures. This might be because the time for solvent evaporation was dramatically shortened and resulting a rapid increase of the viscosity of the precursor solution. However, it is considered that the mechanical properties were mainly dominated by the PVDF–HFP network. Therefore, the decrease of the crosslinking reaction extent did not strongly contribute to the mechanical

properties. As shown in Figure IV-12, the evaporation temperature scarcely affected the dissipated energy of the IPN ion gels. The crystallinity of the PVDF segment in the IPN ion gel was hardly dependent on the evaporation temperature, as shown in Figure IV-11(b). This might be because the chemically cross-linked poly(DMAAm-*co*-NSA) network interpenetrated with the PVDF–HFP network and inhibited the crystallization of PVDF segments. These relationships among the mechanical properties, dissipated energy, and crystallinity of the PVDF segment of the IPN ion gels also suggest that the IPN ion gel mechanical properties were dominated by the PVDF crystalline portion, which dissipated the loaded energy like a sacrificial bond.

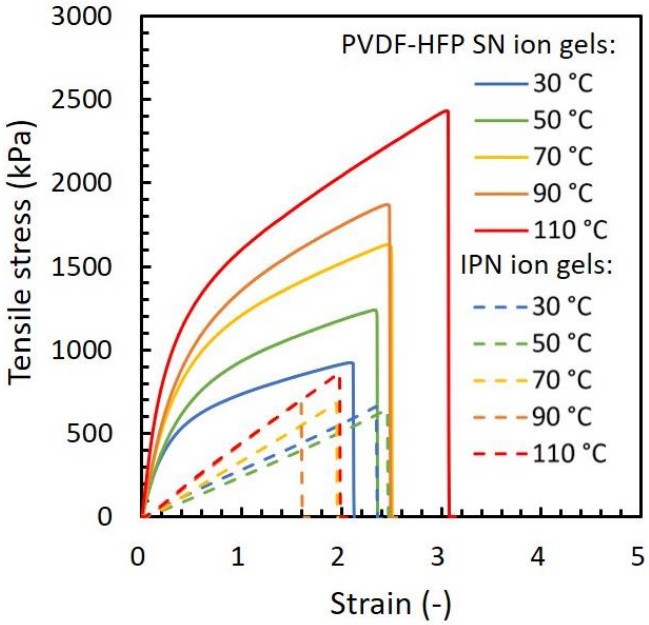

Figure IV-8. Stress–strain curves measured by the uniaxial tensile test of the PVDF–HFP SN ion gels and the IPN ion gels fabricated at different evaporation temperatures. The PVDF–HFP/IPN ratio of the IPN ion gels is fixed at 0.5 g/g. The IL content of the ion gels was fixed at 80 wt%.

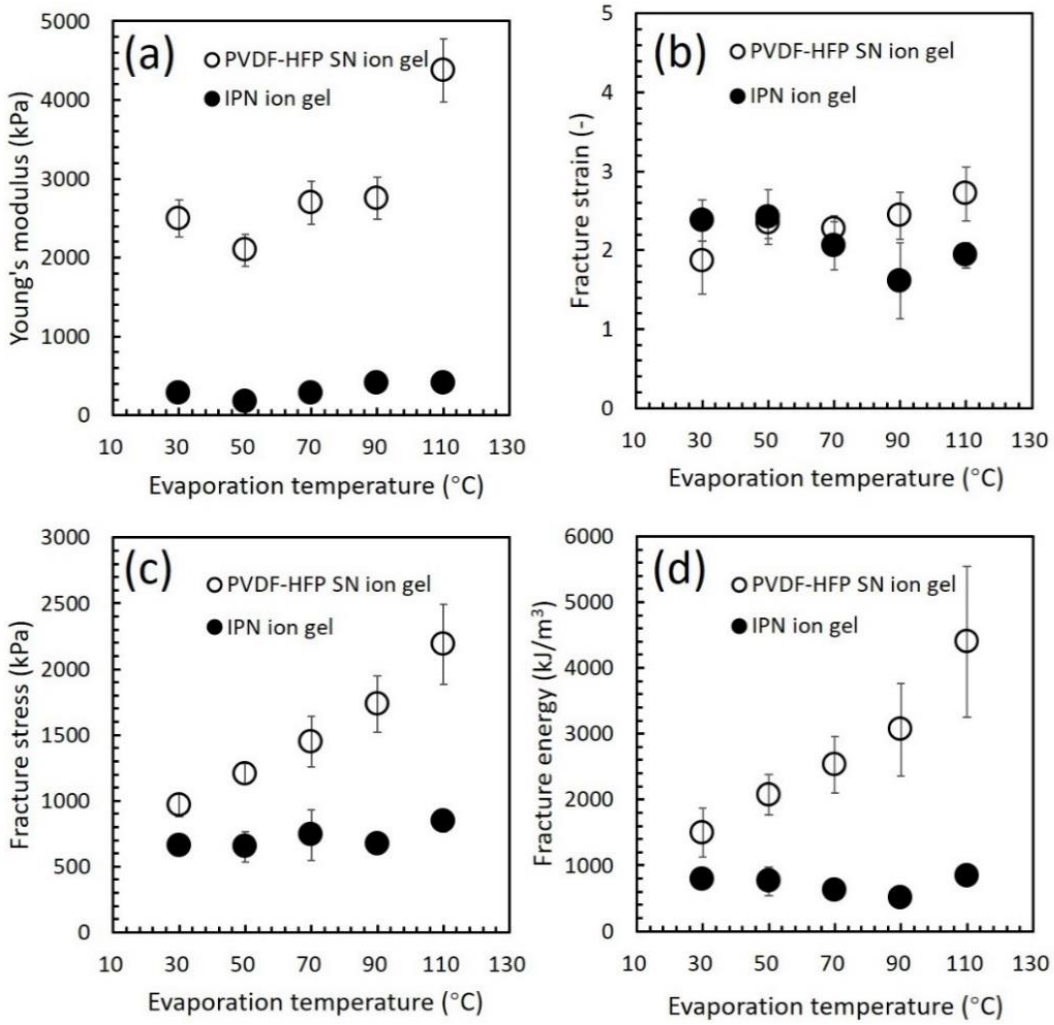

Figure IV-9. (a) Young's modulus, (b) fracture strain, (c) fracture stress, and (d) fracture energy of the ion gels fabricated at different evaporation temperatures. The PVDF–HFP content in the PVDF–HFP/poly(DMAAm-co-NSA) networks of the IPN ion gel is 50 wt%. The IL content of the ion gels was fixed at 80 wt%.

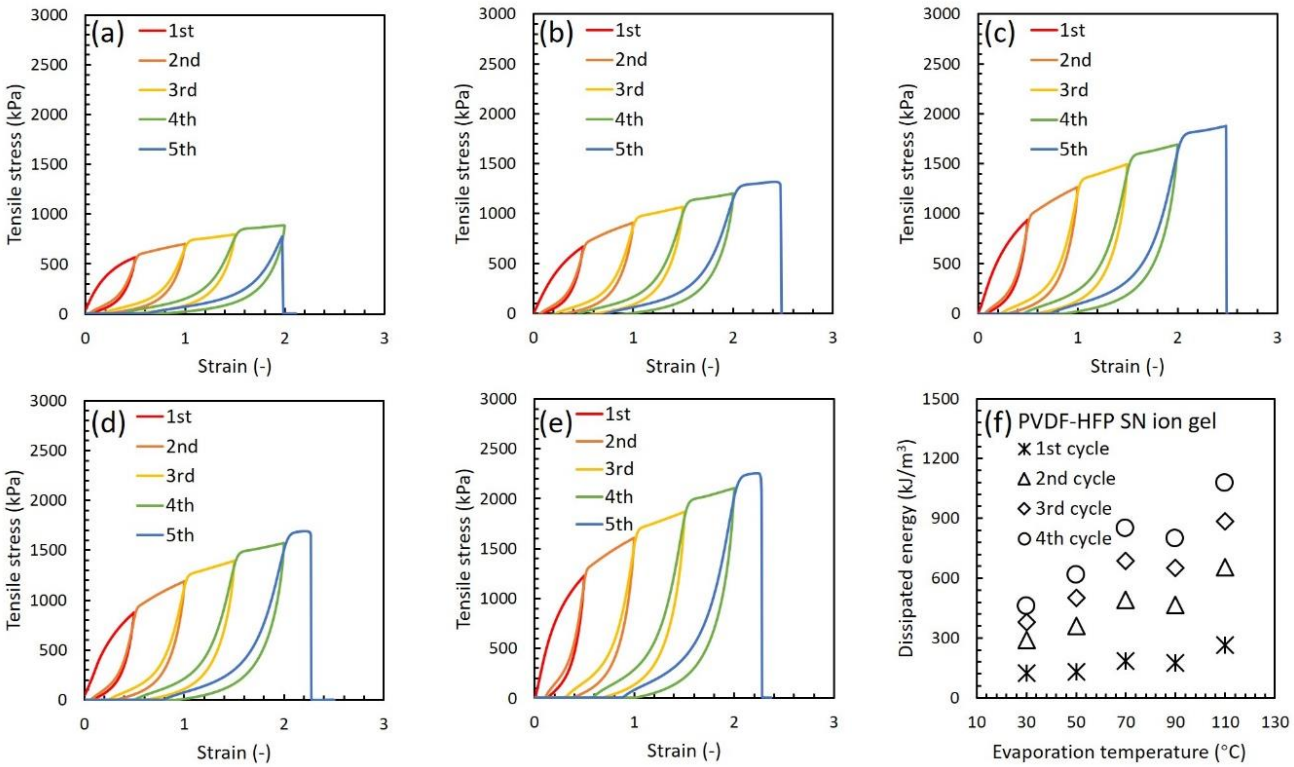

Figure IV-10. Cyclic tensile stress–strain curves of the PVDF–HFP SN ion gels prepared at the evaporation temperatures of (a) 30 ºC; (b) 50 ºC; (c) 70 ºC; (d) 90 ºC; and (e) 110 ºC, respectively. (f) Dissipated energy calculated from the cyclic tensile stress–strain curves of the PVDF–HFP SN ion gels fabricated under different evaporation temperatures. The PVDF–HFP/IPN ratio was 0.5 g/g. The IL contents of the ion gels were fixed at 80 wt%.

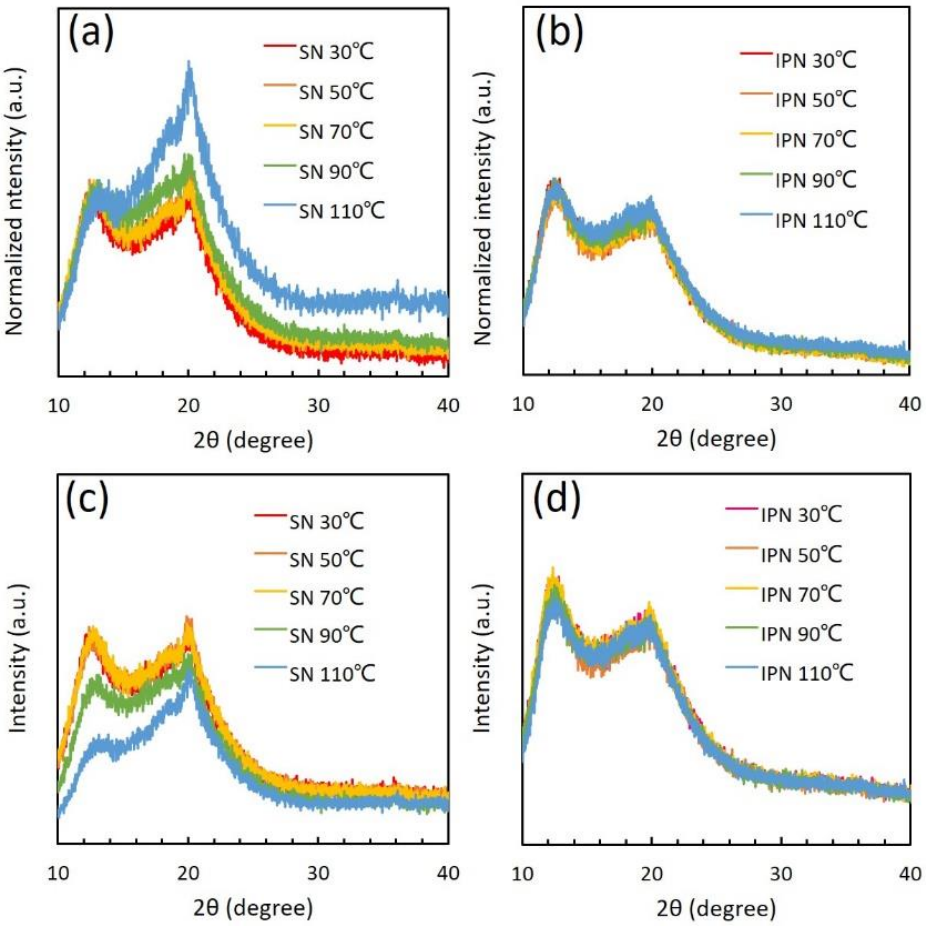

Figure IV-11. XRD patterns of the ion gels fabricated under different evaporation temperatures. The patterns normalized by the structured [Emim][Tf_2N] peak of (a) the PVDF–HFP SN ion gels and (b) the IPN ion gels. The original patterns of (c) PVDF–HFP SN ion gels and (d) IPN ion gels. The IL contents of the ion gels were 80 wt%. The IPN ion gels were prepared with PVDF–HFP/IPN ratio of 0.5 g/g.

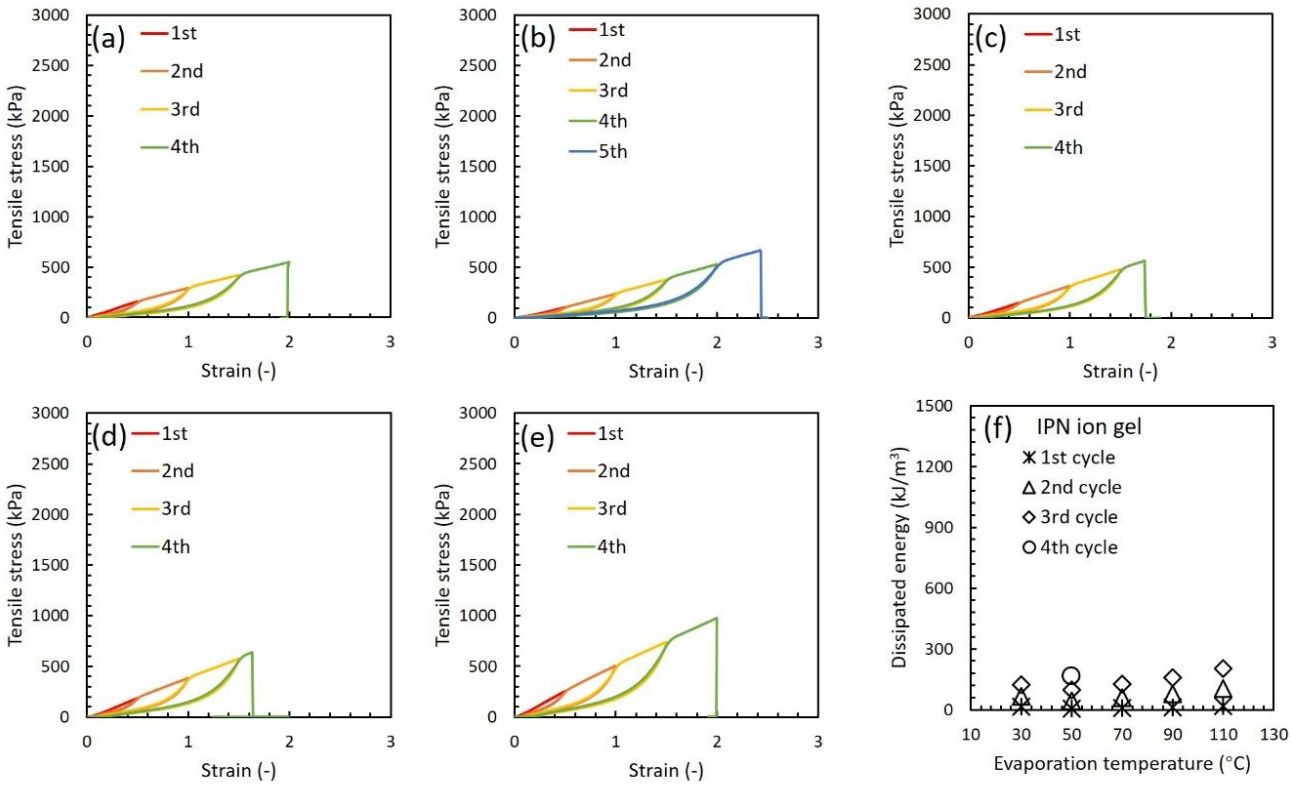

Figure IV-12. Cyclic tensile stress–strain curves of the IPN ion gels prepared at the evaporation temperatures of (a) 30 °C; (b) 50 °C; (c) 70 °C; (d) 90 °C; and (e) 110 °C, respectively. (f) Dissipated energy calculated from the cyclic tensile stress–strain curves of the IPN ion gels fabricated under different evaporation temperatures. The PVDF–HFP/IPN ratio was 0.5 g/g. The IL contents of the ion gels were fixed at 80 wt%.

To the best of our knowledge, the PVDF–HFP SN ion gel fabricated at the evaporation temperature of 110 °C has the highest fracture energy (4396 kJ/m^3) (Figure IV-9(d)) in comparison to the reported ion gels with the same IL content of 80 wt%. However, as shown in Figure IV-13, the PVDF–HFP SN ion gel (PVDF–HFP/IPN ratio of 1 g/g) exhibited poor IL holding property. This is a serious problem for the practical application of ion gels. By contrast, the IL was hardly leaked from the poly(DMAAm-*co*-NSA) ion gel (PVDF–HFP/IPN ratio of 0 g/g) as shown in Figure IV-13(a). This was because of the good compatibility between poly(*N*,*N*-dimethylacrylamide) and [Emim][Tf_2N].[94] Thus, as shown in Figure IV-13(a), for the IPN ion gels, the IL leakage monotonically decreased with the increase in the ratio of poly(DMAAm-*co*-NSA) in the IPN. This result indicated that poly(DMAAm-*co*-NSA) effectively improved the IL holding property of the IPN ion gels. However, as shown in

Figures IV-7 and IV-13(a), the mechanical strength and IL holding property of the IPN ion gel are in a trade-off relationship, i.e. when the PVDF-HFP network ratio increases, the mechanical strength increases but the IL holding property decreases. Therefore, in this study, a PVDF–HFP/IPN ratio of 0.5 g/g was chosen as the optimal composition for the IPN.

The effect of the evaporation temperature on the ion gel IL holding property is shown in Figure IV-13(b). The PVDF–HFP SN ion gel fabricated at elevated evaporation temperatures showed a dramatically reduced IL holding property. By contrast, the IPN ion gels fabricated under different evaporation temperatures showed excellent IL holding properties, as evidenced by their remarkably low IL leakage of the ion gel after compression. This might be attributed to the IPN structure formed in the ion gels. As discussed in previous sections, the crystalline structure formation in PVDF–HFP SN ion gels was facilitated by increasing the evaporation temperature, while the crystallinity was not dependent on the evaporation temperature for IPN ion gel preparation. Therefore, it was considered that the IL holding property decreased with the increase in the amount of the crystalline structure of the PVDF segments. In addition, the results in Figures IV-9 and IV-13(b) indicate that the mechanical properties and IL holding property of the IPN ion gel were independent of the evaporation temperature. This means that IPN ion gels with good mechanical and IL holding properties could be prepared over a wide evaporation temperature range. The preparation of IPN ion gels at elevated temperatures could effectively shorten the preparation time, which has implications for large-scale manufacturing.

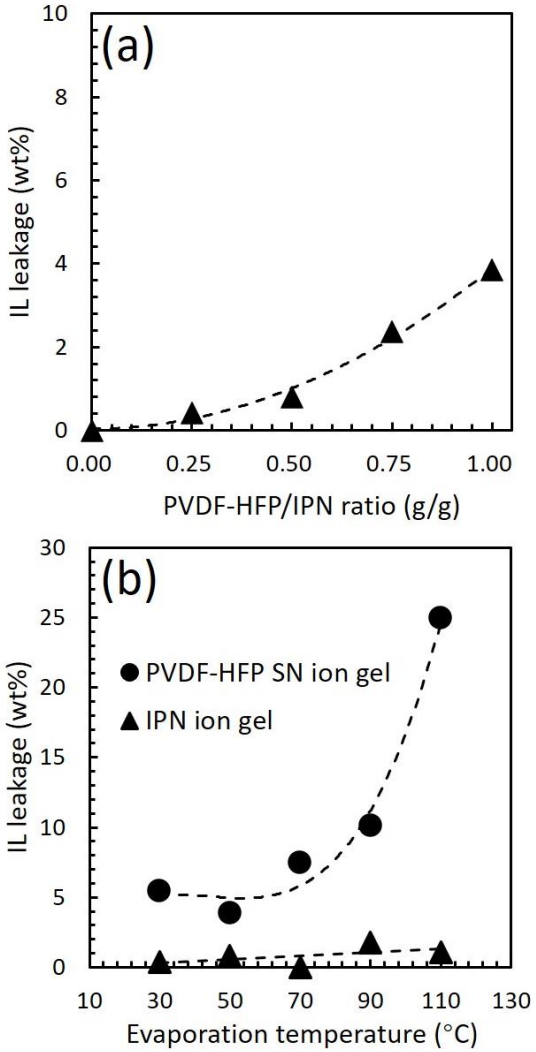

Figure IV-13. IL leakage of the ion gels after compression at the stress of 1.16 MPa: (a) Effect of PVDF–HFP/IPN weight ratios; the ion gels were fabricated at the evaporation temperature of 50 °C. (b) Effect of evaporation temperatures; the ion gels were fabricated with PVDF–HFP/IPN ratio of 0.5 g/g.

An important goal of toughening an ion gel is the fabrication of an ion gel membrane with a high IL content and manipulable mechanical strength. Hence, IPN ion gels with different IL contents were fabricated and investigated. The IL content of the ion gels was measured as described in the experimental section. The IPN ion gels with the IL contents from 80 wt% to 91.3 wt% were prepared. The extents of the crosslinking reaction of the poly(DMAAm-*co*-NSA) network kept the same level even when the IL content in the IPN ion gel increased up to 91.3 wt% (Figure IV-4(c)). The uniaxial tensile stress–strain curves of these IPN ion gels (Figure IV-14) show that the mechanical strength of

the IPN ion gels is highly dependent on their IL content. The detailed mechanical properties are summarized in Figure IV-15. As shown in Figures IV-15(a), (c), and (d), because of the decreasing content of the IPN, Young's modulus, fracture stress, and fracture energy of the IPN ion gels decreased with increasing IL content. The fracture strain of the IPN ion gel was maintained at a constant level with increasing IL content, as shown in Figure IV-15(b).

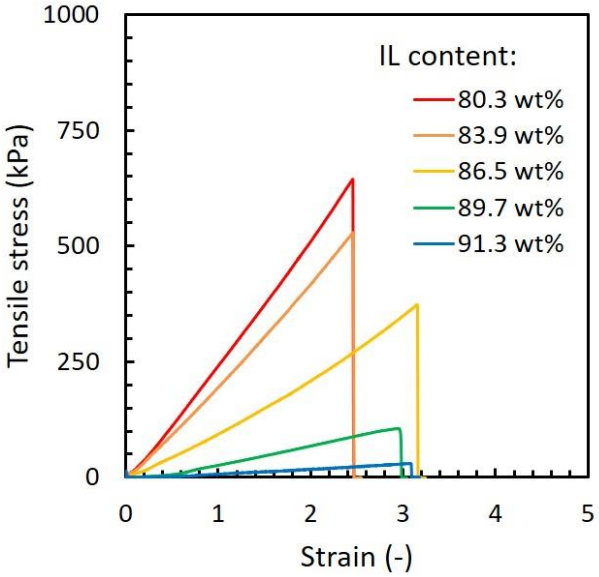

Figure IV-14. Stress–strain curves measured by the uniaxial tensile test of the IPN ion gels with different IL contents. The IPN ion gels were prepared with the PVDF–HFP/IPN ratio of 0.5 g/g at the evaporation temperature of 50 °C.

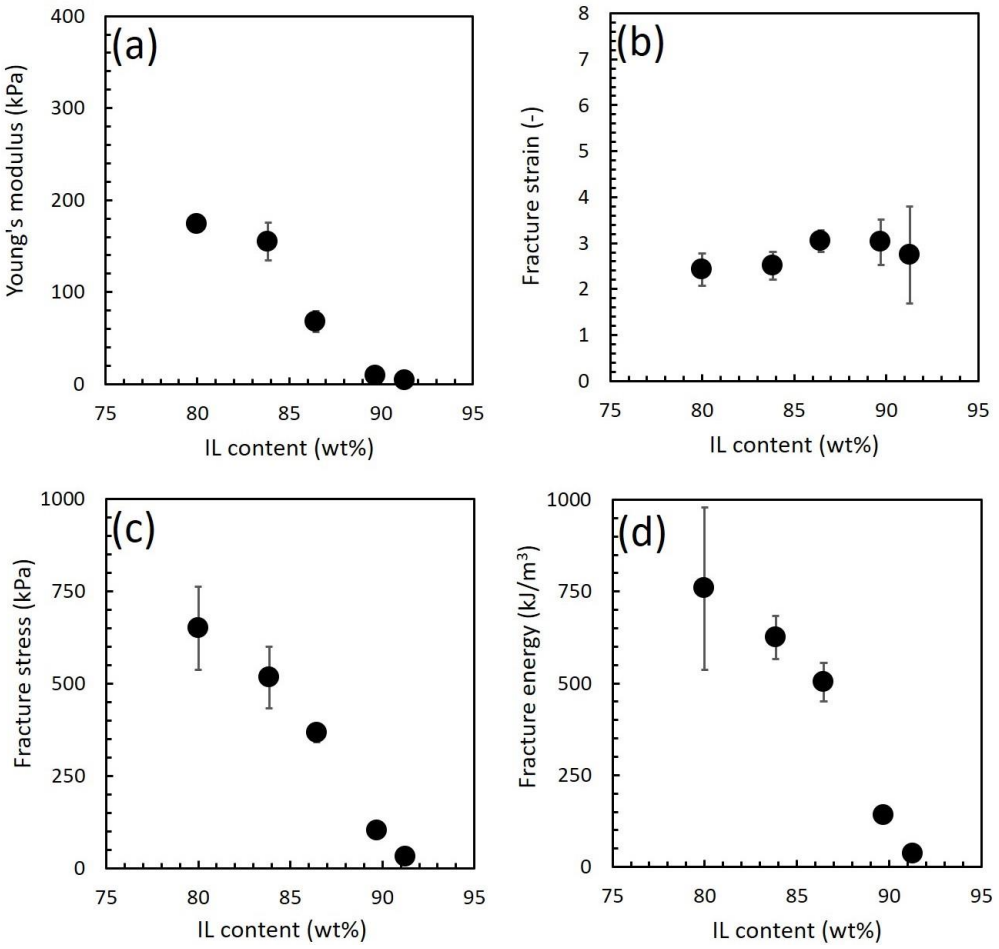

Figure IV-15. (a) Young's modulus, (b) fracture strain, (c) fracture stress, and (d) fracture energy of IPN ion gels with different IL contents. The IPN ion gels were prepared with the PVDF–HFP/IPN ratio of 0.5 g/g under the evaporation temperature of 50 °C.

Cyclic stress loading–unloading tensile tests were also performed on the IPN ion gel with an IL content of 91.3 wt%, as shown in Figure IV-16. The clear hysteresis indicated that the PVDF crystalline part was also formed in the IPN ion gel even when the ion gel has high IL content. To evaluate the IL holding property of an IPN ion gel with high IL content, the IL leakage of the IPN ion gel having 91.3 wt% of the IL was measured after compression. The IL leakage of the IPN ion gel was only 0.81 wt%, similar to the leakage amount of the IPN ion gel with 80 wt% of the IL (0.79 wt%). This result confirmed the good IL holding property of this IPN ion gel even with a high IL content.

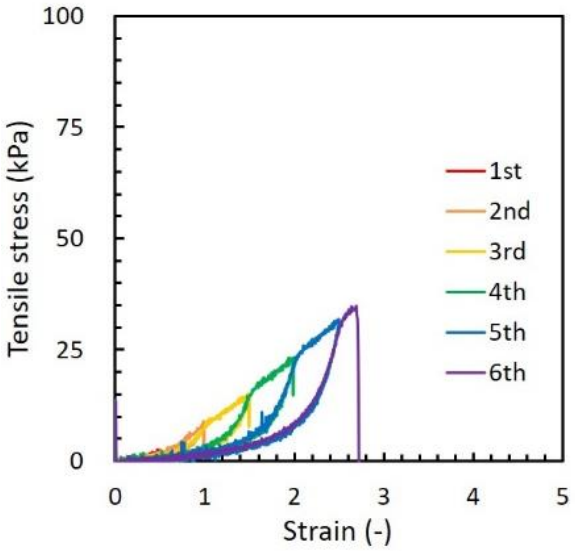

Figure IV-16. Cyclic tensile stress–strain curves of the IPN ion gel with IL content of 91.3 wt%. The IPN ion gel was prepared with PVDF–HFP/IPN ratio of 0.5 g/g under the evaporation temperature of 50 °C.

IV-3-2 Gas separation performance of the IPN ion gel membrane

The investigations above show that IPN ion gels can achieve both excellent IL holding property and high mechanical strength. The IL content of the IPN ion gel could be increased to more than 90 wt% while maintaining a manipulatable toughness. These remarkable properties indicate that IPN ion gels have great potential as gas separation membrane materials. To evaluate the gas separation performance of IPN ion gel membranes, we investigated the CO_2 and N_2 permeabilities and CO_2/N_2 permselectivities of IPN ion gel membranes fabricated under different conditions.

First, the gas separation performance of IPN ion gel membranes with different PVDF–HFP/IPN weight ratios was evaluated. The results are shown in Figure IV-17. The permeabilities of CO_2 and N_2 decreased as the PVDF–HFP ratio in the IPN increased, while the permselectivities were maintained at approximately 27. In general, gas permeation through an ion gel membrane is governed by the solution-diffusion mechanism[72, 95]. When the PVDF–HFP/IPN ratio increased, the crystalline regions in the IPN ion gel membrane increased. The crystalline region is resistant to the diffusion of dissolved gas molecules, resulting in a decrease in the gas permeability of the IPN ion gel membrane. In other words, increasing the poly(DMAAm-*co*-NSA) network ratio in the IPN can improve the gas permeability of the IPN ion gel membranes.

By contrast, the permselectivities were dominated by the solubility selectivity of the gas pair in the IL and hardly affected by the PVDF–HFP ratio. Therefore, from the gas permeation performance point of view, it can be said that the IPN ion gel membrane with a higher poly(DMAAm-*co*-NSA) ratio was preferable.

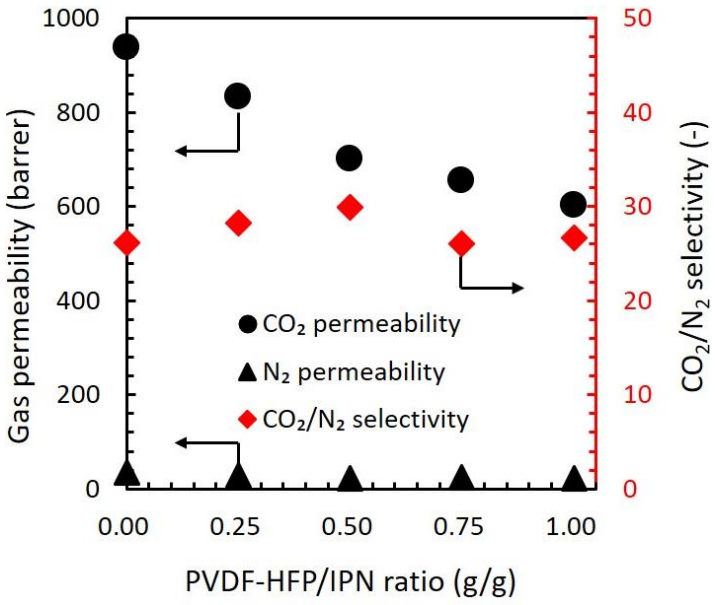

Figure IV-17. Permeabilities of CO_2 and N_2, and CO_2/N_2 permselectivities of the IPN ion gel membranes fabricated with different PVDF–HFP/IPN weight ratios. The ion gel membranes were fabricated with an IL content of 80 wt% at the evaporation temperature of 50 °C. The gas permeabilities were evaluated using 50/50 mol/mol CO_2/N_2 mixed gas at 30 °C under dry and atmospheric pressure conditions.

The gas separation performances of the IPN ion gel membranes and PVDF–HFP SN ion gel membranes fabricated at different evaporation temperatures were also investigated. As shown in Figure IV-18, the CO_2 permeability of the PVDF–HFP SN ion gel membrane decreased with increasing evaporation temperature. This was because when the PVDF–HFP SN ion gel was prepared at a high evaporation temperature, the PVDF segment crystallinity increased, resulting in higher resistance to gas transport. In addition, the CO_2/N_2 permselectivity significantly decreased to 21 when the evaporation temperature was 110 °C. This might be because the structure of the IL in the PVDF–HFP SN ion gel membrane changed when the ion gel was prepared at high evaporation temperatures, and

the CO_2/N_2 solubility selectivity in the IL decreased. As shown in Figure IV-11(c), comparing the XRD patterns of the SN ion gels, the intensity of the peak at 2θ = 12.5°, attributed to the structured IL, dramatically decreased when the evaporation temperature was 110 °C.

For the IPN ion gel membranes, as shown in Figure IV-18(b), the CO_2 permeability and CO_2/N_2 permselectivity were independent of the evaporation temperature. As shown in Figure IV-11(d), the XRD peak at 2θ = 12.5°, attributed to the structured IL, was almost unaffected by evaporation temperature changes. As discussed in the mechanical properties section, the interpenetration of the poly(DMAAm-*co*-NSA) network with the PVDF–HFP network could inhibit the change in the PVDF crystalline structure along with the change in the evaporation temperature. Hence, the CO_2 and N_2 permeabilities did not change because of the uniform structures of not only the PDVF crystalline part but also the IL in the IPN ion gel membranes prepared at different temperatures. From this result, it can be said that the IPN ion gel membrane with high CO_2 permeation performance can be prepared over a wide evaporation temperature range.

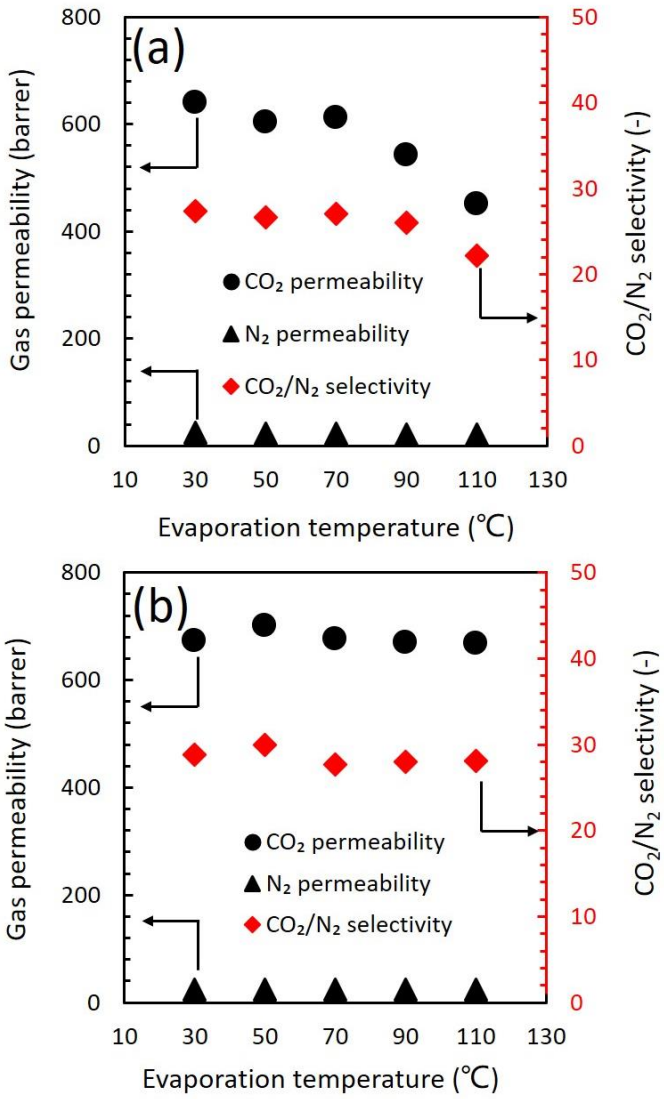

Figure IV-18. Permeabilities of CO_2 and N_2, and CO_2/N_2 permselectivities of the (a) PVDF–HFP SN ion gel membranes, and (b) IPN ion gel membranes fabricated at different evaporation temperatures. The PVDF–HFP/IPN ratio of the IPN ion gels was 0.5 g/g. The IL contents of both the SN and IPN ion gel membranes were 80 wt%. The gas permeability was evaluated using 50/50 mol/mol CO_2/N_2 mixed gas at 30 °C under dry and atmospheric pressure conditions.

Increasing the IL content of an ion gel is an effective way to increase the gas permeance of ion-gel-based membranes [71]. The CO_2 and N_2 permeabilities of IPN ion gel membranes with different IL contents are shown in Figures IV-19(a) and (b). The CO_2 permeability exponentially increased with the increasing IL content of the IPN ion gel membrane. The experimental results correlated well with the estimated CO_2 permeability dotted curve, which was calculated from the solubility coefficient and

the diffusion coefficient of CO_2 in the ion gel according to a previously reported method [71] using Equation I-9 in chapter I. The ion gel was prepared using [Emim][Tf_2N] as the IL; therefore, the diffusion coefficient (D_0 = 7.9 × 10^{-10} m^2/s) and Henry's law constant (39.6 bar) of CO_2 in pure [Emim][Tf_2N] obtained from a reported work were used for the calculation [96]. The IPN ion gel membrane with the IL content of 91.3 wt% displayed excellent CO_2 permeability of 1421 barrer, much higher than that of the IPN ion gel with the IL content of 80 wt% (670 barrer). By contrast, the CO_2/N_2 permselectivity of the IPN ion gel membranes was constant at approximately 27 and was independent of the IL content, as shown in Figure IV-19(c). The constant permselectivity indicated that the IPN ion gel membranes with high IL contents were defect-free, which was also confirmed by the good surface morphology as shown in Figure IV-20.

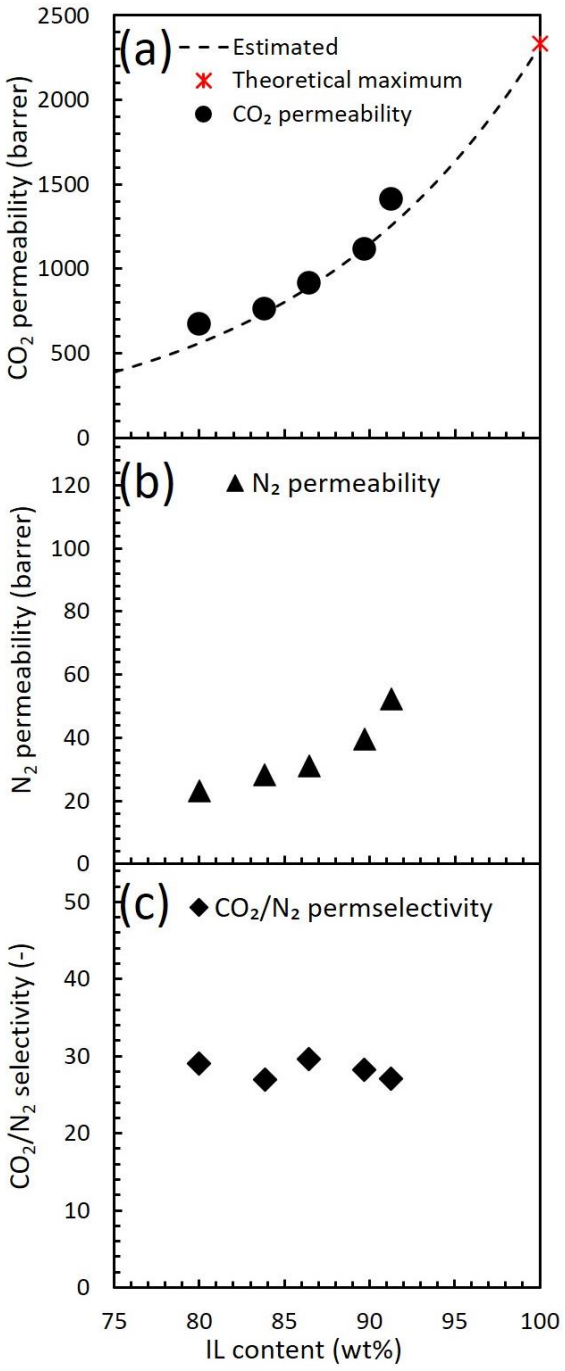

Figure IV-19. Gas separation performance of IPN ion gel membranes with different IL contents: (a) CO_2 permeability; (b) N_2 permeability; (c) CO_2/N_2 permselectivity. The IPN ion gel membranes were fabricated with the PVDF–HFP/IPN ratio of 0.5 g/g at the evaporation temperature of 50 °C. The gas permeability of the IPN ion gel membrane was evaluated using 50/50 mol/mol CO_2/N_2 mixed gas at 30 °C under dry and atmospheric pressure conditions. The estimated curve and the theoretical maximum CO_2 permeability of the [Emim][Tf_2N]-based ion gel membrane was calculated using Equation I-9.

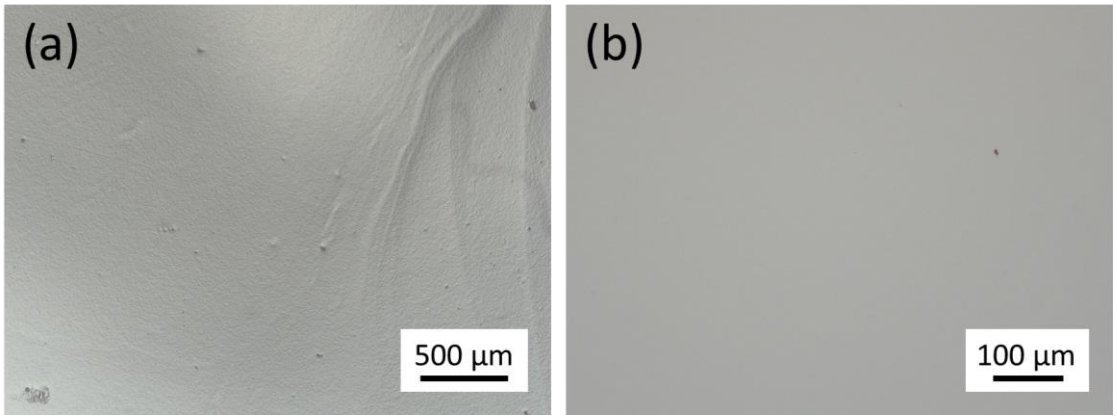

Figure IV-20. Surface morphology of the IPN ion gel with IL content of 91.3 wt%: (a) Image at low magnification and (b) image at high magnification. The IPN ion gels were prepared with PVDF–HFP/IPN ratio of 0.5 g/g at the evaporation temperature of 50 ℃. The morphology was measured by a laser microscope (VK-X3000, KEYENCE Co.).

The ion gel membrane with an IL content of 91.3 wt% was continuously operated for more than 100 h. Constant gas permeabilities and permselectivities (Figure IV-21) indicate good long-term stability of the IPN ion gel membrane. The stable gas separation performance indicated that no IL leaked from the IPN ion gel membrane during the long-time gas permeation test. From this result, it could be confirmed that the IPN ion gel membrane with 91.3 wt% IL had excellent CO_2 permeability, good CO_2/N_2 permselectivity, and good IL holding property. Thus, it can be said that the developed IPN ion gel is a promising material for high-performance CO_2 separation membranes to be used in practical CO_2 separation applications.

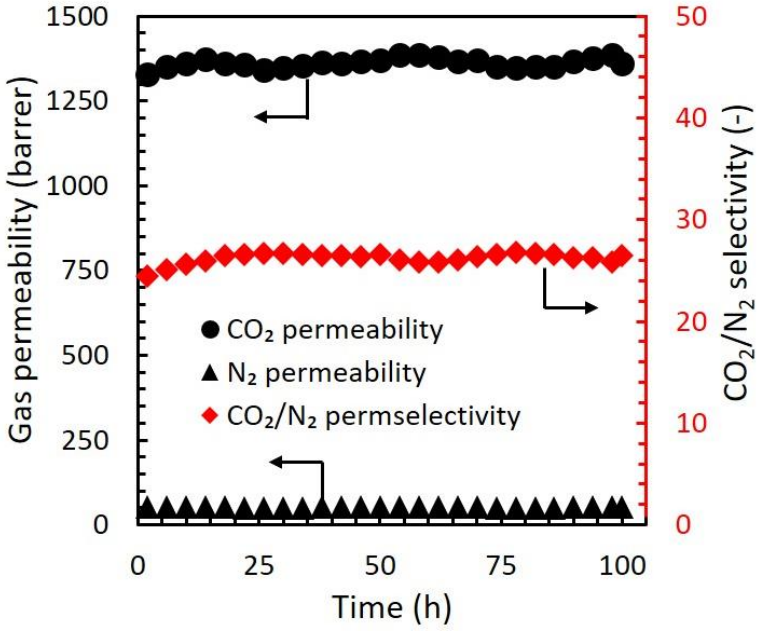

Figure IV-21. Long-term stability during the gas permeation process of the IPN ion gel membrane with the IL content of 91.3 wt%. The IPN ion gel membranes were fabricated with a PVDF–HFP/IPN ratio of 0.5 g/g at the evaporation temperature of 50 °C. The IPN ion gel membrane gas permeability was evaluated using 50/50 mol/mol CO_2/N_2 mixed gas at 30 °C under dry and atmospheric pressure conditions.

IV-4 Conclusion

A novel tough ion-gel-based CO_2 separation membrane with an IPN structure and high IL content was designed and developed. The IPN structure was fabricated by introducing a chemically cross-linked poly(DMAAm-*co*-NSA) network into a physically cross-linked PVDF–HFP network. With increased PVDF–HFP content in the polymer networks, the mechanical strength of the IPN ion gel membrane increased, while the IL holding property and gas permeability decreased. The IPN ion gel membrane (80 wt% of IL) with PVDF-HFP/IPN ratio of 0.5 g/g prepared at the evaporation temperature of 50 °C displayed high fracture energy of 758 kJ/m^3, low IL leakage (0.79 wt%) after compression, high CO_2 permeability of 670 barrer and CO_2/N_2 permselectivity of 27. In addition, the IPN ion gel membrane with a high IL content of 91.3 wt% showed not only excellent CO_2 permeability of 1421 barrer and CO_2/N_2 permselectivity of 27 but also good IL holding property. The high mechanical strength, good IL holding property, high CO_2 permeability, and high CO_2/N_2

permselectivity indicate that the IPN ion gel has good application prospects as a gas separation membrane material.

Chapter V
Development of a composite membrane with an interpenetrating polymer network ion gel layer

V-1 Introduction

For the practical application of ion gel-based membranes, the ion gels should be made into a thin film to decrease the gas transport resistance and improve the gas permeance [97-99]. Until now, fabrication of thin ion gel membrane is challenging, because ion gels are generally weak materials with poor mechanical strength. In Chapter II, the μ-DN ion gel membrane with good mechanical properties and high CO_2 separation performance was developed. Then, a composite membrane with the μ-DN ion gel thin layer was fabricated using spin coating in Chapter III. However, micron-sized particles were formed on the surface of the prepared thin μ-DN ion gel layer. The micron-sized particles would decrease the mechanical strength of the ion gel layer and restrict the preparation of the thinner μ-DN ion gel layer. The IPN ion gel developed in Chapter IV overcame the problem of the formation of the micron-sized particles. The IPN ion gel membrane shows excellent mechanical properties and high CO_2 permeability.

In this study, the composite membrane with ultra-thin IPN ion gel layer was prepared. The IPN ion gel layer was prepared on a poly(dimethylsiloxane) (PDMS) gutter layer by spin coating method. To increase the gas permeance of the composite membrane, the thickness of the IPN ion gel layer was reduced by increasing the dilution degree of the IPN ion gel precursor solution. In addition, the IL content of the IPN ion gel layer was increased to increase the CO_2 permeability of the ion gel layer and thereby improve the separation performance of the composite membrane. Theoretical estimation of the gas permeation performance of the composite membrane was also conducted to prove that IPN ion gel is a good candidate material as a selective layer of a composite membrane for efficient CO_2 separation.

V-2 Experimental section

V-2-1 Materials

Poly(vinylidene fluoride-*co*-hexafluoropropylene) (PVDF-HFP) pellets (Sigma-Aldrich) with M_w of 400000 g/mol and M_n of 130000 g/mol were used as the network material of the IPN ion gel. The other network material is poly(*N*,*N*-dimethylacrylamide-*co*-*N*-succinimidyl acrylate) (poly(DMAAm-*co*-NSA)) with NSA ratio of 2.91 mol% and M_n of 121 kg/mol, which was synthesized in accordance with the method described in the reported works [66, 70]. Diethylene glycol bis(3-aminopropyl) ether (DGBE), purchased from Tokyo Chemical Industry Co., Ltd., was used as the crosslinker of the poly(DMAAm-*co*-NSA). The IL, 1-ethyl-3-methylimidazolium bis(trifluoromethanesulfonyl)imide ([Emim][Tf_2N]), was purchased from Tokyo Chemical Industry Co., Ltd. and used as received. As the diluent of the IPN ion gel precursor solution, acetone (99.5 wt%), purchased from FUJIFILM Wako Pure Chemical Co., Ltd., was used. Sylgard 184 silicone elastomer base and curing agent, purchased from Dow Silicones Co., Ltd, were used for the preparation of the PDMS gutter layer. Poly(sodium 4-styrenesulfonate) (average M_w of ~70000, Sigma-Aldrich co.) was used as a sacrificial layer for the preparation of the gutter layer.

V-2-2 Preparation of IPN ion gel precursor solution

The precursor solution of the PVDF-HFP/poly(DMAAm-*co*-NSA) IPN ion gel was prepared by dissolving PVDF-HFP, poly(DMAAm-*co*-NSA), DGBE and [Emim][Tf_2N] in acetone. The detailed preparation procedures are described elsewhere [100]. In this study, the weight ratio of PVDF–HFP to the sum of IPN precursors (PVDF–HFP, poly(DMAAm-*co*-NSA), and DGBE) was fixed at 0.5 g/g, and molar ratio of DGBE/NSA was fixed at 0.5 mol/mol. The precursor solutions of the IPN ion gel with different dilution degrees were prepared by changing the weight ratio of acetone to the sum of the IL and network precursors. This ratio was defined as *r* to indicate the dilution degree of the IPN ion gel precursor solution. The higher *r* value means the higher dilution degree of the IPN ion gel precursor solution.

V-2-3 Preparation of the support membrane

The PDMS gutter layer was prepared in accordance with the previously reported method [78, 101]. First, the glass plate was cleaned and treated for 5 min by air plasma (YHS-R, Kai Semi-conductor

Co., Ltd.). Poly(sodium 4-styrenesulfonate) aqueous solution (30 wt%) was spin coated on the plasma-treated glass plate at the rotation speed of 3000 rpm for 1 min using a spin coater (MS-A100, Mikasa Co., Ltd.). The glass plate with the poly(sodium 4-styrenesulfonate) layer was dried on a hot plate at 120 ºC for 5 min. The base and curing agent of Sylgard 184 were mixed in 10:1 mass ratio and they were diluted by hexane to adjust the concentration to 5 wt%. This solution was spin coated on the glass plate with the poly(sodium 4-styrenesulfonate) layer at the rotation speed of 4000 rpm for 1 min. Then, it was dried on a hot plate at 120 ºC for 30 min to conduct the crosslinking reaction of the PDMS layer. A PTFE porous membrane (Toyo Roshi Kaisha, Ltd., Japan; pore size: 0.1 μm) was pasted on the PDMS layer and they were immersed in pure water. Because the poly(sodium 4-styrenesulfonate) layer was dissolved in water, the PTFE membrane with the PDMS gutter layer was separated from the glass plate. The PDMS layer surface was washed by pure water to completely remove the residual poly(sodium 4-styrenesulfonate). Finally, it was dried at ambient temperature. The prepared PDMS gutter layer had the CO_2 permeance of 1600 GPU and CO_2/N_2 permselectivity of 5.61.

V-2-4 Preparation and characterization of the self-standing IPN ion gel membrane

Evaluation of the mechanical strength, surface morphology, and CO_2 and N_2 permeability of the IPN ion gel membrane prepared with the precursor solution with different dilution degree was conducted using thick self-standing IPN ion gel membrane. The self-standing IPN ion gel membrane with IL content of 80 wt% was prepared as follows. The precursor solution was poured into an open mold and put in an oven at 50 ℃ for 24 h to roughly evaporate the diluent (acetone). Subsequently, the prepared self-standing IPN ion gel was completely dried on a hot plate at 70 ℃ for 24 h. The thickness of the IPN ion gel membrane was determined by observing the cross section of the membrane using a field-emission scanning electron microscope (FE-SEM JSM-7500F, JEOL Ltd., Japan). The tensile strength of the self-standing IPN ion gels was measured using a universal testing instrument (EZ-LX, Shimadzu CO., Japan). The thickness of dumbbell-shaped IPN ion gel samples was measured using a digital microscope system (LEICA DMS300) and used to calculate the tensile stress. The tensile strain was increased at the rate of 100 mm/min. The loading-unloading cyclic tensile test was carried out to evaluate the dissipated energy caused by the force application. In the cyclic tensile test, the strain was increased by 0.5 per cycle.

V-2-5 Preparation of the composite membrane with thin IPN ion gel layer

The CO_2 permeation performance of the thin IPN ion gel membrane was evaluated using the composite membrane composed of thin IPN ion gel layer, PDMS gutter layer, and porous PTFE support. The composite membrane was prepared as follows. The IPN ion gel precursor solution was spin coated on the support membrane with PDMS gutter layer at the rotation speed of 1000 rpm for 20 s. In this study, just before the use, the PDMS gutter layer was pre-treated by the air plasma for 2.0 s to improve the wettability by the precursor solution. After spin coating the precursor solution, the composite membrane was dried in an oven at 50 ℃ for 24 h. The surface morphology and roughness of the IPN ion gel was measured using a laser microscope (KEYENCE, VK-X3000). The thickness of the IPN ion gel layer was measured using an FE-SEM. To control the thickness of the IPN ion gel layer, the precursor solution with different dilution degree was used. In addition, the precursor solution with large IL content was used to increase the IL content of the IPN ion gel layer. The compositions of the precursor solutions are shown in Table V-1.

Table V-1. Compositions of the precursor solutions for IPN ion gel layer preparation

(a) Compositions of the IPN ion gel precursor solutions with different dilution degrees

	Sample 1	Sample 2	Sample 3	Sample 4	Sample 5	Sample 6	Sample 7
Dilution degree (*r*) (g/g)	1.6	4.0	5.6	8.0	12.8	16	24
IL content (wt%)	80	80	80	80	80	80	80
[Emim][Tf_2N] (g)	5.12	5.12	5.12	5.12	5.12	5.12	5.12
PVDF-HFP (g)	0.64	0.64	0.64	0.64	0.64	0.64	0.64
Poly(DMAAm-*co*-NSA) (g)	0.62	0.62	0.62	0.62	0.62	0.62	0.62
Cross-linker; DGBE (g)	0.02	0.02	0.02	0.02	0.02	0.02	0.02
Acetone (g)	10.24	25.6	35.84	51.2	81.92	102.4	153.6

(b) Compositions of the precursor solutions for the preparation of the IPN ion gel with different IL contents

	Sample 1	Sample 2	Sample 3	Sample 4	Sample 5	Sample 6
Dilution degree (*r*) (g/g)	1.6	12.8	24	1.6	12.8	24
IL content (wt%)	85	85	85	90	90	90
[Emim][Tf_2N] (g)	5.44	5.44	5.44	5.76	5.76	5.76
PVDF-HFP (g)	0.48	0.48	0.48	0.32	0.32	0.32
Poly(DMAAm-*co*-NSA) (g)	0.465	0.465	0.465	0.31	0.31	0.31
Cross-linker; DGBE (g)	0.015	0.015	0.015	0.01	0.01	0.01
Acetone (g)	10.24	81.29	153.6	10.24	81.29	153.6

V-2-6 Gas separation performance evaluation

The CO_2/N_2 separation performance of the IPN ion gel membranes (self-standing and composite membranes) was evaluated by the sweep method using the permeation apparatus described elsewhere [70, 71]. The feed gas was the mixture of 50/50 mol/mol of CO_2 and N_2. It was fed to the gas permeation cell at the constant flow rate of 200 mL/min. The sweep gas (Helium) was fed to the permeation side of the gas permeation cell at the constant flow rate of 40 mL/min. The flow rates of the feed and sweep gases were controlled using a mass flow controller (Hemmi Slide Rule Co., Ltd., Japan). The gas permeation test was conducted at 30 °C and atmospheric pressure. The compositions of the permeated CO_2 and N_2 in the sweep gas was measured using gas chromatograph (GC-8A, Shimadzu Co., Japan) and used to calculate the CO_2 and N_2 permeances.

V-3 Results and discussion

V-3-1 Effect of dilution degree of the precursor solution on the mechanical properties and surface roughness of the IPN ion gel membranes

To prepare an ultra-thin ion gel layer, the ion gel should have high mechanical strength and low surface roughness [69]. In this work, the ultra-thin ion gel layer was prepared using a highly diluted precursor solution of the IPN ion gel. Before the preparation and evaluation of the composite membrane with an ultra-thin IPN ion gel layer, the effect of the dilution degree of the precursor solution on the mechanical strength and surface roughness of the IPN ion gel was investigated. For this

investigation, the self-standing IPN ion gel membranes were used.

The mechanical properties of the IPN ion gels prepared using the precursor solution with different *r* values were evaluated by the uniaxial tensile test. The stress-strain curves are shown in Figure V-1 Young's modulus, fracture stress, fracture strain, and fracture energy of the IPN ion gels determined from the uniaxial tensile stress–strain curves are shown in Figure V-2. From these figures, it was found that the mechanical properties of the IPN ion gels prepared using the precursor solutions with different dilution degrees were nearly the same. This indicates that the dilution degree of the precursor solution does not significantly affect the mechanical strength of the IPN ion gel.

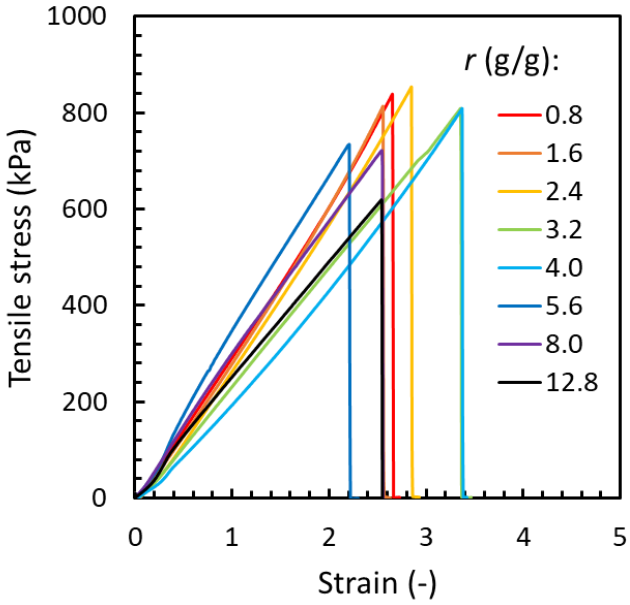

Figure V-1. Uniaxial tensile stress–strain curves of the IPN ion gels as a function of the dilution degree of the ion gel precursor solution. *r* is the weight ratio of acetone to the sum of the IL and network precursors in the precursor solution of the IPN ion gel. IL content of the IPN ion gels was 80 wt%.

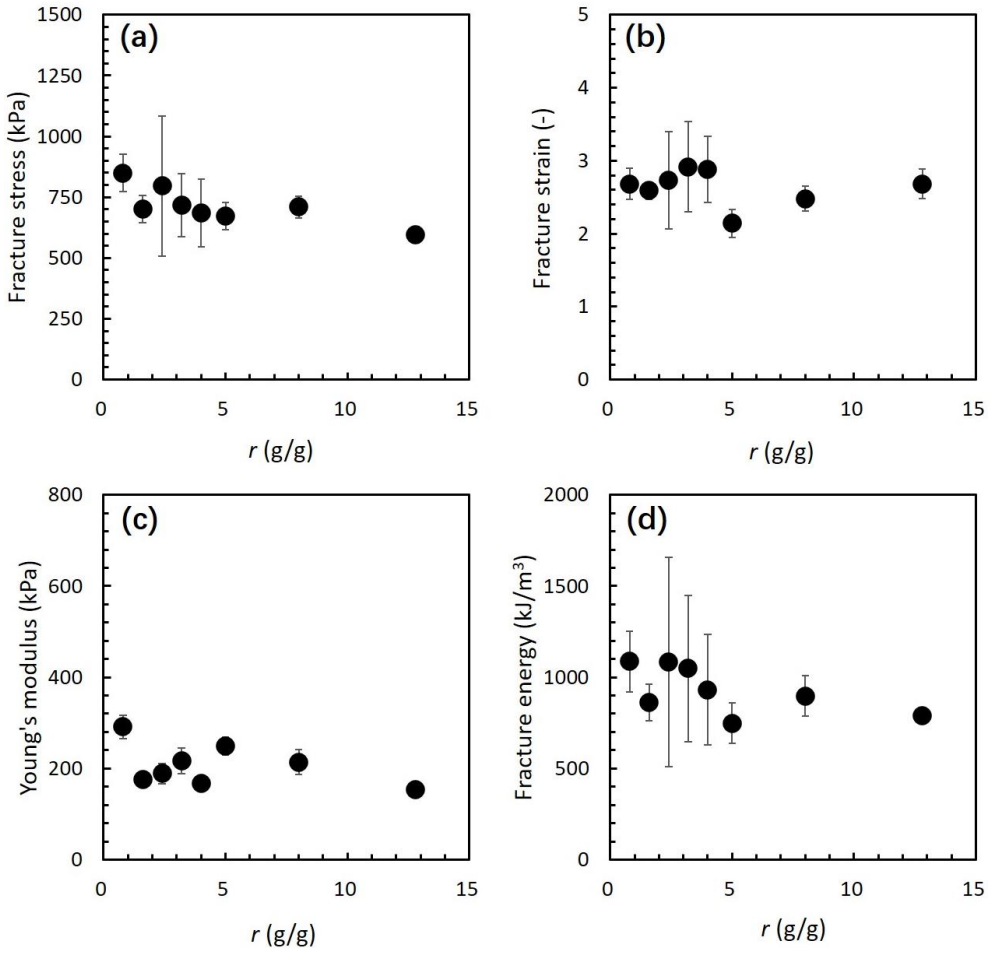

Figure V-2. (a) Young's modulus; (b) fracture strain; (c) fracture stress; and (d) fracture energy of the IPN ion gels as a function of the dilution degree of the ion gel precursor solution. *r* stands for the weight ratio of acetone to the sum of the IL and network precursors in the IPN ion gel precursor solution. IL contents of the IPN ion gels are 80 wt%.

On the other hand, the evaluation of the surface roughness of the IPN ion gel prepared using diluted precursor solution is also important. When an external force is applied to the ion gel layer, the stress would be concentrated on the thin parts, leading the defect formation and making the ion gel break easily. To avoid the defect formation in an ultra-thin ion gel layer of the composite membrane, the ion gel layer should have a low surface roughness. Therefore, the effect of the dilution degree of the precursor solution on the surface roughness of the IPN ion gel layer was investigated. In this investigation, the IPN ion gel layer was prepared on a glass plate by spin coating method. The IPN ion gel precursor solution was spin coated at the rotation speed of 1000 rpm for 20 s, then dried in an oven

at 50 ℃ for 24 h. The surface roughness of the prepared IPN ion gel layer was shown in Figure V-3. As indicated in Figure V-3, the arithmetic mean height (S_a) of the IPN ion gel thin layer decreased with increasing *r* values. The low S_a means the gel surface is smooth. Thus, when the dilution degree of the IPN ion gel precursor solution increases, the surface of the IPN ion gel layer tends to be smooth (Figure V-4). The IPN ion gel layer prepared by the highly diluted precursor solution with 24 g/g of the *r* value had a very smooth surface. This is highly preferred for the preparation of a thin ion gel layer.

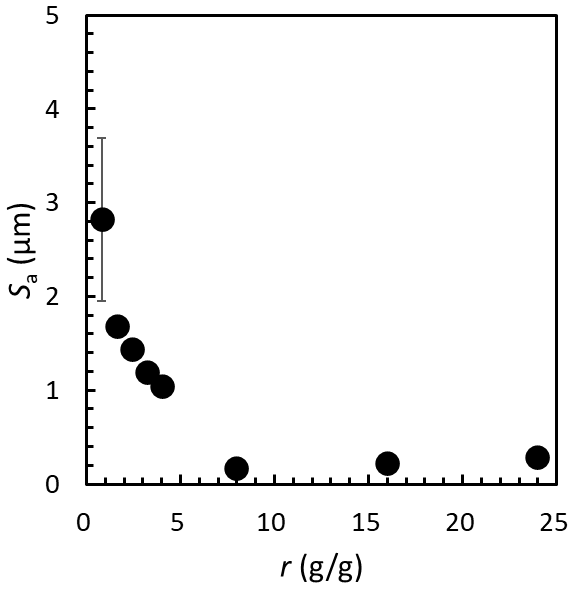

Figure V-3. Effect of dilution degree of the precursor solution on the surface roughness of the IPN ion gel containing 80 wt% of the IL.

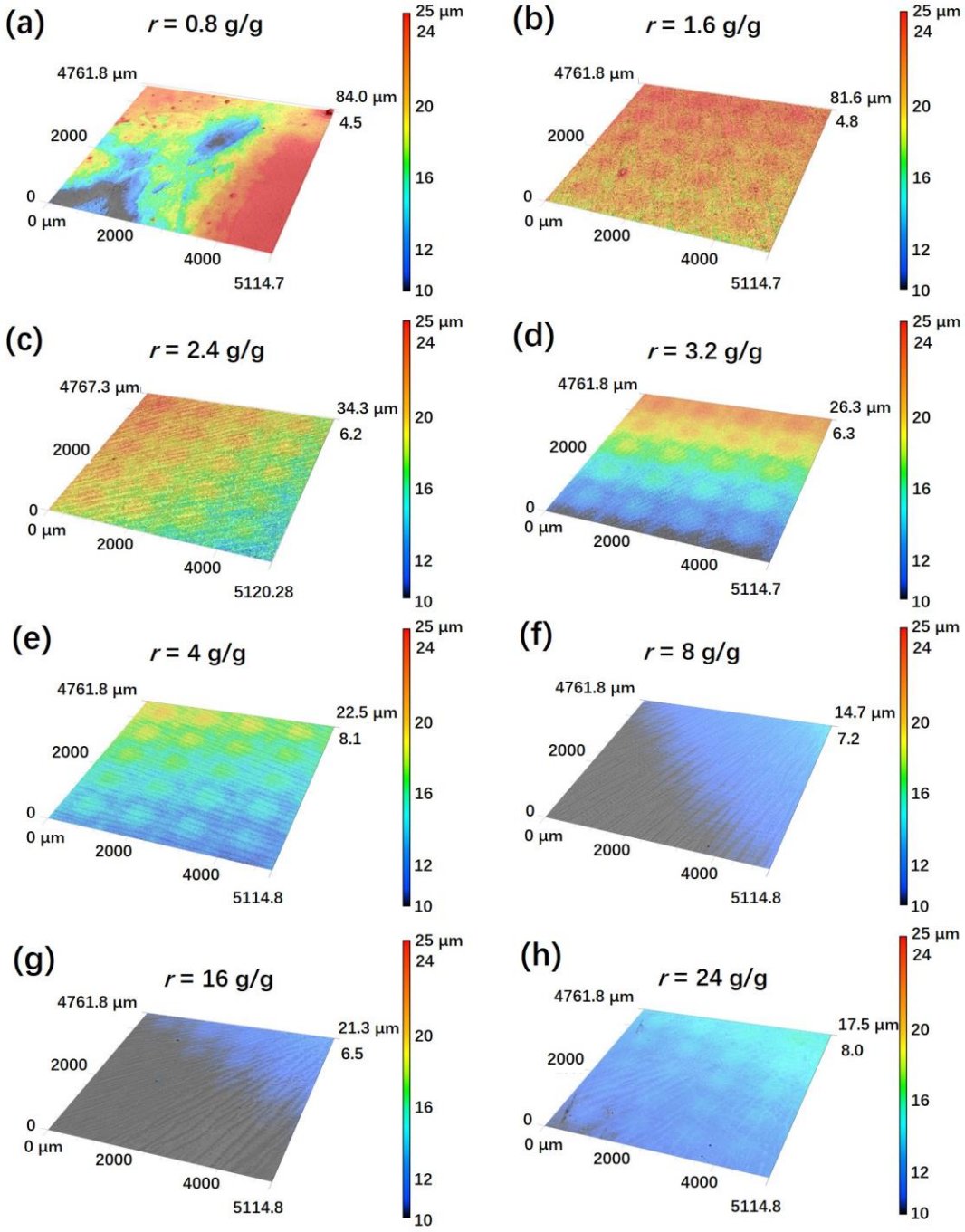

Figure V-4. Surface morphology of the IPN ion gel layer prepared by the precursor solution with *r* of (a) 0.8 g/g, (b) 1.6 g/g, (c) 2.4 g/g, (d) 3.2 g/g, (e) 4 g/g, (f) 8 g/g, (g) 16 g/g, (h) 24 g/g. *r* stands for the weight ratio of acetone to the sum of the IL and network precursors in the IPN ion gel precursor solution. IL contents of the IPN ion gels are 80 wt%.

V-3-2 Effect of dilution degree of the precursor solution on the gas permeation property of

the IPN ion gel membranes

To develop a highly and selectively CO_2 permeable composite membrane with ultra-thin IPN ion gel layer, the ion gel layer should have high CO_2 permeability and high CO_2/N_2 selectivity. Regarding the CO_2 permeation property, it was concerned that the dilution of the precursor solution of the IPN ion gel layer would affect to the CO_2 permeability and CO_2/N_2 selectivity. Thus, subsequently, the effect of the dilution degree of the precursor solution on the gas separation performance of the IPN ion gel membranes was investigated. In this investigation, the CO_2 and N_2 permeabilities were evaluated using thick self-standing IPN ion gel membranes prepared from the precursor solutions with different dilution degrees. The results are shown in Figure V-5. As shown in Figure V-5(a), the CO_2 permeabilities and CO_2/N_2 selectivities were maintained almost constant at different *r* values. This means the dilution degree of the precursor solution did not affect the gas permeation property of the IPN ion gel. This result is preferable for the preparation of ultra-thin IPN ion gel layer using diluted precursor solution. Moreover, the CO_2 permeance showed proportional relationship with the inversed thickness of the IPN ion gel membrane (Figure V-5(b)). From Figure V-5(b), the CO_2 permeability of the IPN ion gel membrane was not dependent on the membrane thickness, and was determined as 747.2 barrer.

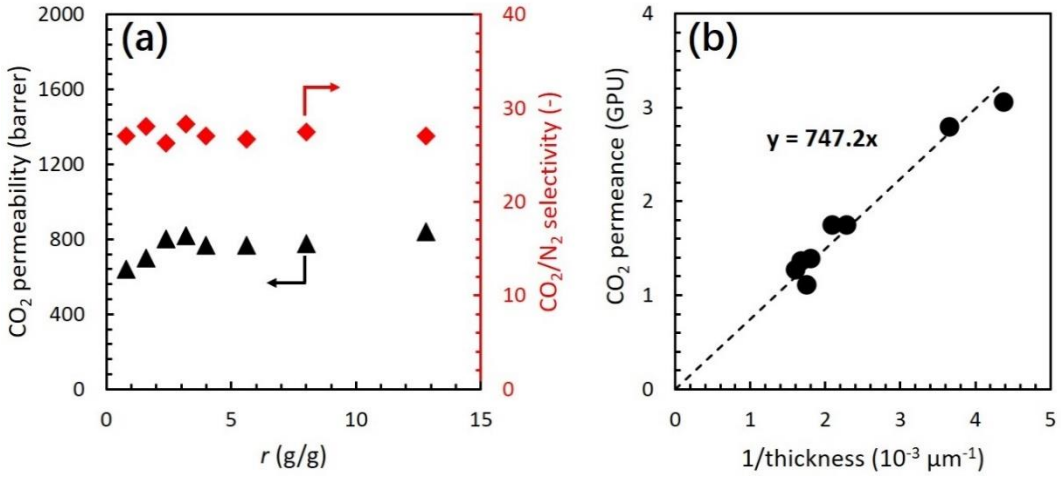

Figure V-5. CO_2 permeation property of the IPN ion gel membrane prepared using the precursor solution with different dilution degrees. (a) Effect of dilution degree on the CO_2 permeability and CO_2/N_2 permselectivity and (b) Relationship between the CO_2 permeance and inversed thickness of the IPN ion gel membrane. The IL contents of the IPN ion gel membranes were 80 wt%. The gas permeation performance was evaluated at 30 °C under dry and atmospheric pressure condition.

V-3-3 Optimization of the gutter layer for the IPN ion gel layer formation

As indicated before, the IPN ion gel membrane maintained the high mechanical strength, low surface roughness, and high and selective CO_2 permeability even when the highly diluted precursor solution was used. Hence, subsequently, the composite membrane composed of porous support membrane, PDMS gutter layer, and the thin IPN ion gel layer was prepared using the highly diluted precursor solution of the IPN ion gel. The IPN ion gel precursor solutions with different *r* values were spin coated on the PDMS gutter layers of the support membranes to prepare the composite membranes. The IL content of the IPN ion gel layer was 80 wt%.

First, the composite membrane was prepared by spin coating the precursor solution on the as-prepared PDMS gutter layer without any surface treatment. The gas permeation performance of the composite membrane is shown in Figure V-6(a). The CO_2 and N_2 permeances of the composite membrane increased with increasing *r* values but the CO_2/N_2 permselectivity dramatically decreased due to the severe defect formation as shown in Figure V-6(b).

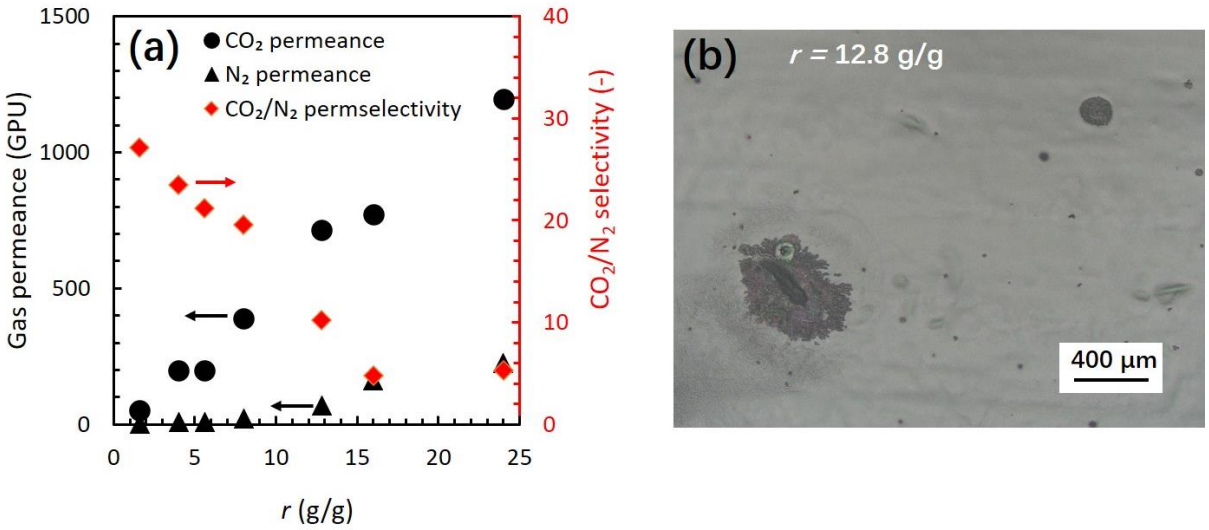

Figure V-6. (a) CO_2/N_2 separation performance of the composite membranes with the IPN ion gel layer prepared using the precursor solution with different *r* values. The IL content of the IPN ion gel layer is 80 wt%. (b) Surface morphology of the composite membrane with the IPN ion gel layer prepared on the as-prepared PDMS gutter layer with no plasma treatment. The precursor solution with *r* value of 12.8 g/g was used.

It was considered that the defect formation was because of the poor wettability between the surface of the as-prepared PDMS gutter layer and the precursor solution of the IPN ion gel and [Emim][Tf_2N]. As shown in Figure V-7(a) at the data for 0 s of the plasma treatment time, the contact angle of [Emim][Tf_2N] on the as-prepared PDMS gutter layer was very high (about 80°). Because the diluent (acetone) is highly volatile, it would be removed rapidly from the precursor solution after spin coating on the PDMS gutter layer. The evaporation of the diluent caused the deterioration of the surface wettability, and the defect formation of the IPN ion gel layer occurred. Therefore, to improve the wettability, the PDMS gutter layer was treated by air plasma before the formation of the IPN ion gel layer. As shown in Figure V-7(a), the contact angles of not only the precursor solution of the IPN ion gel but also [Emim][Tf_2N] on the PDMS gutter layer effectively decreased with increasing plasma treatment time. As shown in Figure V-7(b), even when the plasma treatment was conducted at only 2 s, the visible defects were disappeared. Therefore, it was confirmed that the plasma treatment was effective to prevent the defect formation in the thin IPN ion gel layer. However, on the other hand, it is well known that the plasma treatment affects the gas permeation performance of the PDMS gutter layer [69, 102]. Thus, to determine the preferable plasma treatment time from both wettability and gas permeability points of view, the effect of plasma treatment time on the CO_2 and N_2 permeation properties of the PDMS gutter layer and composite membrane were evaluated. The results are shown in Figures V-7(c) and (d). As for the PDMS gutter layer, along with the increase in the plasma treatment time, the CO_2 permeance decreased, but the CO_2/N_2 permselectivity was slightly increased. That is because of the decrease of the free volume in the gutter layer resulted from the conversion of polysiloxane structure to SiO_x structure after plasma treatment [103-105].

It was reported that the CO_2/N_2 permselectivity of a PDMS membrane is between 5 to 10 [106, 107]. Thus, the CO_2/N_2 permselectivity of the PDMS gutter layers shown in Figure V-7(d) indicates that no significant defect was formed in the PDMS gutter layer by the plasma irradiation. As for the composite membrane, the CO_2/N_2 permselectivity significantly increased from 12 for the as-prepared one to 20 for that after the plasma treatment for 2 s. This improvement of the CO_2/N_2 permselectivity of the composite membrane was because of the no defect formation in the IPN ion gel layer fabricated on the plasma-treated PDMS gutter layer. When the plasma treatment time was more than 2 s, the CO_2/N_2 permselectivity maintained almost constant. Therefore, it was confirmed that 2 s of the plasma

treatment was enough to form the defect-free IPN ion gel layer on the PDMS gutter layer. Regarding the CO_2 permeance of the composite membrane, it was monotonically decreased with the increase in the plasma treatment time. This is because the CO_2 permeance of the PDMS gutter layer decreases with the increasing plasma treatment time, i.e. the diffusion of the dissolved gases in the PDMS gutter layer strongly affected to the overall gas permeation of the composite membrane. Therefore, from the CO_2 permeance point of view, it was decided that the PDMS gutter layer should be treated by plasma for 2 s before IPN ion gel layer formation.

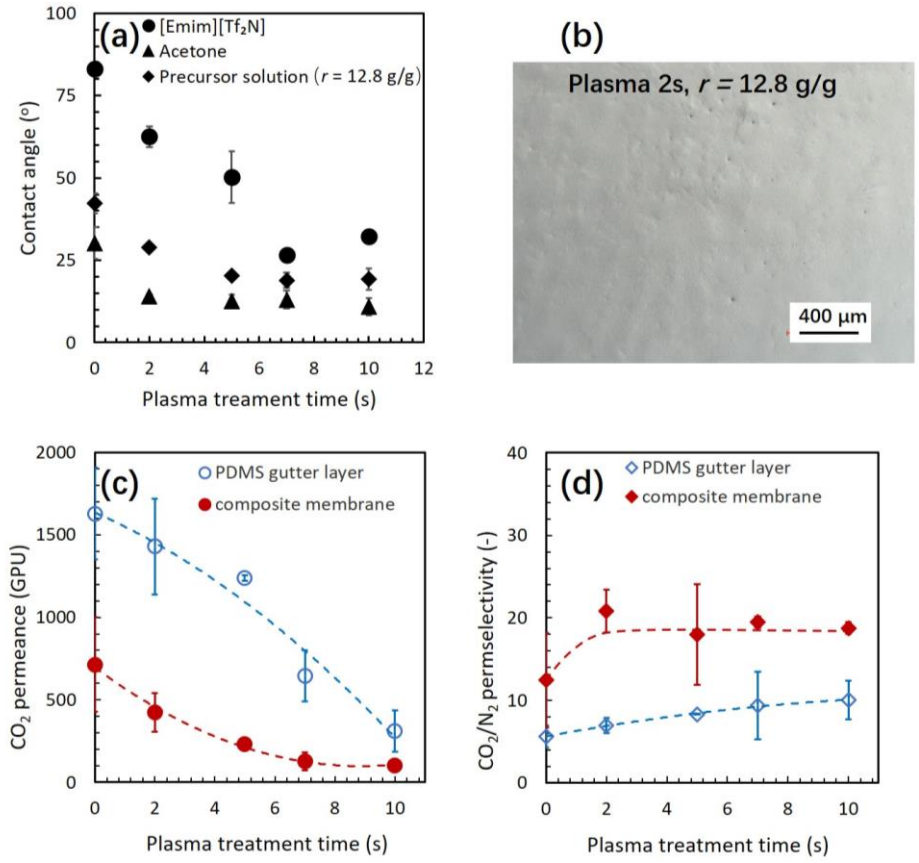

Figure V-7. Effects of the plasma treatment time on the PDMS gutter layer. (a) The contact angles of the [Emim][Tf_2N], acetone, and ion gel precursor solution on the PDMS gutter layer, (b) Surface morphology of the composite membrane prepared on the PDMS gutter layer treated by air plasma for 2s, and (c) CO_2 permeance and (d) CO_2/N_2 permselectivity of the PDMS gutter layer and the composite membrane. The precursor solution with 12.8 g/g of the *r* value was used. The weight percentage of the IL/(polymers and IL) in the precursor solution and IPN ion gel was 80 wt%. The gas permeation performance was evaluated at 30 °C under dry and atmospheric pressure condition.

V-3-4 Gas permeation performance of the composite membrane with the thin IPN ion gel layer prepared using highly diluent precursor solution

Using the PDMS gutter layer treated by plasma for 2 s, the composite membrane with the thin IPN ion gel layer was fabricated, and the CO_2 and N_2 permeances and CO_2/N_2 permselectivity were evaluated. To prepare the composite membrane, the IPN ion gel precursor solutions with different *r* values were used to control the gel layer thickness. The results are shown in Figure V-8. As shown in Figure V-8(a), the CO_2 permeance effectively increased from 45 to 613 GPU with increasing the dilution degree of the precursor solution. This monotonic increase would be due to the decrease of the ion gel layer thickness. On the other hand, the CO_2/N_2 permselectivity slightly decreased with the increase in the dilution degree. Although the decrease in the CO_2/N_2 permselectivity might be caused by the defect formation in the IPN ion gel layer, the surface morphology of the IPN ion gel layer formed using the precursor solution with r = 24 g/g was very smooth and defect-free (Figure V-8(b)). Thus, it was considered that the defect formation in the IPN ion gel layer was not the reason of the decrease of the CO_2/N_2 permselectivity. The other possible reason for the decrease in the CO_2/N_2 permselectivity was the inclement of the contribution of the PDMS gutter layer to total gas permeation property of the composite membrane along with the decrease in the IPN ion gel layer thickness.

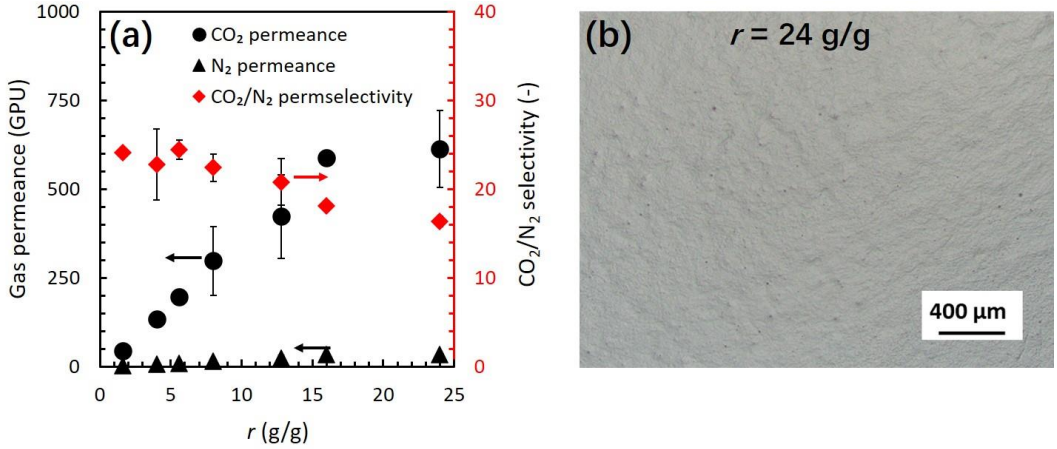

Figure V-8. CO_2 and N_2 permeation performances of the composite membrane with plasma treated PDMS gutter layer and IPN ion gel layer. (a) Effect of dilution degree on the CO_2 and N_2 permeances and CO_2/N_2 permselectivity and (b) Surface morphology of the composite membrane with the IPN ion gel layer prepared using the precursor solution with 24 g/g of the *r* value. The PDMS gutter layer treated by air plasma for 2 s was used. The weight percentage of the IL/(polymers and IL) in the precursor solution and IPN ion gel was 80 wt%.

The gas permeation performance of a composite membrane could be estimated by resistance model [77]. The composite membrane fabricated in this study is composed of a selective IPN ion gel layer (layer 1), a PDMS gutter layer (layer 2) and a porous PTFE support membrane (layer 3). In these diffusion resistance layers, the gas transport resistance in the porous support membrane can be ignored. Therefore, the permeance of gas species "*i*" of the composite membrane, $R_{\mathrm{i,total}}$, can be expressed by Equation V-1 [69].

$$R_{\mathrm{i,total}} = \frac{1}{\left(\frac{\delta_1}{P_{\mathrm{i},1}} + \frac{1}{R_{\mathrm{i},2}}\right)} \qquad (\mathrm{V}-1)$$

where *R* and *P* are permeance and permeability, respectively. δ_1 is the thickness of the IPN ion gel layer. The subscript "*i*" is CO_2 and N_2. The subscripts "total", "1", and "2" mean the composite layer of the PDMS and IPN ion gel layers, IPN ion gel layer, and PDMS layer, respectively. The permselectivity of the composite membrane, α_{total}, can be expressed by Equation V-2

$$\alpha_{\mathrm{total}} = \frac{R_{\mathrm{CO_2,total}}}{R_{\mathrm{N_2,total}}} = \frac{\left(\frac{\delta_1}{P_{\mathrm{N_2},1}} + \frac{1}{R_{\mathrm{N_2},2}}\right)}{\left(\frac{\delta_1}{P_{\mathrm{CO_2},1}} + \frac{1}{R_{\mathrm{CO_2},2}}\right)} \qquad (\mathrm{V}-2)$$

From Equations V-1 and V-2, Equation V-3 can be derived.

$$\alpha_{\mathrm{total}} = \alpha_1 \cdot \left(1 - \frac{R_{\mathrm{CO_2,total}}}{R_{\mathrm{CO_2},2}}\right) + \frac{R_{\mathrm{CO_2,total}}}{R_{\mathrm{N_2},2}} \qquad (\mathrm{V}-3)$$

where α_1 is the CO_2/N_2 permselectivity of the IPN ion gel layer ($\alpha_1 = P_{\mathrm{CO_2},1}/P_{\mathrm{N_2},1} = 27$). The CO_2 permeance, $R_{\mathrm{CO_2},2}$, and N_2 permeance, $R_{\mathrm{N_2},2}$, of the PDMS gutter layer treated by plasma for 2 s were 1400 GPU and 238 GPU, respectively (Figures V-7(c) and (d)). Therefore, the relationship between $R_{\mathrm{CO_2,total}}$ and α_{total} can be estimated by Equation V-3. The estimated result is shown in Figure V-9 along with the experimental data shown in Figure V-8(a). As shown in this figure, the estimated curve is well in agreement with the experimental results. It is worthy to note that the theoretically estimated CO_2/N_2 permselectivity of the composite membrane decreases with the increase in the CO_2 permeance of the composite membrane, $R_{\mathrm{CO_2,total}}$. In other words, the theoretical calculation denotes that the permselectivity decreases with increasing $R_{\mathrm{CO_2,total}}$ even if the IPN ion gel layer has no defect. The reason of the decrease of the estimated permselectivity is because the permselectivity of the PDMS gutter layer is low as about 6 (Figure V-7(d)), and the contribution of the PDMS gutter layer resistance to the total resistance becomes large with the increase of the IPN ion gel layer permeance. Thus, based

on the analysis by the theoretical model (Equation V-3), it was strongly suggested that the IPN ion gel layer formed on the plasma treated PDMS gutter layer were defect-free.

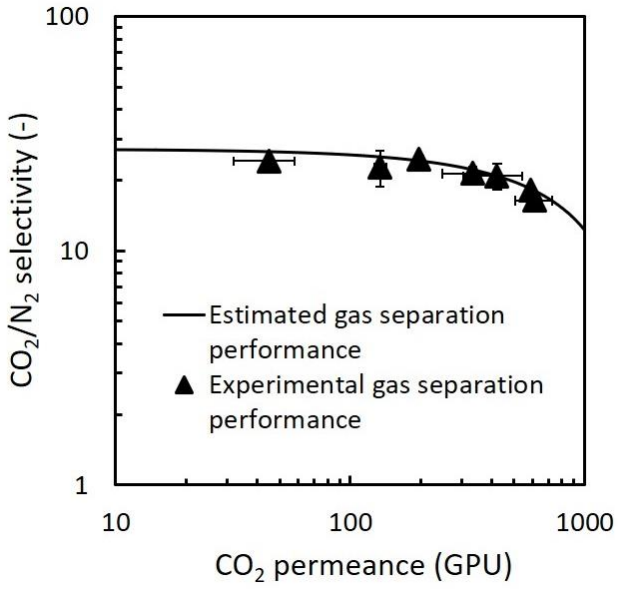

Figure V-9. Theoretically estimated relationship between the CO_2/N_2 permselectivity and the CO_2 permeance of the composite membrane. The experimental data are also plotted to compare the correlation between the estimated result with the experimental data. The composite membranes were prepared by spin coating the precursor solution with different dilution degrees on the PDMS gutter layer treated by plasma for 2 s. The experimental result was the same as those shown in Figure V-8(a). The estimated curve was calculated by Equation V-3.

The ion gel layer thicknesses of the composite membranes were measured by SEM observation and are shown in Figures V-10(a) and (b). The thicknesses significantly decreased from 20 μm to 600 nm when *r* value increased from 1.6 to 24 g/g. This result indicates that increasing the dilution degree of the precursor solution effectively decreases the thickness of the IPN ion gel layer. Using Equations V-1 and V-2, and the ion gel layer thickness δ_1, we can estimate the CO_2 permeance and the CO_2/N_2 permselectivity of the composite membrane. The relationship between the CO_2 permeance and the CO_2/N_2 permselectivity, and the ion gel layer thickness are shown in Figures V-10(c) and (d). The estimated results were in good agreement with the experimental data, indicating that the thicknesses of the IPN ion gel layer measured in Figures V-10(a) and (b) are reasonable. Therefore, it was

confirmed that the composite membrane with ultra-thin and defect-free IPN ion gel layer can be easily formed using highly diluted precursor solution.

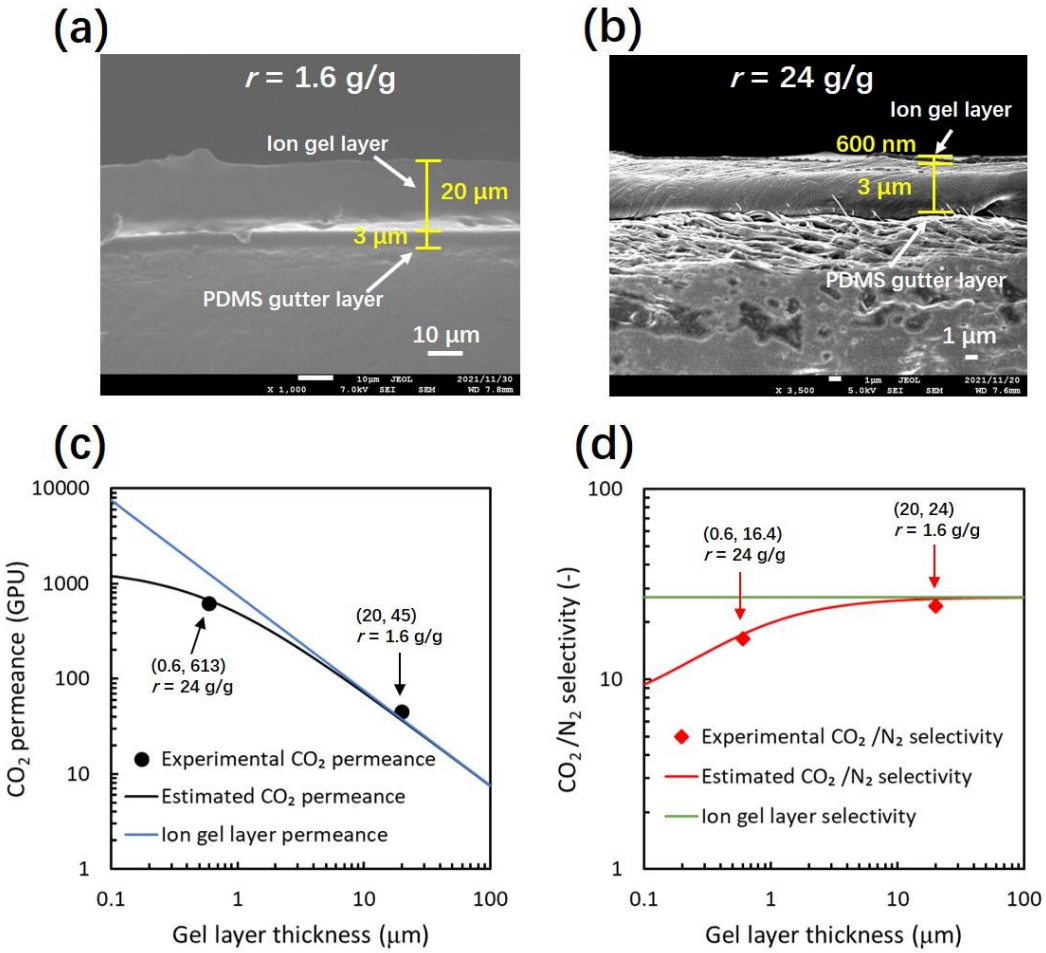

Figure V-10. The IPN ion gel layer thickness of the composite membrane. SEM images of the cross section of the composite membranes with the IPN ion gel layer prepared using the precursor solution with (a) 1.6 g/g and (b) 24 g/g of the *r* values. The composite membranes were prepared using the support membrane with the PDMS gutter layer treated by plasma for 2 s. Relationships between (c) CO_2 permeance and (d) CO_2/N_2 permselectivity of the composite membranes and the ion gel layer thickness. The estimated CO_2 permeance and CO_2/N_2 permselectivity of the composite membranes in parts (c) and (d) were calculated from Equations V-1 and V-2, respectively.

V-3-5 Gas permeation performance of the composite membrane with the thin IPN ion gel layer having high IL content

Decreasing the thickness of the IPN ion gel layer is effective way to increase the CO_2 permeance of

the composite membrane. On the other hand, increasing the CO_2 permeability of the ion gel layer is the other promising way to increase the CO_2 permeance of the composite membrane. The gas permeability of the IPN ion gel membrane can be increased by increasing the IL content [100]. Therefore, to increase the gas permeation performance of the composite membrane, the IL content of the IPN ion gel layer was increased from 80 wt% to 90 wt%. The effect of the IL content of the IPN ion gel layer on the gas permeation performance of the composite membrane was shown in Figures V-11(a) and (b). As shown in Figure V-11(a), the CO_2 permeance of the composite membrane effectively increased with the increase of the IL content and dilution degree. On the other hand, the CO_2/N_2 permselectivity decreased with increasing the IL content and the dilution degree (Figure V-11(b)). The effect of dilution degree on the CO_2 permeance and CO_2/N_2 permselectivity is the same as that for the composite membrane having the IPN ion gel layer with the IL content of 80 wt%. Regarding the effect of the IL content on the CO_2 permeance, the CO_2 permeance of the composite membrane increased due to the increase of the CO_2 permeability of the IPN ion gel layer with the increase in the IL content. On the other hand, the CO_2/N_2 permselectivity was decreased with the increase in the IL content when the *r* value was over 12.8 g/g. This decrease was due to the increase in the contribution of the PDMS gutter layer resistance to the total resistance by the increasing CO_2 permeability of the IPN ion gel layer (Equation V-3). The experimental CO_2/N_2 permselectivities and the CO_2 permeances of the composite membranes with different IL contents prepared using the precursor solution with different dilution degrees were compared with those estimated from Equation V-3 (Figure V-11(c)). It is clearly indicated that the experimental and theoretically estimated results were in good agreement. This result means that the formed IPN ion gel layer with 90 wt% of the IL content had no defect, which was also confirmed from the surface observation of the composite membrane (Figure V-11(d)). Therefore, it was demonstrated that the increase of the IL content of the IPN ion gel layer is effective to increase the CO_2 permeance of the composite membrane.

The thickness of the gel layer with 90 wt% of the IL was determined from the experimental result and Equation V-1. The CO_2 permeance of the composite membrane having the IPN ion gel layer with 90 wt% of the IL were 778 GPU (Figure V-11(a)). In our previous work, we determined the CO_2 permeability and the CO_2/N_2 permeability of the self-standing IPN ion gel membrane with 90 wt% of the IL as 1116 barrer and 27, respectively [100]. On the other hand, the CO_2 permeance of the plasma

treated PDMS gutter layer was 1400 GPU (Figure V-7(c)). Using these values and Equation V-1, the thickness of the IPN ion gel layer of the composite membrane having the IPN ion gel layer with 90 wt% of the IL was determined as 600 nm. Thus, it was confirmed that the ultra-thin IPN ion gel layer was also successfully prepared even if the IL content in the gel layer was 90 wt%.

Using the determined thickness and the CO_2 permeability of the IPN ion gel layer, the CO_2 permeance of the IPN ion gel layer was calculated as 1860 GPU. This CO_2 permeance of 1860 GPU and the CO_2/N_2 permselectivity of 27 of the IPN ion gel layer are higher than those of the gutter layer (1400 GPU and 6, respectively). This means the insufficient CO_2 permeance of the PDMS gutter layer severely restricted the total CO_2 separation performance of the composite membrane.

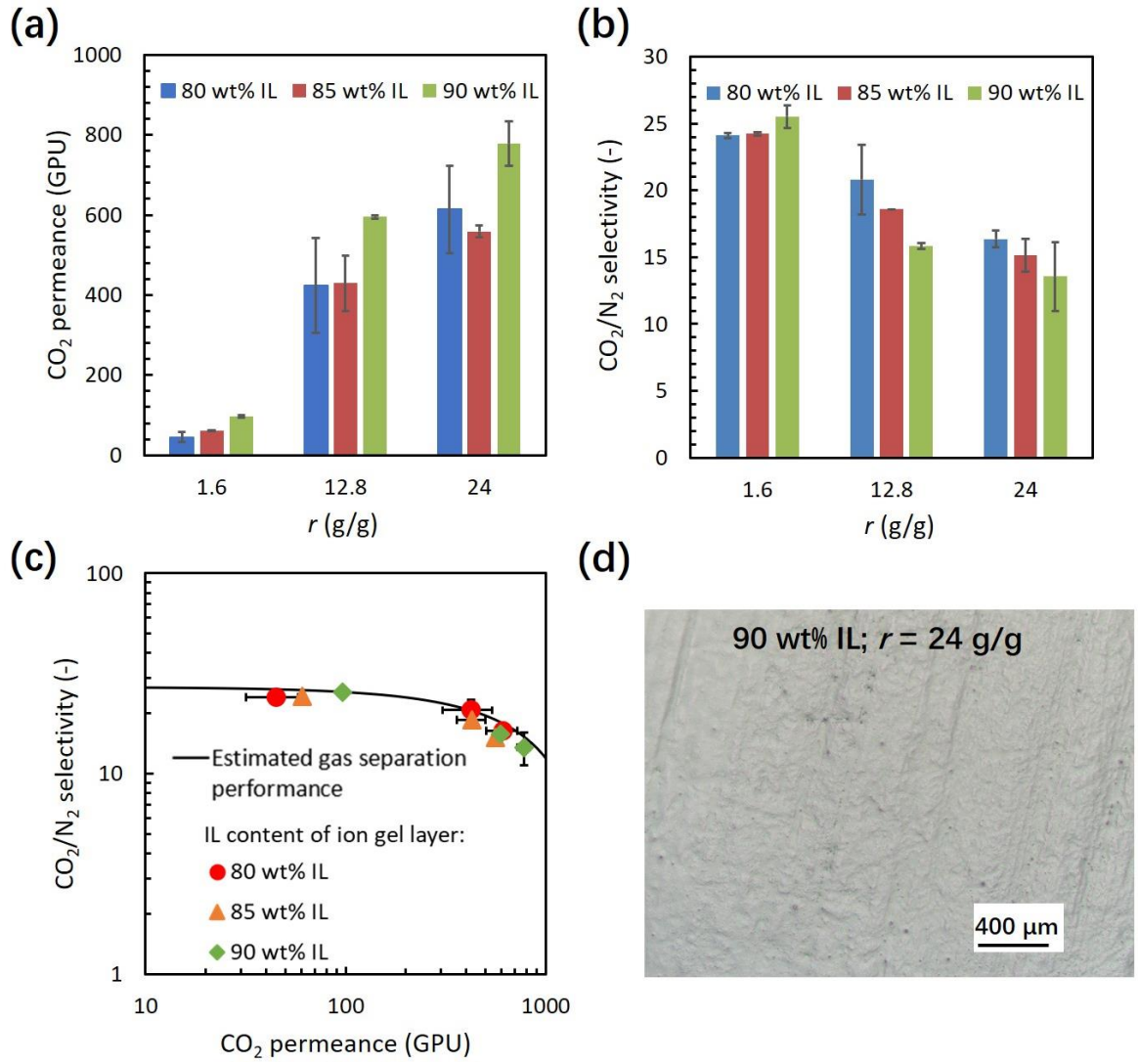

Figure V-11. Effect of the IL content of the IPN ion gel layer on the (a) CO_2 permeance and (b) CO_2/N_2

permselectivity of the composite membranes prepared using the precursor solution with different *r* values. The PDMS gutter layer treated by plasma for 2 s was used to prepare the composite membranes. (c) Comparison between the experimental data and the theoretically estimated relationship between the CO_2/N_2 selectivity and the CO_2 permeance of the composite membranes with the IPN ion gel layer having different IL contents. The estimated line was calculated by Equation V-3. (d) Surface morphology of the composite membrane having the IPN ion gel layer with 90 wt% of the IL prepared using the precursor solution with *r* value of 24 g/g.

V-3-6 Estimation of the CO_2 permeation performance of the composite membrane with a high-performance gutter layer

As mentioned above, the CO_2 permeance of the gutter layer strongly affects the overall CO_2 permeance of the composite membrane with highly CO_2 permeable thin IPN ion gel layer. Unfortunately, in the current stage, because it is hard for us to prepare a highly CO_2 permeable gutter layer, the highest CO_2 permeance of our developed composite membrane was 778 GPU, which is still less than 1000 GPU. However, in recent years, the development of a gutter layer has been progressing, and some of state-of-the-art gutter layers has very high CO_2 permeance (> 8000 GPU) [78, 79, 108-115]. If the high-performance gutter layer can be used to prepare our composite membrane, there is no doubting that the CO_2 permeance of the composite membrane with the best IPN ion gel layer developed in this work becomes very high. Here, we estimated the performance of the composite membrane with high performance gutter layer.

Figure V-12 shows the effect of IPN ion gel layer thickness on the CO_2 permeance and CO_2/N_2 permselectivity of the composite membrane composed of the gutter layer with different CO_2 permeance and the IPN ion gel layer containing 90 wt% of the IL. The CO_2 permeance and the CO_2/N_2 permselectivity of the composite membrane could be effectively improved by increasing the CO_2 permeance of the gutter layer. If the CO_2 permeance of the PDMS gutter layer is more than 5000 GPU, the CO_2 permeance and CO_2/N_2 permselectivity of the composite membrane with 600 nm IPN ion gel layer could be more than 1350 GPU and over 21, respectively. These performances satisfactory meet the required values for the CO_2 capture for the flue gas from the coal-fired power plant (>1000 GPU of the CO_2 permeance and >20 of the CO_2/N_2 permselectivity [32]).

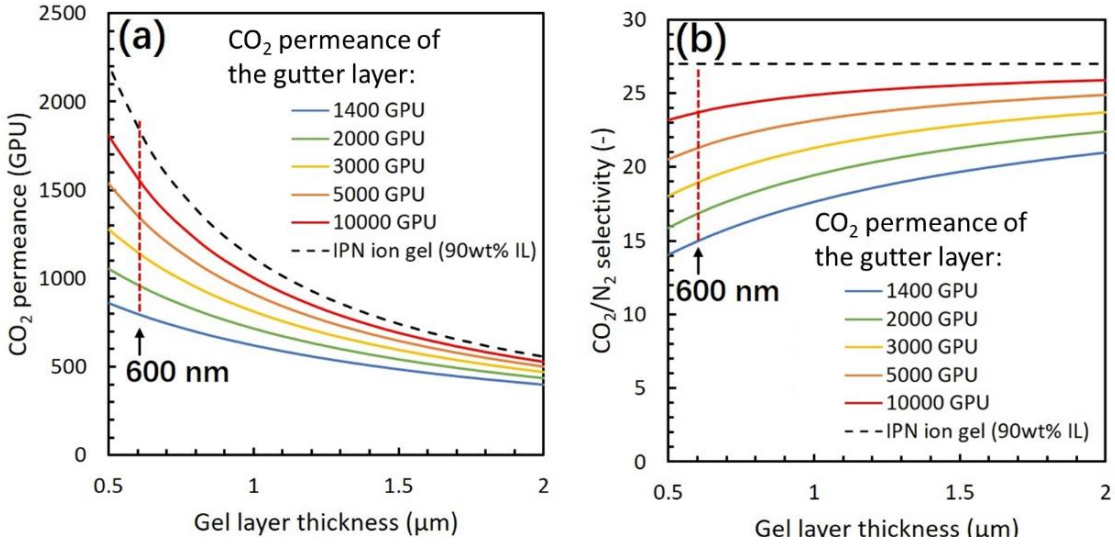

Figure V-12. Effect of gel layer thickness on the CO_2 permeance and CO_2/N_2 permselectivity of the composite membrane composed of the gutter layer with different CO_2 permeance and the IPN ion gel layer containing 90 wt% of the IL. (a) CO_2 permeance estimated by Equation V-1 and (b) CO_2/N_2 permselectivity estimated by Equation V-2. For the calculation, the CO_2 permeability and CO_2/N_2 permselectivity of the IPN ion gel layer were fixed at 1116 barrer and 27, respectively. The CO_2/N_2 permselectivity of the PDMS gutter layer was fixed at 6.

V-4 Conclusion

The composite membrane with an ultra-thin (thickness of 600nm) and defect-free IPN ion gel layer has been successfully prepared on a PDMS gutter layer by spin coating method. The thickness of the IPN ion gel layer could be significantly decreased from 20 μm to 600 nm by increasing the dilution degree of the IPN ion gel precursor solution. Due to the high mechanical strength and good IL holding property of the IPN ion gel, the ultra-thin and defect-free IPN ion gel layer with up to 90 wt% of the IL was successfully prepared. By decreasing the thickness and increasing the IL content of the IPN ion gel layer, the CO_2 permeance of the composite membrane was effectively improved from 45 to 778 GPU. It was confirmed from the theoretical analysis that the CO_2 permeance and the CO_2/N_2 selectivity of the IPN ion gel layer with 600 nm thickness and 90 wt% of the IL content were determined as 1860 GPU and 27, respectively. Estimation of the CO_2 separation performance of the composite membrane with a high-performance gutter layer and the IPN ion gel layer indicated that the IPN gel is a good optional material as a selective layer of a composite membranes for efficient CO_2 separation.

Chapter VI
Conclusions

To overcome the weak mechanical strength of ion gel membranes and fabricate thin ion gel membranes to achieve high CO_2 permeance. Two types of dual-network-based tough ion gel membranes are developed in this study. One is the inorganic/organic μ-DN ion gel membrane (Chapter II). The other one is the IPN ion gel composed of semi-crystalline and cross-linkable polymers (Chapter IV). Both two types of tough ion gels were successfully made into a thin selective layer of a composite membrane (Chapter III and Chapter V). The prepared composite membranes displayed highly improved CO_2 permeance. The IPN ion gel thin layer overcomes the high roughness of the μ-DN ion gel layer, which is preferred for thin ion gel membrane preparation. The composite membrane with a thin IPN ion gel layer achieved the higher CO_2 permeance than that of the composite membrane with a μ-DN ion gel layer. The CO_2 permeance and the CO_2/N_2 permselectivity of the IPN ion gel layer alone having 90 wt% IL were respectively estimated as 1860 GPU and 27, which indicates that IPN gel is a good optional material for the thin ion gel membrane preparation. It is expected that a composite membrane with CO_2 permeance over 1000 GPU and CO_2/N_2 selectivity over 20 could be developed using IPN ion gel as the selective layer. The composite membrane would meet the requirement of the membrane performance for practical carbon capture. Additionally, if the CO_2-phlic ILs such as [Emim][$B(CN)_4$] could be used to prepare the IPN ion gel membrane, the membrane could achieve much higher CO_2 permeation performance.

On the other hand, from the investigations of this dissertation, it was found that for high-performance thin ion gel membrane preparation, the ion gels need to have good mechanical properties, high CO_2 permeability, low surface roughness, and the polymer network which can be formed in an open space.

The detailed conclusions of this study are summarized as follows.

1. Development of a tough ion-gel-based CO_2 separation membrane with the micro-double-network formed from non-volatile network precursors

In Chapter II, an inorganic/organic μ-DN ion gel membrane was fabricated using non-volatile network precursors. By optimizing the molecular weight of the cross-linkable polymer and the

organic/inorganic network composition, the μ-DN ion gel membrane exhibits high mechanical strength with a fracture energy of 765 kJ/m^3. Regarding the gas separation performance, the μ-DN ion gel membrane fabricated using a poly(DMAAm-*co*-NSA) with the NSA ratio of 1.18 mol% shows approximately 920 barrer of the CO_2 permeability, which is much higher than those of the classic inorganic/organic DN ion gel membranes fabricated using volatile network precursors (556 barrer) and the supported ionic liquid membranes (617 barrer). The good mechanical properties and high CO_2 separation performance indicates a good potential of the μ-DN ion gel as a membrane material for CO_2 separation

2. Preparation of a composite membrane with an inorganic/organic micro-double-network ion gel layer

A composite membrane with a μ-DN ion gel layer was developed in Chapter III. The mechanical properties and surface roughness of the μ-DN ion gel fabricated in an open space were optimized for the preparation of thin μ-DN ion gel layer. By adjusting the inorganic/organic network structure, the mechanical strength of the μ-DN ion gel was optimized to achieve a fracture energy of 636 kJ/m^3. Based on the optimized preparation conditions, the μ-DN ion gel was made into a thin selective layer of a composite membrane using the spin coating method. The fabricated composite membrane displays the highly improved CO_2 permeance (119 GPU) comparing to the self-standing μ-DN ion gel membrane (< 10 GPU). The good stability of the composite membrane used for long-term separation was also confirmed. However, some micron-sized particles were formed on the surface of the μ-DN ion gel layer, which would decrease the mechanical properties of the μ-DN ion gel layer and was considered as a disadvantage of the μ-DN ion gel for thin ion gel membrane preparation.

3. Novel tough ion-gel-based CO_2 separation membrane with interpenetrating polymer network composed of semi-crystalline and cross-linkable polymers

In Chapter IV, to overcome the problem of the micron-sized particles formation in the μ-DN ion gel layer, a novel tough ion gel constructed from an interpenetrating polymer network (IPN) composed of semi-crystalline and cross-linkable polymers was developed in an open space. The IPN ion gel shows a highly smoother surface morphology than that of the μ-DN ion gel, which is preferred for thin ion

gel membrane preparation. A IPN ion gel containing 80 wt% of the IL and prepared under optimized conditions displays high tensile fracture energy (758 kJ/m^3). The IPN ion gel membrane with a high IL content of 91.3 wt% was successfully fabricated and showed high CO_2 permeability of 1421 barrer and CO_2/N_2 permselectivity of 27. The good performance of the IPN ion gel membrane indicates a great potential of the IPN ion gel to be used as a base material for developing high-permeance thin ion gel membranes.

4. Development of a composite membrane with an interpenetrating polymer network ion gel layer

In chapter V, a composite membrane with a thin and defect-free IPN ion gel layer was developed. The IPN ion gel layer with high IL content (80 – 90wt%) was prepared on a PDMS gutter layer by spin coating. The thickness of the IPN ion gel layer was reduced from 20 μm to 600 nm via increasing the dilution degree of the ion gel precursor solution, and the CO_2 permeance of the composite membrane increases from 45 to 613 GPU. By increasing the IL content of the IPN ion gel layer to 90 wt%, the prepared composite membrane displays the CO_2 permeance of 778 GPU and CO_2/N_2 selectivity of 15. The CO_2 permeance and the CO_2/N_2 permselectivity of the IPN ion gel layer alone having 90 wt% IL were respectively estimated as 1860 GPU and 27. The excellent gas permeation performance proves that IPN gel is a good optional material for the thin ion gel membrane preparation.

References

[1] R.A. Begum, K. Sohag, S.M.S. Abdullah, M. Jaafar, CO_2 emissions, energy consumption, economic and population growth in Malaysia, Renew. Sustain. Energy Rev., 41 (2015) 594-601.

[2] A. Rehman, H. Ma, I. Ozturk, R. Ulucak, Sustainable development and pollution: the effects of CO_2 emission on population growth, food production, economic development, and energy consumption in Pakistan, Environ. Sci. .Pollut. Res. Int., 29 (2022) 17319-17330.

[3] B. Ekwurzel, J. Boneham, M. Dalton, R. Heede, R.J. Mera, M.R. Allen, P.C. Frumhoff, The rise in global atmospheric CO_2, surface temperature, and sea level from emissions traced to major carbon producers, Clim. Change, 144 (2017) 579-590.

[4] M.Z. Jacobson, Review of solutions to global warming, air pollution, and energy security, Energy Environ. Sci., 2 (2009) 148-173.

[5] T.M. Gür, Carbon Dioxide Emissions, Capture, Storage and Utilization: Review of Materials, Processes and Technologies, Prog. Energy Combust. Sci., 89 (2022) 100965.

[6] H. Ritchie, M. Roser, CO_2 and greenhouse gas emissions, Our world in data, (2020).

[7] J.M. Christensen, A. Olhoff, Emissions gap report 2019, United Nations Environment Programme (UNEP): Gigiri Nairobi, Kenya, (2019).

[8] M. Allen, M. Babiker, Y. Chen, H.C. de Coninck, IPCC SR15: Summary for policymakers, in: IPCC Special Report Global Warming of 1.5 ºC, Intergovernmental Panel on Climate Change, (2018).

[9] D.Y. Leung, G. Caramanna, M.M. Maroto-Valer, An overview of current status of carbon dioxide capture and storage technologies, Renew. Sustain. Energy Rev., 39 (2014) 426-443.

[10] A.A. Olajire, CO_2 capture and separation technologies for end-of-pipe applications–a review, Energy, 35 (2010) 2610-2628.

[11] Y. Wang, L. Zhao, A. Otto, M. Robinius, D. Stolten, A review of post-combustion CO_2 capture technologies from coal-fired power plants, Energy Procedia, 114 (2017) 650-665.

[12] D. Jansen, M. Gazzani, G. Manzolini, E. van Dijk, M. Carbo, Pre-combustion CO_2 capture, Int. J. Greenh. Gas Control, 40 (2015) 167-187.

[13] M. Kanniche, R. Gros-Bonnivard, P. Jaud, J. Valle-Marcos, J.-M. Amann, C. Bouallou, Pre-combustion, post-combustion and oxy-combustion in thermal power plant for CO_2 capture, Appl.

Therm. Eng., 30 (2010) 53-62.

[14] L.C. Tome, I.M. Marrucho, Ionic liquid-based materials: A platform to design engineered CO_2 separation membranes, Chem. Soc. Rev., 45 (2016) 2785-2824.

[15] A.S. Bhown, B.C. Freeman, Analysis and status of post-combustion carbon dioxide capture technologies, Environ. Sci. Technol., 45 (2011) 8624-8632.

[16] Y. Zhang, P. Yu, Y. Luo, Absorption of CO_2 by amino acid-functionalized and traditional dicationic ionic liquids: properties, Henry's law constants and mechanisms, Chem. Eng. J., 214 (2013) 355-363.

[17] J. Palgunadi, J.E. Kang, D.Q. Nguyen, J.H. Kim, B.K. Min, S.D. Lee, H. Kim, H.S. Kim, Solubility of CO_2 in dialkylimidazolium dialkylphosphate ionic liquids, Thermochim. Acta, 494 (2009) 94-98.

[18] R.S. Liu, X.D. Shi, C.T. Wang, Y.Z. Gao, S. Xu, G.P. Hao, S. Chen, A.H. Lu, Advances in Post-Combustion CO_2 Capture by Physical Adsorption: From Materials Innovation to Separation Practice, ChemSusChem, 14 (2021) 1428-1471.

[19] R. Ben-Mansour, M. Habib, O. Bamidele, M. Basha, N. Qasem, A. Peedikakkal, T. Laoui, M. Ali, Carbon capture by physical adsorption: materials, experimental investigations and numerical modeling and simulations–a review, Appl. Energy, 161 (2016) 225-255.

[20] F.A. Chowdhury, H. Okabe, S. Shimizu, M. Onoda, Y. Fujioka, Development of novel tertiary amine absorbents for CO_2 capture, Energy Procedia, 1 (2009) 1241-1248.

[21] G.T. Rochelle, Thermal degradation of amines for CO_2 capture, Curr. Opin. Chem. Eng., 1 (2012) 183-190.

[22] S. Fredriksen, K.-J. Jens, Oxidative degradation of aqueous amine solutions of MEA, AMP, MDEA, Pz: A review, Energy Procedia, 37 (2013) 1770-1777.

[23] C.-H. Yu, C.-H. Huang, C.-S. Tan, A Review of CO_2 Capture by Absorption and Adsorption, Aerosol and Air Quality Research, 12 (2012) 745-769.

[24] T. Gelles, S. Lawson, A.A. Rownaghi, F. Rezaei, Recent advances in development of amine functionalized adsorbents for CO_2 capture, Adsorption, 26 (2020) 5-50.

[25] H. Sun, C. Wu, B. Shen, X. Zhang, Y. Zhang, J. Huang, Progress in the development and application of CaO-based adsorbents for CO_2 capture—a review, Mater. Today Sustain., 1 (2018) 1-27.

[26] M. Minelli, E. Papa, V. Medri, F. Miccio, P. Benito, F. Doghieri, E. Landi, Characterization of novel geopolymer–zeolite composites as solid adsorbents for CO_2 capture, Chem. Eng. J., 341 (2018) 505-515.

[27] A. Sayari, Y. Belmabkhout, R. Serna-Guerrero, Flue gas treatment via CO_2 adsorption, Chem. Eng. J., 171 (2011) 760-774.

[28] N. Gargiulo, F. Pepe, D. Caputo, CO_2 adsorption by functionalized nanoporous materials: a review, J. Nanosci. Nanotechnol., 14 (2014) 1811-1822.

[29] A.R. Kulkarni, D.S. Sholl, Analysis of equilibrium-based TSA processes for direct capture of CO_2 from air, Ind. Eng. Chem. Res., 51 (2012) 8631-8645.

[30] M. Olivares-Marín, M.M. Maroto-Valer, Development of adsorbents for CO_2 capture from waste materials: a review, Greenh. Gases: Sci. Technol., 2 (2012) 20-35.

[31] Y. Han, W.W. Ho, Recent advances in polymeric membranes for CO_2 capture, Chin. J. Chem. Eng., 26 (2018) 2238-2254.

[32] T.C. Merkel, H. Lin, X. Wei, R. Baker, Power plant post-combustion carbon dioxide capture: An opportunity for membranes, J. Membr. Sci., 359 (2010) 126-139.

[33] S. Wang, X. Li, H. Wu, Z. Tian, Q. Xin, G. He, D. Peng, S. Chen, Y. Yin, Z. Jiang, Advances in high permeability polymer-based membrane materials for CO_2 separations, Energy Environ. Sci., 9 (2016) 1863-1890.

[34] L.M. Robeson, The upper bound revisited, J. Membr. Sci., 320 (2008) 390-400.

[35] L.M. Robeson, Correlation of separation factor versus permeability for polymeric membranes, J. Membr. Sci., 62 (1991) 165-185.

[36] P. Walden, Molecular weights and electrical conductivity of several fused salts, Bull. Acad. Imper. Sci.(St. Petersburg), 1800 (1914).

[37] L.A. Blanchard, D. Hancu, E.J. Beckman, J.F. Brennecke, Green processing using ionic liquids and CO_2, Nature, 399 (1999) 28-29.

[38] L.C. Tomé, I.M. Marrucho, Ionic liquid-based materials: A platform to design engineered CO_2 separation membranes, Chem. Soc. Rev., 45 (2016) 2785-2824.

[39] P. Scovazzo, A.E. Visser, J.H. Davis Jr, R.D. Rogers, C.A. Koval, D.L. DuBois, R.D. Noble, Supported ionic liquid membranes and facilitated ionic liquid membranes, ACS Publications, (2002).

[40] P. Scovazzo, J. Kieft, D.A. Finan, C. Koval, D. DuBois, R. Noble, Gas separations using non-hexafluorophosphate $[PF_6]^-$ anion supported ionic liquid membranes, J. Membr. Sci., 238 (2004) 57-63.

[41] D. Morgan, L. Ferguson, P. Scovazzo, Diffusivities of gases in room-temperature ionic liquids: data and correlations obtained using a lag-time technique, Ind. Eng. Chem. Res., 44 (2005) 4815-4823.

[42] J. Tang, H. Tang, W. Sun, H. Plancher, M. Radosz, Y. Shen, Poly (ionic liquid) s: a new material with enhanced and fast CO_2 absorption, Chem. Commun., (2005) 3325-3327.

[43] J. Tang, H. Tang, W. Sun, M. Radosz, Y. Shen, Low-pressure CO_2 sorption in ammonium-based poly (ionic liquid) s, Polymer, 46 (2005) 12460-12467.

[44] J.E. Bara, S. Lessmann, C.J. Gabriel, E.S. Hatakeyama, R.D. Noble, D.L. Gin, Synthesis and performance of polymerizable room-temperature ionic liquids as gas separation membranes, Ind. Eng. Chem. Res., 46 (2007) 5397-5404.

[45] J.E. Bara, C.J. Gabriel, E.S. Hatakeyama, T.K. Carlisle, S. Lessmann, R.D. Noble, D.L. Gin, Improving CO_2 selectivity in polymerized room-temperature ionic liquid gas separation membranes through incorporation of polar substituents, J. Membr. Sci., 321 (2008) 3-7.

[46] J.E. Bara, E.S. Hatakeyama, D.L. Gin, R.D. Noble, Improving CO_2 permeability in polymerized room-temperature ionic liquid gas separation membranes through the formation of a solid composite with a room-temperature ionic liquid, Polym. Adv. Technol., 19 (2008) 1415-1420.

[47] Y. Gu, T.P. Lodge, Synthesis and Gas Separation Performance of Triblock Copolymer Ion Gels with a Polymerized Ionic Liquid Mid-Block, Macromolecules, 44 (2011) 1732-1736.

[48] A.R. Nabais, L.A. Neves, L.C. Tomé, Mixed-Matrix Ion Gel Membranes for Gas Separation, ACS Applied Polymer Materials, 4 (2022) 3098-3119.

[49] F. Moghadam, E. Kamio, H. Matsuyama, High CO_2 separation performance of amino acid ionic liquid-based double network ion gel membranes in low CO_2 concentration gas mixtures under humid conditions, J. Membr. Sci., 525 (2017) 290-297.

[50] F. Moghadam, E. Kamio, A. Yoshizumi, H. Matsuyama, An amino acid ionic liquid-based tough ion gel membrane for CO_2 capture, Chem. Commun., 51 (2015) 13658-13661.

[51] K. Friess, J.C. Jansen, F. Bazzarelli, P. Izák, V. Jarmarová, M. Kačírková, J. Schauer, G. Clarizia, P. Bernardo, High ionic liquid content polymeric gel membranes: Correlation of membrane structure

with gas and vapour transport properties, J. Membr. Sci., 415-416 (2012) 801-809.

[52] K. Fujii, T. Makino, K. Hashimoto, T. Sakai, M. Kanakubo, M. Shibayama, Carbon dioxide separation using a high-toughness ion gel with a tetra-armed polymer network, Chem. Lett., 44 (2015) 17-19.

[53] K. Fujii, H. Asai, T. Ueki, T. Sakai, S. Imaizumi, U.-i. Chung, M. Watanabe, M. Shibayama, High-performance ion gel with tetra-PEG network, Soft Matter, 8 (2012) 1756-1759.

[54] T.P. Lodge, T. Ueki, Mechanically tunable, readily processable ion gels by self-assembly of block copolymers in ionic liquids, Acc. Chem. Res., 49 (2016) 2107-2114.

[55] T.P. Lodge, A unique platform for materials design, Science, 321 (2008) 50-51.

[56] B. Tang, S.P. White, C.D. Frisbie, T.P. Lodge, Synergistic increase in ionic conductivity and modulus of triblock copolymer ion gels, Macromolecules, 48 (2015) 4942-4950.

[57] Y. Gu, E.L. Cussler, T.P. Lodge, ABA-triblock copolymer ion gels for CO_2 separation applications, J. Membr. Sci., 423 (2012) 20-26.

[58] Y. Gu, S. Zhang, L. Martinetti, K.H. Lee, L.D. McIntosh, C.D. Frisbie, T.P. Lodge, High toughness, high conductivity ion gels by sequential triblock copolymer self-assembly and chemical cross-linking, J. Am. Chem. Soc., 135 (2013) 9652-9655.

[59] J.P. Gong, Why are double network hydrogels so tough?, Soft Matter, 6 (2010) 2583-2590.

[60] J.P. Gong, Y. Katsuyama, T. Kurokawa, Y. Osada, Double-network hydrogels with extremely high mechanical strength, Adv. Mater., 15 (2003) 1155-1158.

[61] J. Lan, Y. Li, B. Yan, C. Yin, R. Ran, L.Y. Shi, Transparent Stretchable Dual-Network Ionogel with Temperature Tolerance for High-Performance Flexible Strain Sensors, ACS Appl. Mater. interfaces, 12 (2020) 37597-37606.

[62] Z. Tang, X. Lyu, A. Xiao, Z. Shen, X. Fan, High-Performance Double-Network Ion Gels with Fast Thermal Healing Capability via Dynamic Covalent Bonds, Chem. Mater., 30 (2018) 7752-7759.

[63] F. Moghadam, E. Kamio, T. Yoshioka, H. Matsuyama, New approach for the fabrication of double-network ion-gel membranes with high CO_2/N_2 separation performance based on facilitated transport, J. Membr. Sci., 530 (2017) 166-175.

[64] H. Arafune, S. Honma, T. Morinaga, T. Kamijo, M. Miura, H. Furukawa, T. Sato, Highly Robust and Low Frictional Double-Network Ion Gel, Adv. Mater. Interfaces, 4 (2017) 1700074.

[65] Y. Ding, J. Zhang, L. Chang, X. Zhang, H. Liu, L. Jiang, Preparation of high-performance ionogels with excellent transparency, good mechanical strength, and high conductivity, Adv. Mater., 29 (2017) 1704253.

[66] E. Kamio, M. Kinoshita, T. Yasui, T.P. Lodge, H. Matsuyama, Preparation of Inorganic/Organic Double-Network Ion Gels Using a Cross-Linkable Polymer in an Open System, Macromolecules, 53 (2020) 8529-8538.

[67] T. Yasui, E. Kamio, H. Matsuyama, Inorganic/Organic Double-Network Ion Gels with Partially Developed Silica-Particle Network, Langmuir, 34 (2018) 10622-10633.

[68] E. Kamio, T. Yasui, Y. Iida, J.P. Gong, H. Matsuyama, Inorganic/Organic Double-Network Gels Containing Ionic Liquids, Adv. Mater., 29 (2017) 1704118.

[69] J. Zhang, E. Kamio, M. Kinoshita, A. Matsuoka, K. Nakagawa, T. Yoshioka, H. Matsuyama, Inorganic/Organic Micro-Double-Network Ion Gel-Based Composite Membrane with Enhanced Mechanical Strength and CO_2 Permeance, Ind. Eng. Chem. Res., 60 (2021) 12698-12708.

[70] J. Zhang, E. Kamio, A. Matsuoka, K. Nakagawa, T. Yoshioka, H. Matsuyama, Development of a Micro-Double-Network Ion Gel-Based CO_2 Separation Membrane from Nonvolatile Network Precursors, Ind. Eng. Chem. Res., 60 (2021) 12640-12649.

[71] E. Kamio, M. Minakata, Y. Iida, T. Yasui, A. Matsuoka, H. Matsuyama, Inorganic/organic double-network ion gel membrane with a high ionic liquid content for CO_2 separation, Polym. J., 53 (2020) 137-147.

[72] X. Yan, S. Anguille, M. Bendahan, P. Moulin, Ionic liquids combined with membrane separation processes: a review, Sep. Purif. Technol., 222 (2019) 230-253.

[73] S. Kasahara, E. Kamio, R. Minami, H. Matsuyama, A facilitated transport ion-gel membrane for propylene/propane separation using silver ion as a carrier, J. Membr. Sci., 431 (2013) 121-130.

[74] W.J. Koros, D.R. Paul, Sorption and transport of CO_2 above and below the glass transition of poly (ethylene terephthalate), Polym. Eng. Sci., 20 (1980) 14-19.

[75] S.S. Moganty, R.E. Baltus, Diffusivity of carbon dioxide in room-temperature ionic liquids, Ind. Eng. Chem. Res., 49 (2010) 9370-9376.

[76] A. Ogston, The spaces in a uniform random suspension of fibres, Trans. Faraday Society, 54 (1958) 1754-1757.

[77] J.M. Henis, M.K. Tripodi, Composite hollow fiber membranes for gas separation: the resistance model approach, J. Membr. Sci., 8 (1981) 233-246.

[78] S. Fujikawa, M. Ariyoshi, R. Selyanchyn, T. Kunitake, Ultra-fast, selective CO_2 permeation by free-standing siloxane nanomembranes, Chem. Lett., 48 (2019) 1351-1354.

[79] R. Selyanchyn, M. Ariyoshi, S. Fujikawa, Thickness effect on CO_2/N_2 separation in double layer Pebax-1657®/PDMS membranes, Membranes, 8 (2018) 121.

[80] L. Zhao, E. Riensche, R. Menzer, L. Blum, D. Stolten, A parametric study of CO_2/N_2 gas separation membrane processes for post-combustion capture, J. Membr. Sci., 325 (2008) 284-294.

[81] B. Amsden, Solute diffusion within hydrogels. Mechanisms and models, Macromolecules, 31 (1998) 8382-8395.

[82] T. Yasui, S. Fujinami, T. Hoshino, E. Kamio, H. Matsuyama, Energy dissipation via the internal fracture of the silica particle network in inorganic/organic double network ion gels, Soft matter, 16 (2020) 2363-2370.

[83] 久高 陸, 無機/有機ダブルネットワークイオンゲル薄膜調製に及ぼすゲル前駆体溶液の希釈効果, 卒業論文: 神戸大学工学部応用化学科, (2021).

[84] 木ノ下 雅之, 無機/有機ダブルネットワークイオンゲル薄膜創製のための高分子ネットワーク形成技術の確立, 修士論文: 神戸大学大学院工学研究科応用化学専攻, (2020).

[85] G.G. kumar, A.R. Kim, K.S. Nahm, D.J. Yoo, R. Elizabeth, High ion and lower molecular transportation of the poly vinylidene fluoride–hexa fluoro propylene hybrid membranes for the high temperature and lower humidity direct methanol fuel cell applications, J. Power Sources, 195 (2010) 5922-5928.

[86] G. Gnana kumar, A.R. Kim, K.S. Nahm, D. Jin Yoo, High proton conductivity and low fuel crossover of polyvinylidene fluoride–hexafluoro propylene–silica sulfuric acid composite membranes for direct methanol fuel cells, Curr. Appl. Phys., 11 (2011) 896-902.

[87] N. Senthilkumar, K.J. Babu, G. Gnana kumar, A.R. Kim, D.J. Yoo, Flexible Electrospun PVdF-HFP/Ni/Co Membranes for Efficient and Highly Selective Enzyme Free Glucose Detection, Ind. Eng. Chem. Res., 53 (2014) 10347-10357.

[88] B. Huang, Y. Zhang, M. Que, Y. Xiao, Y. Jiang, K. Yuan, Y. Chen, A facile in situ approach to ion

gel based polymer electrolytes for flexible lithium batteries, RSC Adv., 7 (2017) 54391-54398.

[89] M. Zia ul Mustafa, H. bin Mukhtar, N.A.H. Md Nordin, H.A. Mannan, R. Nasir, N. Fazil, Recent Developments and Applications of Ionic Liquids in Gas Separation Membranes, Chem. Eng. Technol., 42 (2019) 2580-2593.

[90] J.C. Jansen, K. Friess, G. Clarizia, J. Schauer, P. Izák, High Ionic Liquid Content Polymeric Gel Membranes: Preparation and Performance, Macromolecules, 44 (2011) 39-45.

[91] J. Guan, J. Shen, X. Chen, H. Wang, Q. Chen, J. Li, Y. Li, Crystal Forms and Microphase Structures of Poly(vinylidene fluoride-co-hexafluoropropylene) Physically and Chemically Incorporated with Ionic Liquids, Macromolecules, 52 (2018) 385-394.

[92] F. Huang, Q. Wei, J. Wang, Y. Cai, Y. Huang, Effect of temperature on structure, morphology and crystallinity of PVDF nanofibers via electrospinning, e-Polymers, 8 (2008).

[93] J. Gregorio, Rinaldo, M. Cestari, Effect of crystallization temperature on the crystalline phase content and morphology of poly (vinylidene fluoride), J. Polym. Sci., Part B: Polym. Phys., 32 (1994) 859-870.

[94] T. Ueki, M. Watanabe, Polymers in ionic liquids: dawn of neoteric solvents and innovative materials, Bull. Chem. Soc. Jpn., 85 (2012) 33-50.

[95] L.C. Tome, I.M. Marrucho, Ionic liquid-based materials: a platform to design engineered CO_2 separation membranes, Chem. Soc. Rev., 45 (2016) 2785-2824.

[96] D. Camper, C. Becker, C. Koval, R. Noble, Diffusion and solubility measurements in room temperature ionic liquids, Ind. Eng. Chem. Res., 45 (2006) 445-450.

[97] K. Xie, Q. Fu, G.G. Qiao, P.A. Webley, Recent progress on fabrication methods of polymeric thin film gas separation membranes for CO_2 capture, J. Membr. Sci., 572 (2019) 38-60.

[98] J. Zhou, M.M. Mok, M.G. Cowan, W.M. McDanel, T.K. Carlisle, D.L. Gin, R.D. Noble, High-permeance room-temperature ionic-liquid-based membranes for CO_2/N_2 separation, Ind. Eng. Chem. Res., 53 (2014) 20064-20067.

[99] C. Ma, M. Wang, Z. Wang, M. Gao, J. Wang, Recent progress on thin film composite membranes for CO_2 separation, J. CO_2 Util., 42 (2020) 101296.

[100] J. Zhang, E. Kamio, A. Matsuoka, K. Nakagawa, T. Yoshioka, H. Matsuyama, Novel Tough Ion-Gel-Based CO_2 Separation Membrane with Interpenetrating Polymer Network Composed of

Semicrystalline and Cross-Linkable Polymers, Ind. Eng. Chem. Res., 61 (2022) 4648-4658.

[101] O. Selyanchyn, R. Selyanchyn, S. Fujikawa, Critical role of the molecular interface in double-layered Pebax-1657/PDMS nanomembranes for highly efficient CO_2/N_2 gas separation, ACS Appl. Mater. Interfaces, 12 (2020) 33196-33209.

[102] H. Matsuyama, M. Teramoto, K. Hirai, Effect of plasma treatment on CO_2 permeability and selectivity of poly (dimethylsiloxane) membrane, J. Membr. Sci., 99 (1995) 139-147.

[103] H. Hillborg, J. Ankner, U.W. Gedde, G. Smith, H. Yasuda, K. Wikström, Crosslinked polydimethylsiloxane exposed to oxygen plasma studied by neutron reflectometry and other surface specific techniques, Polymer, 41 (2000) 6851-6863.

[104] J.-T. Chen, Y.-J. Fu, K.-L. Tung, S.-H. Huang, W.-S. Hung, S.J. Lue, C.-C. Hu, K.-R. Lee, J.-Y. Lai, Surface modification of poly (dimethylsiloxane) by atmospheric pressure high temperature plasma torch to prepare high-performance gas separation membranes, J. Membr. Sci., 440 (2013) 1-8.

[105] K. Tsuji, M. Nakaya, A. Uedono, A. Hotta, Enhancement of the gas barrier property of polypropylene by introducing plasma-treated silane coating with SiO_x-modified top-surface, Surf. Coat. Technol., 284 (2015) 377-383.

[106] G.-L. Zhuang, C.-F. Wu, M.-Y. Wey, H.-H. Tseng, Impacts of Green Synthesis Process on Asymmetric Hybrid PDMS Membrane for Efficient CO_2/N_2 Separation, Membranes, 11 (2021) 59.

[107] G. Li, K. Knozowska, J. Kujawa, A. Tonkonogovas, A. Stankevičius, W. Kujawski, Fabrication of Polydimethysiloxane (PDMS) Dense Layer on Polyetherimide (PEI) Hollow Fiber Support for the Efficient CO_2/N_2 Separation Membranes, Polymers, 13 (2021) 756.

[108] M. Ariyoshi, S. Fujikawa, T. Kunitake, Robust, Hyper-Permeable Nanomembrane Composites of Poly (dimethylsiloxane) and Cellulose Nanofibers, ACS Appl. Mater. Interfaces, (2021).

[109] Q. Fu, A. Halim, J. Kim, J.M. Scofield, P.A. Gurr, S.E. Kentish, G.G. Qiao, Highly permeable membrane materials for CO 2 capture, J. Mater. Chem. A, 1 (2013) 13769-13778.

[110] A. Halim, Q. Fu, Q. Yong, P.A. Gurr, S.E. Kentish, G.G. Qiao, Soft polymeric nanoparticle additives for next generation gas separation membranes, J. Mater. Chem. A, 2 (2014) 4999-5009.

[111] Q. Fu, E.H. Wong, J. Kim, J.M. Scofield, P.A. Gurr, S.E. Kentish, G.G. Qiao, The effect of soft nanoparticles morphologies on thin film composite membrane performance, J. Mater. Chem. A, 2 (2014) 17751-17756.

[112] P. Li, Z. Wang, W. Li, Y. Liu, J. Wang, S. Wang, High-performance multilayer composite membranes with mussel-inspired polydopamine as a versatile molecular bridge for CO_2 separation, ACS Appl. Mater. Interfaces, 7 (2015) 15481-15493.

[113] C.Z. Liang, T.S. Chung, Ultrahigh flux composite hollow fiber membrane via highly crosslinked PDMS for recovery of hydrocarbons: propane and propene, Macromol. Rapid Commun., 39 (2018) 1700535.

[114] P. Li, H.Z. Chen, T.-S. Chung, The effects of substrate characteristics and pre-wetting agents on PAN–PDMS composite hollow fiber membranes for CO_2/N_2 and O_2/N_2 separation, J. Membr. Sci., 434 (2013) 18-25.

[115] M.J. Yoo, K.H. Kim, J.H. Lee, T.W. Kim, C.W. Chung, Y.H. Cho, H.B. Park, Ultrathin gutter layer for high-performance thin-film composite membranes for CO_2 separation, J. Membr. Sci., 566 (2018) 336-345.

List of Publications

[1] Jinhui Zhang, Eiji Kamio, Atsushi Matsuoka, Keizo Nakagawa, Tomohisa Yoshioka, Hideto Matsuyama: Development of a Micro-Double-Network Ion Gel-Based CO_2 Separation Membrane from Nonvolatile Network Precursors. Industrial & Engineering Chemistry Research, 60, 12640-12649, 2021. **(Chapter II)**

[2] Jinhui Zhang, Eiji Kamio, Masayuki Kinoshita, Atsushi Matsuoka, Keizo Nakagawa, Tomohisa Yoshioka, Hideto Matsuyama: Inorganic/Organic Micro-Double-Network Ion Gel-Based Composite Membrane with Enhanced Mechanical Strength and CO_2 Permeance. Industrial & Engineering Chemistry Research, 60, 12698-12708, 2021. **(Chapter III)**

[3] Jinhui Zhang, Eiji Kamio, Atsushi Matsuoka, Keizo Nakagawa, Tomohisa Yoshioka, Hideto Matsuyama: Novel Tough Ion-Gel-Based CO_2 Separation Membrane with Interpenetrating Polymer Network Composed of Semicrystalline and Cross-Linkable Polymers. Industrial & Engineering Chemistry Research, 61, 4648-4658, 2022. **(Chapter IV)**

[4] Jinhui Zhang, Eiji Kamio, Atsushi Matsuoka, Keizo Nakagawa, Tomohisa Yoshioka, Hideto Matsuyama: Fundamental investigation on development of composite membrane with thin ion gel layer for CO_2 separation. (Submitted). **(Chapter V)**

Acknowledgement

Time flies and three years of study are about to come to an end. During these three years of study in Professor Hideto Matsuyama's research group at Kobe University, I have learned and improved a lot. What I learn in Kobe university will play an important role in helping me in my future life. I would like to thank all the people who provided me with help.

First, I am deeply grateful to Prof. Hideto Matsuyama for giving me the chance to study in his group and providing the advanced research platform and the patient guidance to me. I am impressed by his deep knowledge base. I could not have successfully completed my research without the help of Prof. Hideto Matsuyama.

I sincerely thank Prof. Eiji Kamio for his guidance and help in my research. I was greatly impressed by his rigorous scientific attitude and agile scientific thinking. Without his constant encouragement and help in experiments and papers, I could not overcome the difficulties to complete my studies here. Once again, thank you very much for your kind help.

I am very grateful to Prof. Ryosuke Takagi, Prof. Tomohisa Yoshioka, Prof. Keizo Nakagawa, Prof. Rajabzadeh Kahnamouei Saeid, Dr. Atsushi Matsuoka, Dr. Chuanjie Fang, Dr. Cuijing Liu and Dr. Kecheng Guan for the guidance and advice on my research work, which have really helped a lot.

I would like to thank Masayuki Kinoshita, Jumpei Segawa, and Masayuki Minakata for helping me with my experiments. Your support helped me to get used to the study and life here quickly.

I would like to thank my families. Their support is the source of my working motivation.

Thank you to all the teachers, classmates and friends who have ever helped me. They are too many to be mentioned here, but I will remember all of you forever. Thank you so much everyone.

The support from the China Scholarship Council (CSC) is also acknowledged.

ZHANG JINHUI
Kobe University, Japan
May 2022

Doctoral Dissertation, Kobe University
"Fundamental investigation on the development of tough ion gel-based thin membranes for CO_2 separation", 135 pages
Submitted on 13, 07, 2022
The date of publication is printed in cover of repository version published in Kobe University Repository Kernel.